Nanostructures based on cyclic C_6

by

Stanislav Kuzmin

A thesis
presented to the University of Waterloo
in fulfilment of the
thesis requirement for the degree of
Doctor of Philosophy
in
Physics

Waterloo, Ontario, Canada 2013

AUTHOR'S DECLARATION

I hereby declare that I am the sole author of this thesis. This is a true copy of the thesis, including any required final revisions, as accepted by my examiners.

I understand that my thesis may be made electronically available to the public.

ABSTRACT

The properties of a new family of carbon structures based on stacked cyclic C_6 rings and intercalated cyclic C_6 structures: $(C_6)_n$ and $(C_6)_nMe_{n-1}$ have been studied theoretically using a*b initio* DFT (Density Functional Theory). Calculations of the structural, electronic, and vibrational properties of a range of these molecules have been carried out using DFT techniques with the best correspondence to experimental results. The chemical and structural stability of structures based on stacks of cyclic C_6 has also been estimated for pure carbon molecules $(C_6)_n$ and for metal-organic sandwich molecules intercalated with Fe and Ru atoms. These have $(C_6)_nFe_{n-1}$ and $(C_6)_n Ru_{n-1}$ compositions, respectively

These structures are predicted to show a variety of new electronic, vibrational and magnetic properties. Ultra-small diameter tubular molecules are also found to have unique rotational electron states and high atomic orbital pi-sigma hybridization giving rise to a high density of electron states. All phonons in these structures have collinear wave vectors leading to an ultrahigh density of phonon states in dominant modes suggesting that some of these structures may exhibit superconductivity.

These properties, as well as a predicted high electron mobility, make these structures promising as components in nanoelectronics. Experiments using femto-second laser pulses for the irradiation of organic liquids suggest that such structures may appear under certain conditions. In particular, a new type of iron carbide has been found in these experiments.

ACKNOWLEDGMENTS

I would like to express my sincere gratitude to my advisor and teacher Professor Walter Duley. Due to his deep wisdom and patience I returned into physics and wrote this work.

I would especially like to thank Dr. Michal Wesolowski. His amazing talent for experimental work produced fascinating results in our collaborative experiments.

Special acknowledgments to Dr. Z. Leonenko and Dr. J.H.Sanderson for access to their laser and Atom Force Microscope facilities. They also provided me with informative comments and helpful discussions. I would also like to thanks the rest of my advisory committee, Dr. Marsel Nooijen and Dr. Elisabeth Nicol for taking the time to meet with me when question arose and for their informative insights into my work.

My thanks also goes to my external examiner on my oral thesis defence committee Dr. Michael G. Cottam for his kindness and showing enthusiasm in my work, that helped me a lot.

Finally, I cannot thank my beloved wife Masha enough for moral support and endless help with editing of this manuscript.

Table of Contents:

CHAPTER 1

INTRODUCTION

Carbon is undoubtedly one of the most remarkable chemical elements. It is the backbone of organic compounds, and life itself would not be possible without carbon. In addition, most carbon allotropes and many carbon-based compounds demonstrate extreme values of chemical and physical properties (stiffness, hardness, electron mobility, etc.). For the last two centuries, carbon has been a central focus of studies in chemistry and physics. Despite this activity, the more we find out about carbon-based structures, the more we realize that many of the properties of carbon remain undiscovered. Carbon-based materials have been widely adopted in modern nanoelectronics due to their semiconducting and conducting properties. Some of carbon-based structures such as nanotubes, fullerenes, and graphene [1,2] are widely used in physics. All these structures have unique electronic and vibrational properties (*e.g.* high electron mobility, high Debye temperature), that are exceptional among those of known substances.

Theoretical studies of new carbon-based structures and their novel properties are of great practical interest due to potential use for these materials in the design of electronic devices in future applications. Carbon-based materials can have high electron mobility combined with a high density of states, as well as some additional properties, e.g. ferromagnetism, superconductivity, and enhanced sensitivity to spin orientation of conduction electrons. Most of the organic polymers that are currently used in nanoelectronics have very low electron mobility due to trapping of electrons by hydrogen atoms. Indeed, high electron mobility has been seen in hydrogen free carbon materials [2,3]. These structures then have great potential as the best candidates for nanoelectronics applications.

This thesis is an outline of a series of studies into a new type of carbon sandwich compound based on stacks of cyclic C_6 and intercalated cyclic C_6, notably $(C_6)_n$ and $(C_6)_nM_{n-1}$ [4-7]. These studies focus on the conductive, magnetic, superconductive, vibrational and other properties, particularly those relevant in the development of modern nanoelectronics. A common property of these low dimensionality structures involves characteristic features related to electron band structure, superconductivity, intermolecular magnetic field, which makes them especially attractive for new applications in nanoelectronics, specifically those in spintronics and superconductivity.

1.1. Allotropes of carbon

From ancient times, mankind has known about two allotropes of carbon: ***graphite*** and ***diamond***. These two materials have very different physical properties. While diamond is mechanically hard, optically transparent and electrically insulating, graphite is mechanically soft, optically opaque and electrically conductive. It has been known at least from the XVIII century [8] that both of these materials are a form of carbon. However, the reason for the difference between the two allotropes became clear only in the XIX century with the development of the theory of chemical bonds between atoms. Explicit study of chemical structure became possible only after the development of x-ray diffraction (XRD) methods. For the application of XRD in the determination of crystal structure, Von Laue was awarded the Nobel Prize in Physics in 1914 [9]. The structural study by XRD of diamond was made by W.H. and W.L. Braggs [10] in 1913. They discovered that atoms in diamond are arranged in a tetrahedral lattice with a bond spacing of 0.152 nm. The crystalline structure of graphite was described in 1924 by Bernal [11]. While

previous researchers proposed that graphite has an hexagonal lattice, Bernal revealed the hexagonal intra-planar and stacked inter-planar structures of the material.

The study of disordered carbon materials began in the late 1950s by Bernard Redfern and Cowlard and Lewis) [12,13] with the description of ***glassy carbon*** (g-carbon) also called vitreous carbon. This allotrope combines glassy and ceramic properties with those of graphite. Most importantly, this material is characterized by a high hardness, low density, low electrical resistance, low friction, extreme resistance to chemical attack and impermeability to gases and liquids. Glassy carbon is widely used today as an electrode material in electrochemistry. However, the structure of glassy carbon has long been a subject of debate. Early structural models assumed that both sp^2 and sp^3 hybridized bonds between carbon atoms were present, but it is now known that glassy carbon is 100% sp^2-bonded carbon Recent research has suggested that glassy carbon has a structure consisted of network of graphite ribbon stacks [14].

G-carbon is different from ***amorphous carbon*** (a-C), because it consists of two-dimensional structural elements and does not exhibit 'dangling' π-bonds. Amorphous carbon was discovered in the early 1970s when Aisenberg and Chabot used ion-beam deposition to make thin films of this material [15]. Amorphous carbon does not have any long range structural order or crystallinity. As with all amorphous materials, some short-range order can be observed.

The properties of amorphous carbon films vary depending on the parameters used during deposition. One of the most common ways to characterize amorphous carbon is through the ratio of sp^2 to sp^3 hybridized bonds present in this material. Graphite consists purely of sp^2 hybridized bonds, whereas diamond consists purely of sp^3 hybridized bonds. Materials that are high in sp^3 hybridized bonds are referred to as tetrahedral amorphous carbon (ta-C) (owing to the tetrahedral shape formed by sp^3 hybridized bonds) or as diamond-like carbon (DLC). Amorphous carbon

materials may also be stabilized by terminating dangling π-bonds with hydrogen. These materials are then called hydrogenated amorphous carbon (a-C:H).

Another new crystalline allotrope of carbon was discovered in 1967. Bundy and Kasper [16] synthesised a diamond allotrope with a hexagonal lattice structure that was named ***lonsdaleite*** after Kathleen Lonsdale, the crystallographer, who discovered the planar hexagonal structure of benzene. The structure of lonsdaleite is very similar to that of diamond in that all six member rings in the lattice contain carbon atoms linked only by single bonds with 109.5 degrees between each bond. The difference, however, is that not all rings in lonsdaleite take the form of the chair structure; some of them form what is called a boat structure leaving the unbonded distance between adjacent carbon atoms smaller than that of the chair structure. Lonsdaleite is markedly less stable and its hardness is slightly less than that of diamond. Despite the fact that the presence of boat structure rings in lonsdaleite is the mineral's defining characteristic, most rings in its lattice still exhibit the more stable chair conformation. Frondel and Marvin have identified lonsdaleite inclusions encapsulated in meteorites [17].

A new era of carbon structures began in the mid-1980s, when the first ***fullerene*** was discovered by Kroto, Heath, O'Brien, Curl and Smalley [18]. They studied the interaction of intense laser radiation with graphite and examined the vapor product. Time of flight mass spectroscopy (TOF-MS) showed the presence of stable carbon clusters including $C_{60.}$ Further study determined that the structure of this new compound was icosahedral, which is a polygon with 12 pentagonal and 20 hexagonal faces. This compound, also called "buckminsterfullerene" (C_{60}), is the most symmetric of a large class of fullerenes. Fullerenes are pure carbon compounds in which carbon atoms are connected mainly by sp^2 hybridized bonds to form a two-dimensional surface. Topologically this surface can be wrapped into a sphere, ellipsoid or tube. One of the

most important types of fullerenes are nanotubes (NT). Materials containing these structures have been known for thousands years [19]. For example, NTs are mainly responsible for the nanostructure of fine steel, and can also be found in combustion products [20], and encapsulated in ancient meteorites [21]. NTs were discovered independently by two different research groups in the early 1990s [22,23].

Another important allotrope of carbon is ***graphene***, a one-atom thick sheet of graphite. A key advance in the science of graphene came when Geim and Novoselov at Manchester University managed to extract graphene from bulk graphite in 2004 [24]. After that it was discovered that graphene exhibits a set of remarkable physical properties, including an anomalous quantum Hall effect [25,26], which provided direct evidence for mass-less Dirac fermions.

Other carbon allotropes that should be mentioned include polyyne chains first envisioned in the 1960s [27,28] and subsequently studied by many researchers. This material is also referred to as Linear Acetylenic Carbon (LAC), or ***"Carbyne"***. The structure of these compounds consists of a carbon chain with alternating single and triple covalent bonds. An example of another exotic material is carbon ***nanofoam.*** This was prepared by Rode and coworkers [29] via laser ablation of graphite.

1.2. Chemical and physical properties of carbon and metal-carbon periodic structures.

The modern theory of chemical bonding between atoms is based on Molecular Orbital (MO) theory complemented with Valence Bond theory. Valence Bond theory was developed by Lewis in 1916 [30] when he proposed that chemical bonds form by the interaction of two shared bonding electrons. The Heitler-London theory was formulated in 1927 [31] and for the first time enabled the calculation of bonding in the hydrogen molecule. MO theory is a method for

determining molecular structure in which electrons are not assigned to individual bonds, but are treated as moving in the electric field of the nuclei of the whole molecule. The basis of MO theory was laid by Friedrich Hund and Robert Mulliken [32]. The first quantitative use of MO theory was by Lennard-Jones in 1929 [33]. The concept of the hybridization of atomic orbitals was developed by Pauling [34]. He also analyzed the tetravalency of the carbon atom. Rigorous application of MO concepts to quantum mechanical methods led to the development of computational methods in quantum chemistry. The basic calculation formalism in quantum chemistry is the Hartree-Fock method. It is typically used to solve the time-independent Schrödinger equation for a multi-electron atom or molecule. Since there are no known solutions for many-electron systems, the problem is solved numerically. Due to the nonlinearities introduced by the Hartree-Fock approximation, the equations are solved using a nonlinear method such as iteration, which gives rise to the term "self-consistent" field method. The method was first developed by Hartree and then corrected and developed by Fock [35]. The next step in the development of these computational methods was made after proof of the Hohenberg-Sham theorems [36]. These theorems state that the ground state properties of a many-electron system are uniquely determined by an electron density that depends only on three spatial coordinates and that the correct ground state electron density minimizes energy in the system. Thus, it is possible to find a true representation of electron density and geometry in molecules by minimizing the overall energy. This *ab initio* method is called the Density Functional method (DFT) and is the most popular technique in modern quantum computational chemistry.

The unique properties of carbon structures are mainly due to the special properties of the electron structure of carbon atoms. The electron structure of the ground state in a single free carbon atom includes $1s^2$, $2s^2$, $2p^2$ electron configurations, so that carbon has the opportunity to

use four electrons to form bonds with other atoms. The outer electron shells are close to the nucleus and are strongly bonded to the atom. The ionization potential for these electrons is large, so that carbon forms covalent rather than ionic bonds. Only in rare situations, *e.g.* in carbides, does carbon participate in combined covalent-ion-metal bonds. As a result, carbon is then the only element that can build infinite polymer chains that are only a single atom thick without spatial weakening of the bond energy. A consequence of these properties is that carbon-based molecules can be organized in long polymers. Some carbon allotropes such as nanotubes, fullerene, graphene [1,2] have unique physical and chemical properties.

Another feature of the carbon electron structure is that it readily hybridizes bonding of valence electrons. The typical electron hybridizations of orbitals of the same carbon atom are sp, sp^2 and sp^3. In sp hybridization one s and one p orbital are mixed in two orbitals oriented along the inter-nuclear axis. The hybridization of one **s** and two **p** orbitals creates three identical orbitals with trigonal symmetry that lie in-plane with 120 degrees between their axes. Formation of sp^2 hybridization needs one **s** and three **p** orbitals and results in the formation of four identical orbitals having tetragonal symmetry.

Hybridization of atomic orbitals between different carbon atoms to form molecular orbitals is also typical in carbon. In this case, delocalization occurs and electrons are shared simultaneously among several atoms. A typical hybridization of this type is one in which a few carbon π-orbitals combine to create one aromatic orbital as occurs, for example, in benzene. The multiple hybridization of many atomic orbitals into delocalized molecular orbitals can be observed in nanotubes with ultra-small diameters [108].

The diamond allotrope of carbon where all carbon atoms have sp^3 hybridization, is the hardest natural mineral on Earth [37]. Although some artificially grown materials have a hardness and

stiffness higher than diamond, most of these materials are carbon-based. In 2005 it was found that the hardest known material seems to be carbyne [38], with a Young's modulus forty times higher than that of diamond [38]. In was shown however in 2009, that the material with the highest stiffness is graphene [39]. Measurements have demonstrated that graphene has a breaking strength 200 times greater than steel, with a tensile modulus (stiffness) of 1 TPa. In practice (for example, in tool bits) materials used for coatings have similar hardness to diamond, but are much less expensive. Most of these are composite materials based on carbides with transition metals of the IV-VI groups. The most important carbides are cementite (Fe_3C) with an orthorhombic crystal structure [40], titanium carbide (TiC) with face centered cubic crystal structure [41], and tungsten carbide (WC) with hexagonal crystal symmetry.

Despite excellent mechanical properties, carbon-based structures have unique electronic properties that make them potentially useful in the rapidly developing field of nanoelectronics. Of these, graphene has the most remarkable electronic properties of all known substances. Intrinsic graphene is a semi-metal or zero-gap semiconductor. The electronic structure of graphene was realized as early as 1947 by Wallace [42] who showed that the relation between electron energy and momentum is linear for low energies near the six corners of a two-dimensional hexagonal Brillouin zone, leading to zero effective mass for electrons and holes [43]. Due to this linear dispersion relation at low energies, electrons and holes near these six points, two of which are inequivalent, behave like relativistic particles as described by the Dirac equation for spin 1/2 particles [44,45].

Experimental results from transport measurements show that graphene has a remarkably high electron mobility at room temperature, with reported values in excess of $1.5 \cdot 10^4$ $cm^2V^{-1}s^{-1}$ [46]. In addition, the symmetry of the experimentally measured conductance indicates that the mobility

for holes and electrons should be nearly identical [43]. The mobility is also nearly independent of temperature between 10 K and 100 K [25,46,48,49], which implies that the dominant scattering mechanism is due to defects. Scattering by the acoustic phonons in graphene places intrinsic limits on the room temperature mobility of $2 \cdot 10^5$ $cm^2V^{-1}s^{-1}$ at a carrier density of 10^{12} cm^{-2}[49,50,52]. The corresponding resistivity of a graphene sheet would then be 10^{-6} Ω·cm. This is less than the resistivity of silver, which is the lowest resistivity substance known at room temperature [49]. However, for graphene on SiO_2 substrates, scattering of electrons by optical phonons at the substrate is a larger effect at room temperature than scattering by phonons in graphene. This limits the mobility to $4 \cdot 10^4$ cm^2 $V^{-1}s^{-1}$ [49], and the electron velocity, v_F, at the Fermi level exceeds 10^6 m/s. Thus, intercalated layers of graphene represent an optimum combination of the electronic properties needed for transport properties – the highest ever measured mobility of electrons combined with a rather high density of electrons states [53]. The large value of v_F and low-resistance contacts without a Schottky barrier should help reduce switching times to perhaps < 10^{-13}s. Relatively low on/off ratios (reaching only ≈100 because of graphene's minimum conductivity) do not seem to present a fundamental problem for high-frequency applications, and the demonstration of transistors operational at THz frequencies would be an important milestone for graphene-based electronics [46]. Another important property of graphene is its high Debye temperature which exceeds 2300 K [52] and is much higher than in typical metallic systems.

1.3 Electronic properties of fullerenes and sandwich metal-carbon structures

Different types of fullerenes and nanotubes can be considered as derivatives of graphene as nanotubes can be formed from a rolled sheet of graphene, while fullerenes are wrapped pieces of the graphene surface. Thus, the electronic properties of nanotubes and fullerenes are very similar to those of graphene. Studies of the electronic structure of fullerenes [55,101] shows that the electron mobility in intercalated fullerenes exceeds 1 $cm^2/(V\ s)$, while the Debye temperature is ~ 1750K [101]. A notable feature of the electronic properties of fullerenes and nanotubes is the dependence of the localized density of electronic states (LDOS) on local curvature [107,108]. In spherical fullerenes and in nanotubes the LDOS is inversely proportional to the volume of the sphere and the cross sectional area of the tube, respectively. This effect is a consequence of pi-sigma hybridization on the curved graphene surface.

Graphene and its derivatives also have other applications in nanoelectronics related to spin-dependent electron transport phenomena. Graphene is thought to be an ideal material for spintronics due to its small spin-orbit interaction and the near absence of nuclear magnetic moments in carbon. Electrical spin-current injection and detection in graphene has been recently observed at room temperature [56-58]. A spin coherence length > 1 micrometer at room temperature was also observed [57], while control of the spin current polarity with an electrical gate has been demonstrated at low temperature [58].

For sandwich metal-carbon structures (e.g. intercalated graphite) there are potentially many interesting physical properties and a broad spectrum of possible applications [59]. The main goal of intercalation in carbon structures is to increase the density of current carriers, while maintaining mobility close to that of graphite. Graphite intercalation compounds have many

possible applications, specifically involving use in battery and electrode materials, in chemical catalysis and catalytic applications, as conductors, and in the production of carbon fibres. Existence of the long-range structure of intercalated graphite suggest that it may be used for the preparation of materials with large lattice constants for applications in low energy neutron monochromators, etc. The alkali metals K, Cs, Li, and Rb, the alkaline-earth metals Ca and some other compounds (Br_2, $AlCl_3$ and $FeCl_3$) are mostly used as the intercalated species.

Some intercalated graphite structures such as C_2Li, C_8K, C_6Ca, C_6Yb, and C_6Ba with high electron density of states show superconducting properties [60]. High temperature superconductivity has also been predicted in doped hydrogenated graphene [61], or graphane [62], with a critical point higher than the boiling point of nitrogen. Superconductivity in nanotubes and in ropes of nanotubes has been studied extensively (see the review in [191]), and it has been found that the critical temperature increases as the diameter becomes smaller. The highest critical temperature (30K) for nanotubes was reported by Tang et al. [113] in a nanotube with a diameter of 4.2Å.

The first experimental observations of structures consisting of stacks of flat organic aromatic molecules were reported in the 1970s [63]. It was found that flat disc-like organic molecules (benzene-hexa-n-alkanoates or BHn-alkanoates) can self-assemble into columnar structures with thousands of stacked layers. The possibility of π-conductivity along such column structures was noted [64,65]. Early in the 2000s Simpson et al [82] proposed the use of such "columnar superstructures" in nanoelectronics. They used disk-type polycyclic aromatic hydrocarbons (PBAHs), two-dimensional pi-systems decorated by peripheral alkyl chains (C_{78}, C_{96}, C_{132}). These molecules were arranged in columns and it was shown that such compounds exhibit complex electronic functions, and can act as a diode or as a field effect transistor. Such structures

can be used as nano-sized charge transport cables. The main problem of electronic devices based on organic column structures involves the low electron mobility by hydrogen atoms that trap free electrons. This problem could be resolved by using pure carbon or metal-carbon sandwich structures where the electron mobility is comparable with that in graphene.

Erkoc [5] was the first to propose the existence of structures consisting of stacks of different flat pure carbon clusters. Among proposed structures were stacks of dehydrogenated benzene with benzene rings on the edge of structure. He called such structures "benzorods". Later [4] he considers fully dehydrogenated "benzorods" and their thermal stability. In his calculations he applied the Density Functional Theory (DFT) using the pure Hartree-Fock formalism combined with the Austin Model (AM1) semi-empirical method. However, this approach did not allow precise calculations. Reliable vibrational and electron properties cannot be predicted at this theoretical level [81], and subsequent calculations reported in this thesis suggests that there were several miscalculations in Erkoc's optimized molecular structure geometry. For example, the geometry of $(C_6)_n$ stacks sometimes differs substantially from those calculated by Erkoc.

Sandwich structures with metal atoms between benzene rings $Me_{n-1}Bz_n$ can be considered as precursors to metal organic molecules $Me_{n-1}(C_6)_n$ based on cyclic C_6. Metal-benzene compounds have been the subject of much interest since the discovery of V-benzene polymers [83] due to their unique electronic and magnetic properties [84-91]. Many theoretical [84-90,92-95] and experimental [96-99] studies of their properties have been reported. For example, metal-benzene polymers are expected to be good conductors for spin transport [85,88,89] and as components in novel nanoscale devices. It has been suggested that multilayered sandwich molecules based on benzene combined with Ti, Cr, Sc, Fe, Ni, Nb, Ta, and Mn are possible [84,87,89,90,93,94,99] but, to date, such structures have been found only in V-benzene systems.

1.4. Specific features of one-dimensional periodic structures.

Compounds with low dimensionality have unique electronic, vibronic, magnetic, spintronic and other properties [66-75;89]. Of special interest are drastically changed electronic properties in low dimensional systems in compare with two- and three-dimensional. These changes can have a direct influence on transport, optical, superconducting, magnetic, and many other physical properties. These features of one-dimensional interacting many-electron systems are the result of strong spatial confinement accompanied by presence of very strong quantum fluctuations and extra-strong electron correlation [67, 114, 161].

The collective motion of electrons in three-dimensional metals is well described by the Fermi-liquid model, introduced by Landau in 1956 [76], and later developed by Abrikosov and Khalatnikov using diagrammatic perturbation theory [77]. In this model, the system of strongly correlated electrons is replaced by system of quasi-particles carrying both charge and spin. This description is not applicable in one-dimensional systems, where the carriers of charge and spin are separated into charge density and spin density waves, respectively. The first theoretical model of the properties of one-dimensional electron systems was reported by Tomonaga in 1950 [68]. He proposed a general protocol for describing the collective motion of fermions in one spatial dimension in terms harmonic oscillators which is now known as the bosonization method [69]. Tomonaga's work has stimulated many additional theoretical investigations, including that by Luttinger [70]. The outcome of this work has been the development of the basic description of one-dimensional many-body systems in terms of what have become known as Tomonaga-Luttinger (TL) liquids [67-71,73-75]. This concept covers not only fermions but also a wide variety of quantum systems including interacting bosons and spins. There are number of correlated electron systems in which clear evidence for anomalous TL liquid properties has been

found experimentally [67]. Interest in the properties of TL liquids increased after the discovery of high-temperature superconductivity in 1986, where the electron system exists in a pseudo-one dimensional state. Since the original approach initiated by Tomonaga is based on a weak-coupling theory, the main problem involves developing ways to describe the TL liquid in a strong correlation regime. This problem has been studied extensively using a variety of numerical and analytical methods since the early 1990s. Conformal field theory (CFT) [72], which was created in the 1980s in connection with superstring theory, has provided an effective formalism to describe TL liquids in the strong coupling regime in one-dimensional systems.

Strictly speaking, only infinite chains of atoms are one-dimensional systems. All other structures commonly referred to as "one-dimensional" have some additional degrees of freedom and are therefore occasionally called "one-plus-zero-dimensional" [120], or "1+1" dimensional [67] systems. In this case, the application of the pure TL liquid model may be questionable.

The primary representatives of structures with such "one-plus-zero" dimensionality are carbon nanotubes, with geometries that can be represented as a folded graphene strip. Because of this, the structure of a nanotube is uniquely determined by the chiral vector – the combination of graphene lattice vectors that can be built along the circumference of nanotube. This chiral vector is given by a combination of two integers (n,m). If m=0, then the nanotube has a zigzag structure, while if n=m it has an armchair structure. If neither of these solutions applies, then the nanotube is referred to as having "chiral" structure. The electronic structure of large diameter nanotubes is well approximated by the so-called "folding method" [3]. This method originated from the known two-dimensional electronic structure of graphene. Electronic wave functions of the nanotube remain unchanged following a 2π rotation around the principle axis. In addition, the crystalline lattice of the nanotube has additional periodic boundary conditions [3] along its

circumference, leading to the quantization of the electron wave-vector component along the circumference. These quantum states are associated with rotational eigenstates, which combine linear motion along the principle axis with rotation around the nanotube axis.

This approach is applicable not only to nanotubes, but to any structure with a principal rotational or rotational-translational axis. It is then evident that structures with axial symmetry have additional branches in the electron band structure associated with these rotational energy states. If such additional branches cross the Fermi level then conduction electrons have additional density of states. It has also been reported [105] that the density of states (DOS) of electrons near the Fermi level in nanotubes is inversely proportional to tube diameter. Studies of the properties of electrons in nanotubes with ultra-small diameters [106-111] have shown that the hybridization of pi and sigma electrons increases with decreasing tube diameter. As a result, the energy levels corresponding to the HOMO and LUMO states tend to approach each other, and eventually overlap for nanotubes with diameters < 10 Å. Thus, all nanotubes with ultra-small diameter are conductors and have a relatively high DOS. Under these conditions in one-dimensional structures, the Fermi surface reduces to a few points or occasionally to a set of a few circles.

Superconducting properties drastically decrease in response to any reduction in dimensionality [114], and it has been predicted theoretically that superconductivity is not possible in one dimensional structures [112]. The classical microscopic theory of superconductivity developed by Bardeen, Cooper and Schrieffer (BCS) [119] cannot explain this phenomenon. Despite these constraints, superconductivity has been observed in one-dimensioned structures and has been the subject of extensive experimental investigations [115-118]. Superconductivity in small diameter nanotubes exists down to the smallest diameter nanotube [109,175]. Superconductivity has even been reported in a nanotube with diameter of ~ 4.2 Å [113], although, in this case, the

dependence of the energy gap on temperature was depressed by quantum fluctuations. Superconductivity has also been discovered in a broad class of one-dimensional organic material [114] at high pressures. Despite theoretical limitations, superconductivity has been observed in aluminum nano-wires [115-118] where it is enhanced by a yet unknown mechanism.

It has been shown by Migdal [181] that the electron-phonon interaction in these materials, is primarily due to contributions from electrons and phonons having nearly collinear wave vectors. In bulk three-dimensional materials the probability that the wave vectors of arbitrary electrons and phonons will be collinear is very small, so that the energy of the electron-phonon interaction is small compare with that associated with normal vibrations. This phenomenon has become known as "Migdal's theorem". Since all wave vectors are collinear in one-dimensional structures, one can predict that the electron-phonon interaction energy will be comparable to that of the normal vibrations. Hence, it is possible that the conditions for superconductivity will be facilitated in one-dimensional structures due to enhanced electron-phonon interaction.

Theoretical studies of new carbon-based structures and their novel properties are of great practical interest in the design of new generation electronic devices. Development of these materials can be expected to yield structures with high electron mobility combined with a high density of states. It may also be possible to develop materials with ferromagnetic, superconductive and spin orientation properties that will facilitate new applications. Most of the organic polymers currently used in nanoelectronics have very low electron mobility due to trapping of electrons by hydrogen atoms. Thus, hydrogen-free carbon structures are potentially good candidates for new applications in nanoelectronics.

The study of a new type of carbon and metal-carbon sandwich molecules based on stacks of cyclic C_6 and intercalated cyclic C_6 structures could then be an important step in the wonderful

world of carbon materials. The goal of the work described in this thesis is to explore some characteristics of these materials based on promising applications in nanoelectronics and in other physical systems.

1.5. Overview of this thesis

After this introduction, Chapter 2 summarizes the results of the first principles calculation of the stability, geometry and electronic properties of tubular carbon $(C_6)_n$ structures. These represent the simplest molecules formed by stacking dehydrogenated benzene components. High-precision DFT methods are used to improve the validity of theoretical simulations on the stability of these molecules. The electron structure and electron charge distribution in these structures has also been determined theoretically. *Ab initio* DFT calculations are used to explore the chemical and geometric stability of these molecules.

Chapter 3 shows that similar techniques can be used in the theoretical analysis of metal-organic sandwich molecules where cyclic C_6 layers alternate with metal atoms. The resulting analysis indicates that the most stable intercalated structures are those based on cyclic C_6 containing iron or ruthenium atoms.

Chapters 4 and 5 describe the predicted vibrational and electronic properties of finite molecules based on C_6 stacks $(C_6)_n$ and the most stable intercalated C_6 stacks $(C_6)_nFe_{n-1}$and $(C_6)_nRu_{n-1.}$ This analysis yields the configuration of atomic displacements in the most active vibrational modes and dependence of electronic and vibrational properties on the length of molecule.

Chapter 6 discusses the mechanisms involved in producing superconductivity in nanotubes, and leads to a proposed re-interpretation of the BCS results for one-dimensional structures using

a simple model. This new model is compatible with the BCS formalism but is also consistent with the classical theory in one-dimensional periodic structures. The discussion includes a preliminary investigation into the possibility of superconductivity in $(C_6)_n$ and related metal-organic structures.

Chapter 7 describes the results of some preliminary experiments on irradiation of the organic liquids with laser fs-pulses, including the irradiation of pure benzene, and experiments on the irradiation of solutions of ferrocene in benzene. These experiments indicate that a variety of different organic and metal-organic nanoparticles are created under these conditions, and a simple theoretical model has been developed to describe specific features involving the formation of nanoparticles via laser irradiation of pure benzene. Experiments on the irradiation of ferrocene/benzene solutions indicate that a new type of iron carbide structure may be created under fs irradiation conditions.

The final Chapter summarizes the main theoretical and experimental results of this research, and suggests further directions for this research. A summary is also provided to specifically focus on the novelty of some of these results. These results have been reported in seven papers [6,7,103,104,122,123,125], and two additional papers on one-dimensional superconductivity [104] and outlining the experimental data on laser irradiation of ferrocene solution in benzene and discovery of new type iron carbide [124] are now in preparation.

CHAPTER 2

A NEW TYPE OF TUBULAR CARBON MOLECULE BASED ON MULTI-LAYERED CYCLIC C_6 STRUCTURES

The electronic properties of individual carbon molecules as potential nanowires are of special interest in the rapidly developing field of nanotechnology [126]. One of the primary limitations in this field is a lack of knowledge of the basic properties of molecular conductors with respect to electron transport. Although many studies report on the transport properties of carbon nanotubes [127,128], the novel characteristics of simpler compounds based on carbon rings, chains [126,129], sheets [130,131], and other carbon structures are worthy of further investigation.

Unlike carbon nanotubes (NT), that are formed by rolling of a graphene sheet such that the walls consist of fused C_6 rings, tubular carbon structures can also be created by stacking basic units such as dehydrogenated naphthalene (C_{10}), dehydrogenated phenanthrene (C_{18}), and dehydrogenated coronene (C_{24}). Structures based on stacked molecules are not related to graphene as they do not consist of extended aromatic ring configurations. In the tubular structures described above, the overlap of π electrons between adjacent rings still occurs, leading to the possibility of electronic conduction along the axis of the resulting tubular $(C_N)_n$ structure. Therefore, given these π–π interactions, molecules of this type are worth investigating as potential conductive elements for nano-circuits [64,65].

From a quantum mechanical point of view, the conductive properties of multilayered carbon stack structures appear to arise from the hybridization of local atomic orbitals (AO) from different layers into one molecular orbital (MO) near the Fermi level. In this case electrons belonging to the global MO are delocalized over the volume of the MO. In particular, in a MO that crosses the Fermi level electrons can participate in conducting current through the structure. One can then visualize the MO as forming a conducting channel through the structure. Such links

can be formed through the assembly of stacks of planar carbon structures including aromatic rings via hybridization of aromatic pi-bonds [63-65,82]. Many types of conducting polymers and carbon multilayered structures have been reported [114], but structures based on stacks of cyclic C_6 as discussed in this thesis represent a new class constituting the minimum cross-sectional size for conducting channels assembled from carbon rings.

Hydrogen is known to play an important role in organic compounds and acts to define molecular geometry and chemical stability. In reality, the presence of hydrogen also acts to trap electrons and reduce electron mobility. Thus, the hydrogenation of conducting carbon structures reduces conductivity even in materials with high electron mobility [79]. A major challenge then is to create stable long periodic dehydrogenated carbon structures. One important class of periodic pure carbon structures are nanotubes (NTs) [3,102,148]. These can exhibit extremely high electron mobility [128], over lengths ranging from 10 nm up to 18.5 cm [80]. NTs are widely used as nanowires and in spintronics devices. However, it has been shown [105] that for a single wall nanotube (SWNT) the density of electron states (and, hence, other electronic properties) are inversely proportional to radius. Therefore, small diameter SWNTs are particularly interesting as elements in nanoelectronics. The smallest possible conventional NT consistent with superconductivity was reported to have a ~ 4 Å [106-109,175] diameter (for SWNT (4;1), (5;0), (3;3)). Such SWNTs are rolled from graphene ribbons. A similar unconventional NT structure based on stacks of cyclic C_6 would have a diameter of ~ 3 Å (see Fig.2-2).

This chapter summarizes the results of first principles calculations of the stability, geometry and electronic properties of pure carbon structures based on stacks of cyclic C_6. Some laboratory experiments related to the possible production of these molecules are also discussed.

2.1. Methods of *ab initio* calculation.

Calculations were carried out using density functional theory (DFT) based on the Becke, Lee, Yang and Parr (B3LYP) hybrid-exchange correlation functional and implemented with the Gaussian03 suite of programs [132,133]. The 6–21g, and 6–31g atomic basis sets were used in initial calculations, but final results were obtained using the 6–311g and 6–311g(p,d) atomic basis sets with increased precision. Electronic energy levels and density of states (DOS) were calculated for the ground state using a restricted closed shell calculation method. Bond energies were calculated after optimization of the overall geometry in Gaussian 03 using the 6–311g atomic basis by comparison of the energy of the whole structure and overall energy of separate carbon rings.

2.2. Properties of cyclic C_6.

Over the last 20 years there have been many *ab initio* DFT calculations of the properties of cyclic C_6 [134-142,149] carried out using various formalisms and with a variety of different atomic basis sets. The results of these calculations together with matrix spectra of C_6 molecules [143-146] show that there are two isomers of cyclic C_6, with D3h and D6h symmetries. The ground state of C_6 is concluded to have D3h symmetry while the D6h configuration is associated with a transition state ~0.41 eV above the ground (D3h) state. The results of the present calculations indicate that the energy of the cyclic D6h state is ~0.53 eV lower than that of the linear C_6 isomer and implies that cyclic C_6 is a very stable molecule, but that it will exhibit high chemical activity.

It is expected that cyclic C_6 isomers with different symmetry correspond to different types of hybridization of HOMO orbitals. Cyclic C_6 with D3h symmetry corresponds to a molecule where

three of the six carbon atoms have sp^3 orbital hybridization (with 109.5 degrees between orbitals). The more symmetric isomer with D6h symmetry corresponds to sp^2 hybridization of all six carbon atoms in the ring. The energy of this configuration is slightly higher than that of the isomer with D3h symmetry and is accompanied by delocalization of all valence electrons. Thus different symmetries of C_6 ring isomers correspond to different electron densities in the molecule accompanied by distinct electron delocalization.

Cyclic C_6 has been identified in matrix spectra [92-95] and the D3h symmetry of the ground state has been confirmed from infra-red and Raman spectra. Although the D6h isomer of cyclic C_6 has not been observed in the laboratory, there is good reason to believe that this structure could appear when the C_6 group is bonded to other species, especially to another C_6 ring. The results of our first principles calculations show that $(C_6)_n$ molecules tend to approach D6h symmetry as n increases.

2.3. Results and discussion

Although, the benzene ring and cyclic C_6 isomer both have D6h symmetry, and have very similar structures, there are significant differences in the valence electron molecular orbitals in the two species. The structure of molecular orbitals for benzene and cyclic C_6 are shown in Fig.2-1.a and Fig.2-1.b, respectively. It is well-known that six pi-orbitals in benzene molecule hybridized into degenerate aromatic HOMO orbital. It localized as two aromatic rings parallel to the molecular plane from both sides of the molecule (see Fig.2-1.a). Cyclic C_6 also has HOMO orbital hybridized from several electron orbitals, but they are not pure pi-orbitals and some other s- and p- orbitals are also involved. The resulting HOMO orbital has a shape of one large torus in-plane of carbon ring around the molecule (see Fig.2-1.b). Such difference in electronic

structure of benzene and C_6 ring can explain difference in interaction of a few benzene molecules and a few cyclic C_6 molecules.

The intermolecular potential in the benzene dimer arises from the van der Waals interaction and is 20–100 times weaker than that of normal chemical bonds [147]. The two stable configurations for a pair of benzene molecules consist of one in which the planes of the two molecules are perpendicular and another in which the planes are parallel but where one molecule is shifted by half the width of the benzene ring. Unlike in the benzene dimer, the two rings in the stable ground state of $(C_6)_2$ overlap almost completely. In this configuration, each 6-atom ring has C_3 symmetry although the overall molecule exhibits C_i symmetry (Fig. 2-1). In the next largest molecule $(C_6)_3$ all three rings are stacked on top of one another and the overall molecular symmetry is S_6. This stacking configuration is preserved in longer $(C_6)_n$ molecules but individual C_6 rings in some stacks incorporate a small D3h distortion. The tendency toward hexagonal symmetry in longer $(C_6)_n$ molecules occurs because the electron density in the degenerate HOMO orbital in the D6h form of C_6 forms a broad ring around the molecule allowing it to form covalent bonds with adjacent C_6 rings. The presence of C_6 rings with D3h symmetry at the ends of these molecules is related to differences in the properties of C_6 isomers. A high delocalization of electrons in the middle of the $(C_6)_n$ structure requires the C_6 isomer with D6h symmetry corresponding to a highly delocalized electron distribution. Hybridization of HOMO orbitals of this isomer leads to delocalization of the electrons over the central region of the molecule. Rings at the end of the molecule interact only with one neighbouring ring and are less prone to hybridize, so that they retain the D3h symmetry of the ground state of the C_6 ring. Fig. 2-2 shows the optimized geometry and electron density within the HOMO orbitals in $(C_6)_9$ where the stack has the structure $(C_6)_2(C_6)(C_6)_3(C_6)(C_6)_2$ and an overall D6h symmetry. It can be seen that the

electron density assumes an annular form near the end of this molecule. In $(C_6)_9$ the $(C_6)_3$ and $(C_6)_2$ components each form strong bonds to intermediate C_6 molecules.

Bond energies in some $(C_6)_n$ molecules are summarized in Table 2-1. The bond energy between carbon atoms in cyclic C_6 with D6h symmetry was found to be 6.74 eV. This increases to 6.75 eV in C_6 with D3h symmetry. For $(C_6)_2$ where the overall symmetry is C*i*, the average bond energy between carbon atoms inside each of the rings is 5.96 eV, while the bond energy between the two C_6 rings is 7.90 eV. The bond energy between rings in $(C_6)_3$, where the overall symmetry is S_6, is found to increase slightly to 7.98 eV. Table 2-1 shows that the strongest bonds (~8.5–10.5 eV) in the molecules studied occurs between the central C_6 rings in $(C_6)_6$, $(C_6)_7$ and $(C_6)_9$, while the weakest intramolecular bonds (~5.3 eV) are present in central C_6 groups in $(C_6)_n$ with $n \geq 5$. This may be one reason why it is not possible to find a stable tubular configuration for $(C_6)_4$. The weakest intermolecular bond (4.90 eV) is found between central C_6 rings and the outer $(C_6)_2$ groups in $(C_6)_6$.

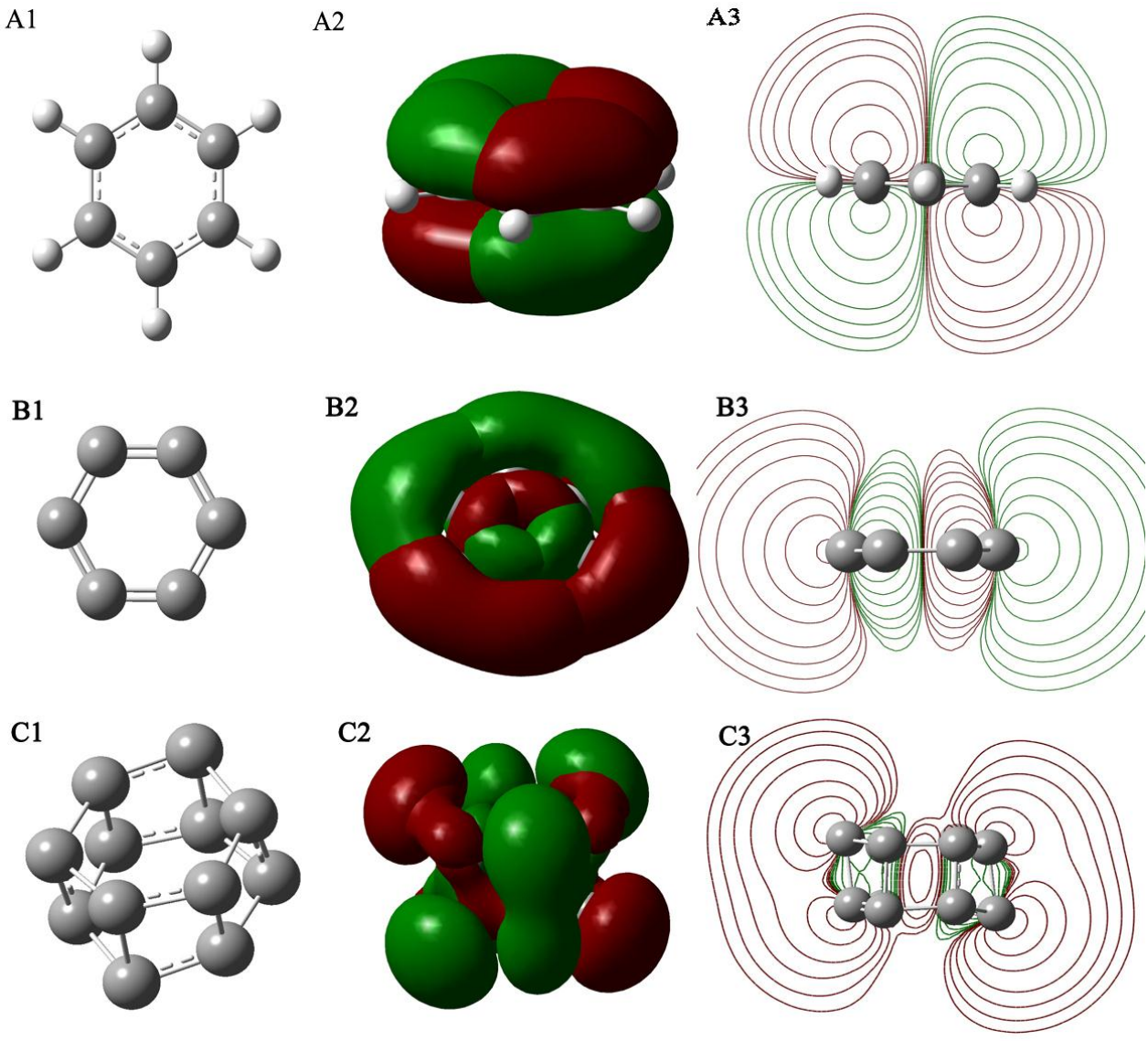

Fig. 2-1.A comparison of electron density in the HOMO orbital of (a) benzene; (b) cyclic C_6; and (c) $(C_6)_2$. Left: molecular geometry. Middle: shape of the degenerate HOMO orbital. Right: electron density in the HOMO orbital.

$(C_6)_n$		C_6	$(C_6)_2$	$(C_6)_3$	$(C_6)_5$	$(C_6)_6$	$(C_6)_7$	$(C_6)_8$	$(C_6)_9$
Symmetry		(D_{6h})	(C_i)	(S_6)	(D_{6h})	(D_{6h})	(D_{6h})	(D_{6h})	(D_{6h})
C_6-$(C_6)_n$ (n=2,3)		-	-	-	6.63	4.90	-	6.19	6.55
$(C_6)_2$-$(C_6)_3$		-	-	-	-	-	5.32	-	-
C-C in C_6		6.75	-	-	5.30	5.34	-	5.34	5.32
Edge $(C_6)_2$	C_6-C_6	-	7.90	-	6.54	6.42	6.61	6.63	6.51
	C-C	-	5.96	-	5.87	5.88	5.87	5.87	5.40
Center $(C_6)_2$	C_6-C_6	-	-	-	-	-	-	5.34	-
	C-C	-	-	-	-	-	-	5.42	-
Center $(C_6)_3$	C_6-C_6	-	-	7.98	-	-	8.55	-	8.45
	C-C	-	-	6.05	-	-	5.38	-	5.87
Center C_6-C_6		-	-	-	-	10.53	-	-	-

Table 2-1
Bond energies in eV of components in multi-layered cyclic C_6 structures. Bond energies between individual components as well as C–C bond energies within C_6 rings areidentified. Highest symmetries are indicated, but molecules often also have small low symmetry distortions. For example, all larger molecules combine D6h with a small D3h component.

A comparison between the electron distribution in HOMO and LUMO orbitals in some of the molecules studied is shown in Fig. 2-3. It is evident that the geometry of the larger tubular molecules becomes similar to that of nanotubes. The electron distribution in the HOMO orbitals in molecules with 7 or more layers tends to assume a limiting distribution in which the electron density is concentrated toward the ends of the molecule (Fig.2-3), while that within the LUMO orbitals has a dumbbell configuration with a low electron density at the center of the molecule. All larger molecules terminate in $(C_6)_2$ fragments but internal components consist of $(C_6)_2$ and $(C_6)_3$ structures separated by one C_6 ring. The interlayer separation at the center of these molecules is found to be 0.163±0.2 nm (Table 2-2) which is almost exactly 50% of the separation between planes in crystalline graphite.

The energy gap between the highest occupied molecular orbital (HOMO) and the lowest unoccupied molecular orbital (LUMO) has been calculated for molecules up to $(C_6)_{16}$, (Fig.2-4). It was found that electrons in the HOMO states are highly delocalized and that the energy gap between the LUMO and HOMO levels approaches 2.28±0.02 eV, while the ionization energy tends to 6.8±0.3 eV. The electron affinity is nearly 4.65 eV in the largest molecules studied. Evidently, the electronic properties of these molecules rapidly approach limiting values as more C_6 groups are added suggesting that it may be possible to construct $(C_6)_n$ with many layers. A characteristic feature is a periodicity in the distance between C_6 layers involving a structure in which 2–3 layer C_6 rings are separated by individual C_6 rings. The energy gap is in agreement with the observed dependence of the energy gap in semiconducting "zigzag" nanotubes scaled by a factor 1/d, where d is the nanotube diameter [148]. This is one more example of the similarity between electronic and vibrational structures in "classical" "zigzag" SWNTs and those in molecules based on multi-layer stacks of cyclic C_6.

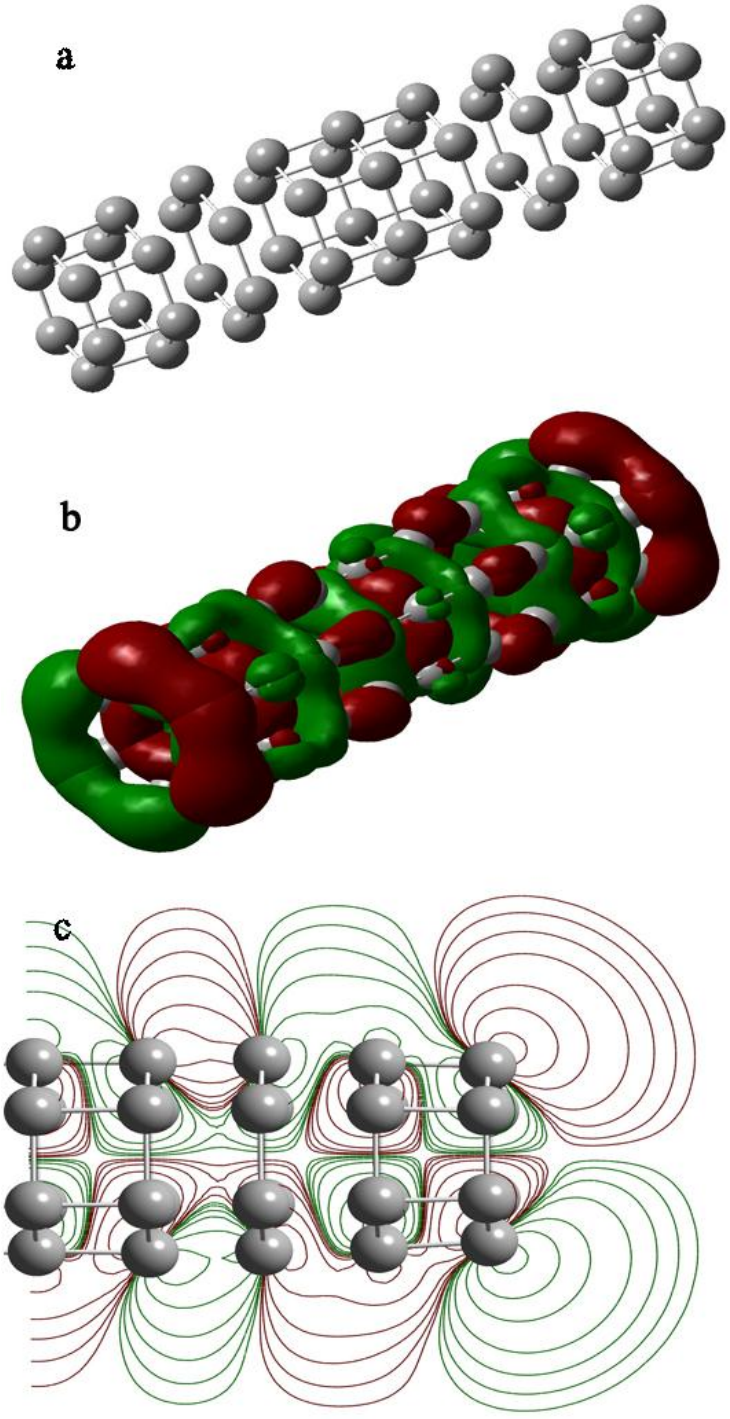

Fig. 2-2.Structure and electron density in the HOMO orbitals in $(C_6)_9$. (a) Overall optimized geometry. (b) HOMO orbitals. (c) Electron density distribution in the HOMO orbitals near one end of the molecule.

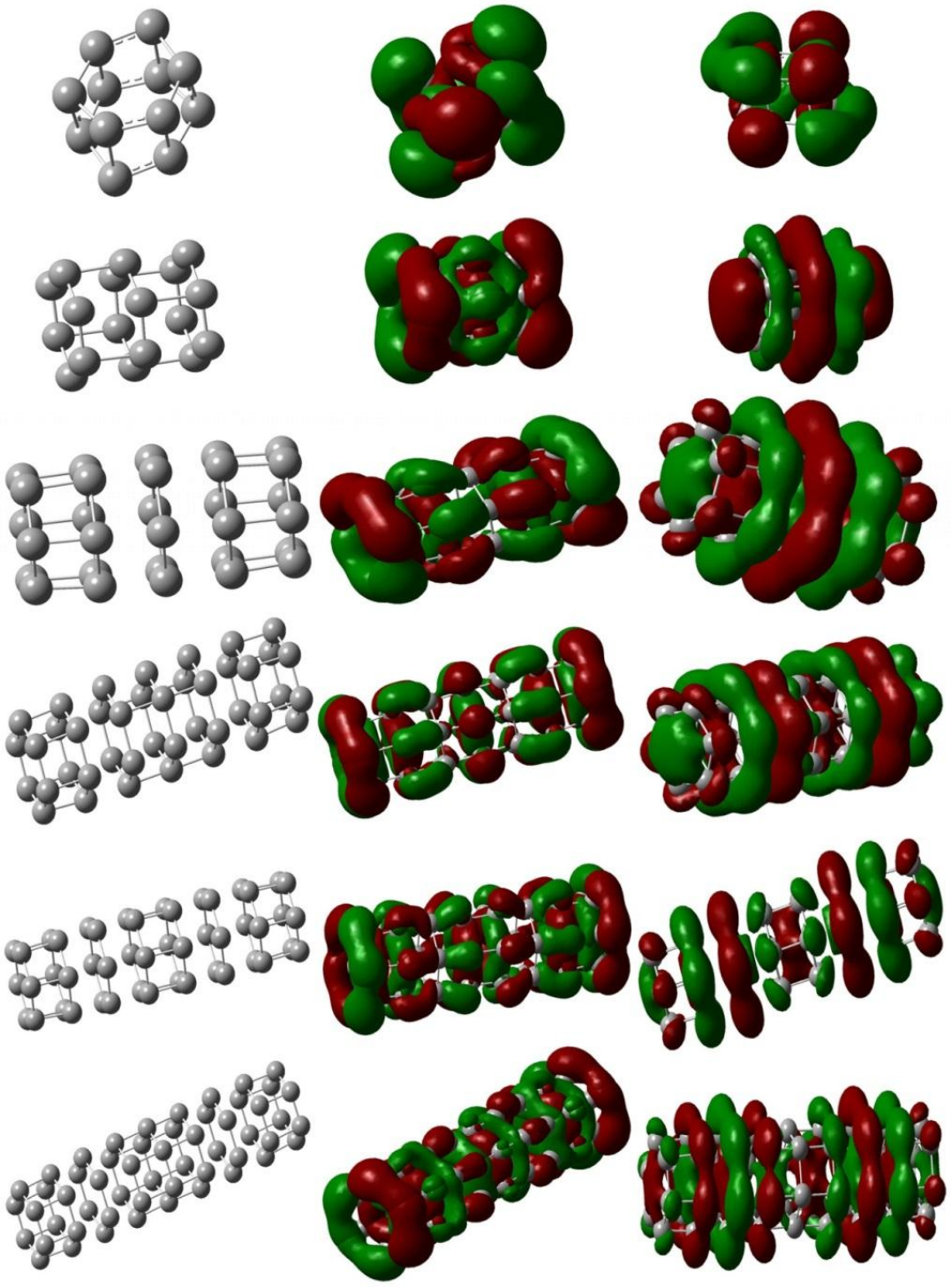

Fig.2-3. HOMO and LUMO orbitals in some multi-layered $(C_6)_n$ structures. The left column shows the geometry of the molecule. The middle and right-hand columns show the distribution of electron density in the HOMO and LUMO orbitals, respectively. Molecules are (from top to bottom): $(C_6)_2$, $(C_6)_3$, $(C_6)_5$, $(C_6)_7$, $(C_6)_8$, $(C_6)_9$.

Structure	$(C_6)_2$	$(C_6)_3$	$(C_6)_5$	$(C_6)_6$	$(C_6)_7$	$(C_6)_8$	$(C_6)_9$
	R_{12}= 0.150 (average)	R_{12}= 0.159	R_{12}= 0.157 R_{23}= 0.164	R_{12}= 0.159 R_{23}= 0.165 R_{34}= 0.164	R_{12}= 0.158 R_{23}= 0.166 R_{34}= 0.163	R_{12}= 0.158 R_{23}= 0.165 R_{34}= 0.163 R_{45}= 0.161	R_{12}= 0.159 R_{23}= 0.165 R_{34}= 0.164 R_{45}= 0.162

Table 2-2.Distances (nm) between C_6 layers in stacked $(C_6)_n$ structures. For $(C_2)_3$ and larger molecules layers are labelled 1, 2, etc., starting from the first C_6 ring at the end of the molecule.

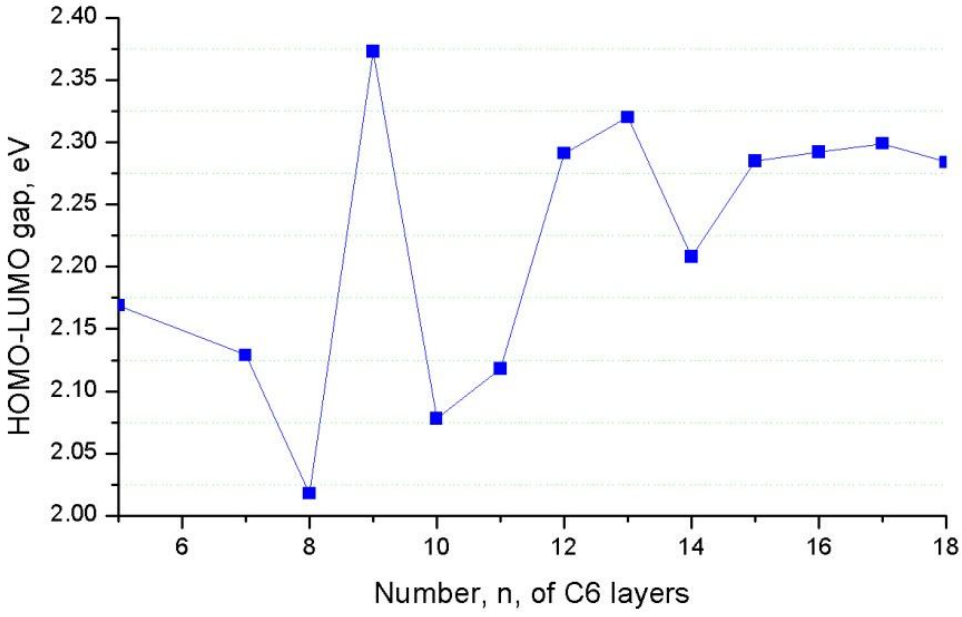

Fig.2-4. Calculated HOMO-LUMO energy gap (eV) plotted vs. n for $(C_6)_n$ molecules. This approaches 2.28 ± 0.02 eV for large n.

2.4. Experimental evidence for pure carbon nanotubes based on stacks of C_6.

In 2004 during a study of multi wall nanotubes (MWNT), Zhao et al. [78] found that the smallest radius nanotube is only 3Å in diameter (Fig.2-5). They associated this nanotube with the (2;2) armchair structure because of its geometry. The present calculations do not support this interpretation. Indeed, it has been argued that ultra-small radius nanotubes [106-109,175] cannot exist a standard NTs with diameters < 3.6Å (for the (4;1) structure).

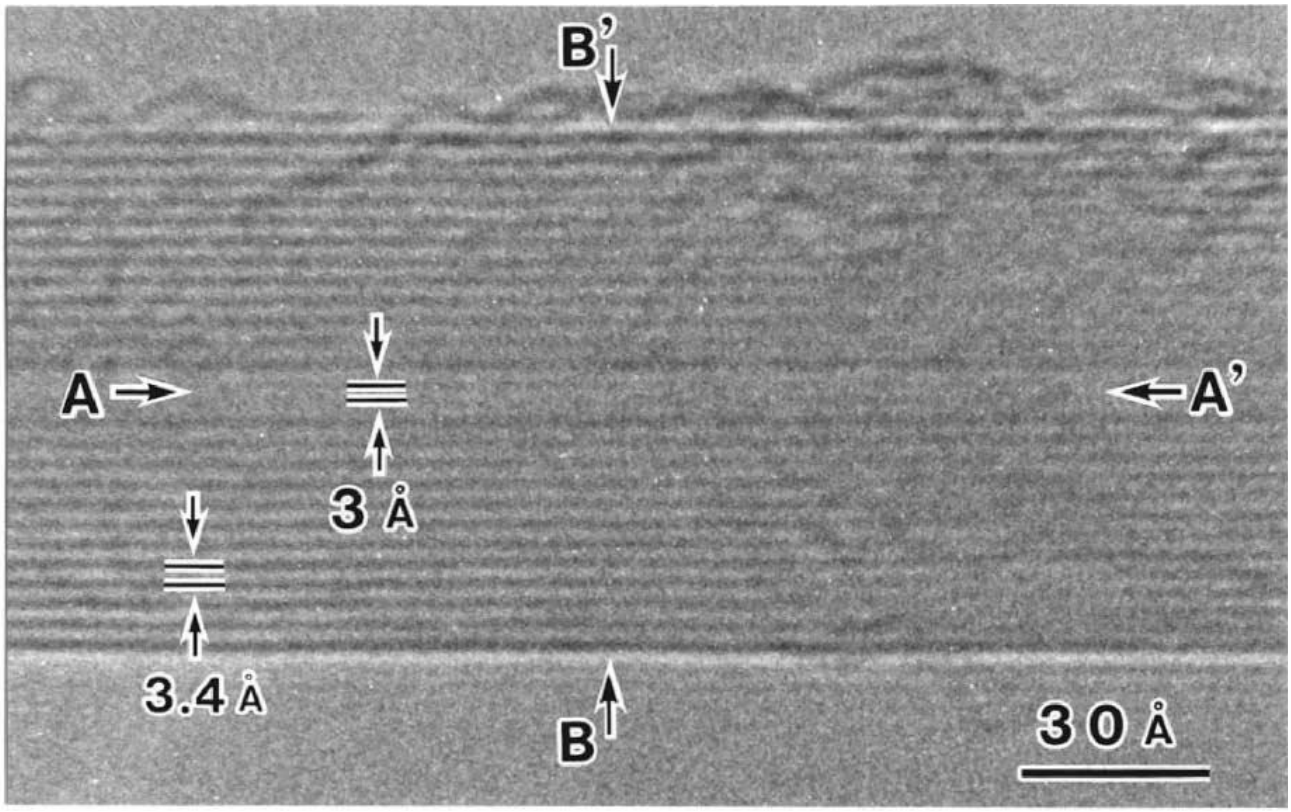

Fig.2-5. Transmission electron microscopy (TEM) image of 3 Å CNT formed inside MWNT. The diameter of 3 Å SWNT and the interlayer space of MWNT, 3.4 Å, are indicated by a pair of lines marked by arrows. Each end is marked by two horizontal arrows, *A* and *A'*.
Photo is taken from [78]

Nanotubes with a smaller diameter do not have smooth edges, but some sort of zigzag boundary line. Thus, on the HRTEM photo shown above, the edge of a (2;2) nanotube would appear as a zigzag, or dashed line. Fig.2-5 shows that the inner nanotube has a weak, but well-defined straight line. The (2;2) structure is not in fact a nanotube because it consists of two elementary graphite ribbons parallel to each other. The modelling of a (2;2) nanotube with precise DFT methods (Gaussian-09 software in atomic basis B3LYP/6-311(p,d)) shows the structures proposed by Zhao et al. are unstable. On the other hand, a structure based on $(C_6)_n$ stacks provides a good fit to this 3Å nanotube, as $(C_6)_n$ structures have an inner diameter of 2.72Å, and an outer diameter of 3.14Å with an average diameter of 2.9Å. The straight edge of such molecules agrees with the geometry observed in experiment. This suggests that the structure shown in Fig 2-5 is the first experimental evidence of the existence of $(C_6)_n$ stacks.

2-5. Conclusions

The first principles have been used to investigate the structure and electronic properties of carbon nanotubes formed by stacking individual C_6 rings. It is found that these structures are quite stable with inter-ring bond energies exceeding 5.3 eV in larger stacks. Most of the electron orbitals near the Fermi level are delocalized over the entire molecular structure. In longer stacks a higher proportion of C_6 rings participate in orbital hybridization resulting in increased delocalization of the electron near the Fermi level. Tubular $(C_6)_n$ structures based on multilayer stacked cyclic C_6 are expected to exhibit a range of unique physical and electronic properties combined with high stability. With inter-ring bond energies in $(C_6)_n$ of 5.5-8.5 eV these structures should have high electron mobility.

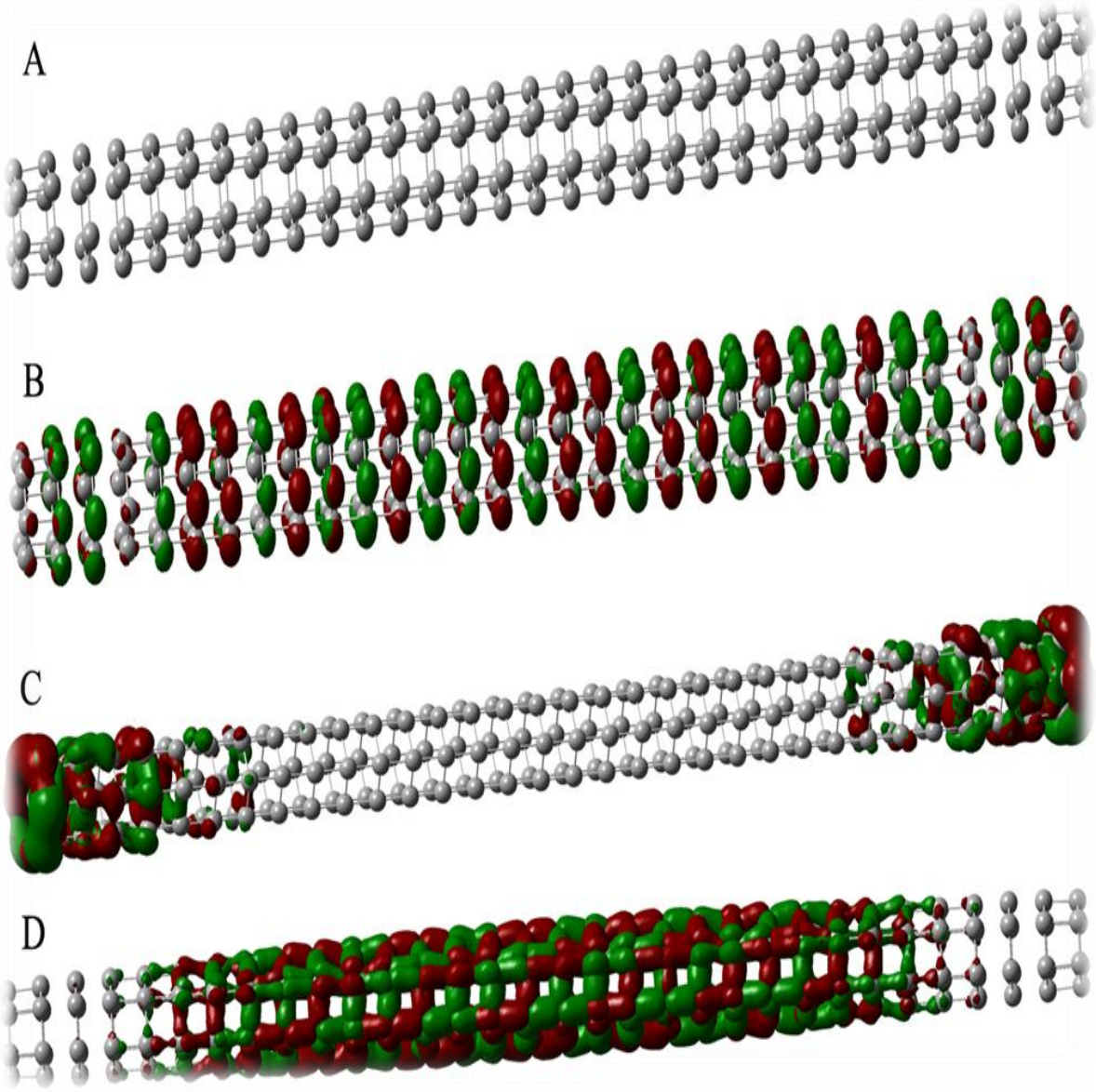

Fig.2-6. Structure and electron density in the HOMO orbitals in $(C_6)_{32}$.
A) Overall optimized geometry. B) LUMO orbital C) HOMO orbital
D) HOMO-1 orbitals

The resulting tubular molecules consist of groups of $(C_6)_2$ and $(C_6)_3$ separated by individual C_6 rings in an aperiodic structure, although the aperiodicity became smaller in larger molecules. For example, Fig.2-6 shows the structure of a stack of cyclic C_6 with 32 layers together with the shape of the HOMO and LUMO orbitals. In this case an aperiodic structure persists only at the ends of the stack while the interlayer distance in the center of the structure is quite constant.

It is suggested that the high periodicity of the structure in longer molecules is caused by strong electron hybridization near the Fermi level. Thus, longer molecules are even more stable than short ones. The HOMO–LUMO energy gap, the overall symmetry of the molecule and the separation between rings approach limiting values as length increases, suggesting that long multi-layer $(C_6)_n$ tubes are possible. The high extent of electron delocalization near the Fermi level could be a strong prerequisite to conductive or semi-conductive properties.

Evidence of the existence of tubular carbon structures based on stacks of cyclic C_6 can be clearly seen in the report of Zhao et al. [78], indicating that $(C_6)_n$ structures may be found inside of MWNTs. One asks, however, if these structures can exist only inside MWNTs, or can they be produced in stable form as free-standing structures?

CHAPTER 3

MULTILAYER CYCLIC C_6 STRUCTURES INTERCALATED WITH METAL ATOMS

The difference in electronic properties of benzene and cyclic C_6 ring was considered in previous Chapter. The molecular geometries of benzene and cyclic C_6 ring are very similar. Though, the cyclic C_6 ring does not have aromatic orbitals for which benzene is famous for.

The same way could be compared the geometry and properties of sandwich complexes benzene-metal and (cyclic C_6)-metal. Although both of these structures have similar geometry, they are markedly different in electron structure. The difference between orbital distributions in benzene and in cyclic C_6 makes it possible for cyclic C_6 to form metal-sandwich compounds that would be unstable in systems based on benzene [4].

Metal-benzene compounds have been the subject of much interest since the discovery of V-benzene polymers [83]. Many theoretical [84-88,90-95] and experimental [96-99] studies of their unique electronic and magnetic properties have been reported. For example, metal-benzene polymers are expected to be good conductors for spin transport [85,88,89] and as components in novel nanoscale devices. It has been suggested that multilayered sandwich molecules based on benzene combined with Ti, Cr, Sc, Fe, Ni, Nb, Ta, and Mn are possible [84,87,89,90,93,94,99] but, to date, such structures have been found only in V-benzene systems. All these described molecules were insulators with energy gaps exceeding 3 eV. It could be expected that exploiting of dehydrogenated benzene (another words cyclic C_6 rings) instead of benzene in such multilayered sandwich metalorganic structures should essentially improve electronic properties.

We proposed a new structure based on layers of cyclic C_6 intercalated with metal atoms [7] that could be designated by structural formula $(C_6)_nM_{n-1}$ (where M – metal atom) . *Ab initio*

calculations showed a possibility of existence of polymeric inorganic metal-carbon molecules in which C_6 is combined with different metals.

All calculations of the geometry, as well as electronic and vibrational properties of these compounds were carried out with GAUSSIAN-03/09 [133] using the most precise DFT (density functional theory) methods consistent with computational efficiency. For molecules incorporating Li, K, Ca, Fe, Mn, and V calculations were carried out on a B3LYP/6-311G∗ and B3LYP/6-31G∗ basis. For molecules incorporating heavier metals a Beckethree-parameter Perdew-Wang-1971 functional combined with Los Alamos National Laboratory 2-double-zeta (B3PW91/LANL2DZ) basis was used.

3.1. Geometry and stability of the chemical bonds in metalorganic structures $(C_6)_nM_{n-1}$.

According to recent reports [96-99], in the first four periods of the periodic table, only V can form long stable sandwich molecules with benzene. On the basis of the present study, it was found that many more atoms can form sandwich molecules based on cyclic C_6. In particular, Li, K, Ca, Na, Fe, V, Mg, and Mn all combine in this way with cyclic C_6.

We calculated from first principles of DFT optimized geometry, chemical bonding energy, electron density and shape of electron orbitals. The conclusions about stability of metalorganic molecules $(C_6)_nM_{n-1}$ with different metals were made from study of different factors. The most important parameters of stability are bonding energy between cyclic C_6 ring and metal atom and average bonding energy per atom. Another factor is existence of sandwich molecules $(C_6)_nM_{n-1}$ with different length (with different number of layers n). Also is very important for estimation of the structural and chemical stability molecular symmetry and existence of structural distortions.

The most promising structures involve C_6 in combination with group VIII transition metals in the periodic table, specifically Fe, Ru, and Os, and some adjacent elements, including V, Mn, Tc, Re, and Ir. Other partners include the alkali metals (Li, Na, K, Rb) as well as some alkaline earth metals (Mg, Ca,Ba). Be and Hg can also form similar molecules with help of van der Waals forces. The most energetically stable molecules were found those involving Fe and Ru. In general, it was found a correlation between increasing stability in MC_6 molecules, where M denotes metal, and the atomic weight of the metal. Stability was also increased with the overall length of the molecule.

The highest-stability compounds are those incorporating Fe and Ru in a $(C_6)_nM_{n-1}$ structure. Sandwich molecules $(C_6)_nMn_{n-1}$ appear to have some chemical instability that is indicated by structural distortions in these compounds (see Fig.3-2). $(C_6)_nV_{n-1}$ molecules are found to be stable only when n≥4, and (C6)nMgn−1 is stable only with n = 4 as (C6)5Mg4 and (C6)3Mg2 are both unstable. For groups 1 and 2 atoms, Table 3-1 shows that the Li(C6) bond energy is much smaller than the M(C6) bond energy in other molecules, so these molecules have marginal stability. In addition, it was found that molecules incorporating Ca, K, and Na are asymmetric, indicating that they may tend to be unstable. Among elements in the fifth and sixth periods, only Rb, Ba, Tc, and Ru compounds are found to form stable molecules $(C_6)_nM_{n-1}$. Some other elements, notably Cs, Re, Os, and Ir, form stable molecules, but often their structures are distorted or the order of symmetry is lowered. The common types of distortion are absence of the stable symmetry of individual cyclic C_6 rings and their relative disorientation (Fig.3-2). In the most symmetric molecules, where the overall symmetry is *D*6*h*, the intrinsic symmetry of cyclic C_6 is *C*6 and all rings have the same orientation relative to the principle molecular axis (Fig.3-1).

Structure	Calculation method	Molecular symmetry	Average bond length between two cyclic C_6, Å	Average length of the bond in cyclic C_6 in the central ring, Å	Average metal-C_6bond energy (eV)	Average charge on metal atom	Presence of structural distortion
$(C_6)_3Fe_2$	b3lyp/6-311g*	D3h	3.15	1.4	10.29	0.833	
$(C_6)_3K_2$	b3lyp/6-311g*	C3	5.783	1.36	3.73	0.801	
$(C_6)_3Li_2$	b3lyp/6-311g*	C6	4.034	1.37	0.22	0.196	
$(C_6)_3Ca_2$	b3lyp/6-311g*	C3	4.834	1.40	12.05	1.274	
$(C_6)_3Na_2$	b3lyp/6-311g*	D3h	4.96	1.36	2.97	0.662	
$(C_6)_3Ba_2$	b3pw91/lanl2dz	C3	5.77	1.41	9.90	1.807	
$(C_6)_3Cs_2$	b3pw91/lanl2dz	C3	6.92	1.37	3.58	0.924	
$(C_6)_3Ir_2$	b3pw91/lanl2dz	D6h	3.56	1.47	8.69	1.148	
$(C_6)_3Mn_2$	b3lyp/6-311g*	C2h	3.32	1.40	8.66	0.869	√
$(C_6)_3Os_2$	b3pw91/lanl2dz	D6h	3.57	1.47	4.47	0.939	
$(C_6)_3Rb_2$	b3pw91/lanl2dz	D3h	6.53	1.37	3.68	0.911	
$(C_6)_3Re_2$	b3pw91/lanl2dz	near D2	3.6	1.46	10.84	0.523	√
$(C_6)_3Ru_2$	b3pw91/lanl2dz	D6h	3.59	1.45	17.93	0.615	
$(C_6)_3Tc_2$	b3pw91/lanl2dz	near D6h	3.6	1.46	5.57	0.625	√
$(C_6)_4Fe_3$	b3lyp/6-311g*	D3h	3.19	1.41	11.63	0.836	
$(C_6)_4K_3$	b3lyp/6-31g*	C3	5.76	1.36	2.33	0.644	√
$(C_6)_4Li_3$	b3lyp/6-311g*	D3h	4.12	1.36	2.94	0.229	√
$(C_6)_4Ba_3$	b3pw91/lanl2dz	C3	5.92	1.41	9.73	1.898	
$(C_6)_4Cs_3$	b3pw91/lanl2dz	C3	6.92	1.37	1.94	0.933	
$(C_6)_4Ir_3$	b3pw91/lanl2dz	near D6h	3.77	1.41	2.96	1.132	√
$(C_6)_4V_3$	b3lyp/6-311g*	near D3d	3.67	1.4	5.39	0.976	
$(C_6)_4Mn_3$	b3lyp/6-311g*	C2v	3.09	1.39	2.38	0.872	√
$(C_6)_4Mg_3$	b3lyp/6-31g*	≈D3d	3.97	1.4	1.8	0.104	
$(C_6)_4Rb_3$	b3pw91/lanl2dz	near D3h	6.46	1.37	2.19	0.927	
$(C_6)_4Ru_3$	b3pw91/lanl2dz	D6h	3.57	1.46	3.78	0.892	
$(C_6)_4Tc_3$	b3pw91/lanl2dz	D6h	3.54	1.46	5.45	0.916	
$(C_6)_3Fe_2$	b3lyp/6-311g*	D3h	3.15	1.4	10.29	0.833	

Table 3-1. Geometry and bond parameters in metal-organic molecules $(C_6)_nM_{n-1}$ with n = 3,4

only when $n \geq 4$, and $(C_6)_nMg_{n-1}$ is stable only with n = 4 as $(C_6)_5Mg_4$ and $(C_6)_3Mg_2$ are both unstable. For groups 1 and 2 atoms, Table 3-1 shows that the $Li(C_6)$ bond energy is much smaller than the $M(C_6)$ bond energy in other molecules, so these molecules have marginal stability. In addition, it was found that molecules incorporating Ca, K, and Na are asymmetric, indicating that they may tend to be unstable. Among elements in the fifth and sixth periods, only Rb, Ba, Tc, and Ru compounds are found to form stable molecules $(C_6)_nM_{n-1}$. Some other elements, notably Cs, Re, Os, and Ir, form stable molecules, but often their structures are distorted or the order of symmetry is lowered. The common types of distortion are absence of the stable symmetry of individual cyclic C_6 rings and their relative disorientation (Fig.3-2). In the most symmetric molecules, where the overall symmetry is *D*6*h*, the intrinsic symmetry of cyclic C_6 is *C*6 and all rings have the same orientation relative to the principle molecular axis (Fig.3-1).

All long molecules incorporating Fe and Ru are examples of this type. If the orientation of cyclic C_6 with symmetry C6 is not regular, for example, as in $(C_6)_3Li_2$, then we find that the overall symmetry becomes C3.

Another configuration occurs when two or more cyclic C6 have C3 symmetry and all cyclic rings are oriented in the same way, then the molecule has D3h symmetry. This structure occurs in $(C6)_3Fe_2$. This reduces to C3 symmetry when all the cyclic rings have different orientations. Some examples of structures that are subject to different distortions induced by constraints on bonding are shown in Fig. 3-2. From discussion in previous Chapter it could be concluded that D3h molecular symmetry caused by weak hybridization of the electrons in the structure, while D6h symmetry prove strong electron delocalization. Also chemical bonding in structures with D6h symmetry should be stronger.

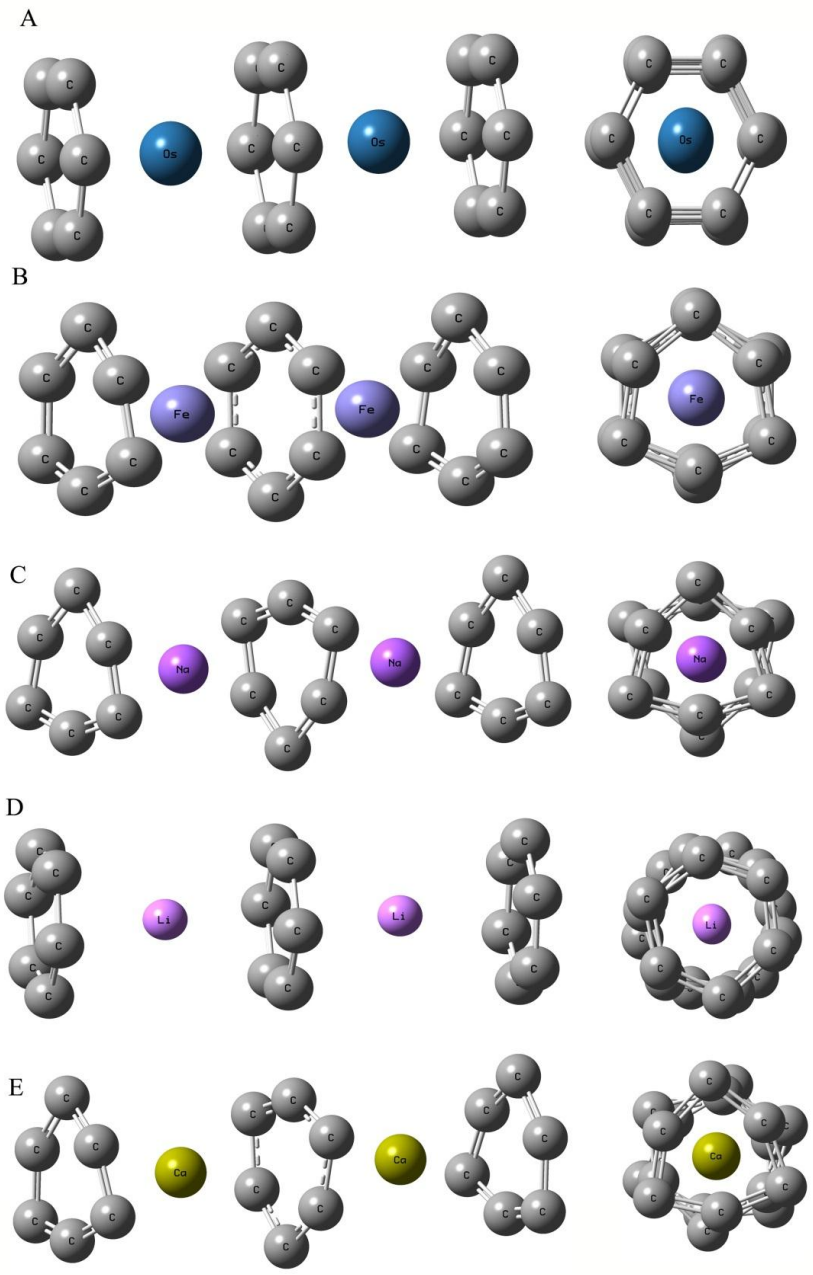

Fig. 3-1. Examples of the different symmetries in sandwich molecules *M*-(cyclic C_6) for molecules $(C_6)_3M_2$: (a) *D*6*h* symmetry in $(C_6)_3Os_2$ (b) *D*3*h* symmetry in $(C_6)_3Fe_2$ (central ring with C_6 symmetry) (c)*D*3*h* symmetry in $(C_6)_3Na_2$ (central ring with *C*3 symmetry) (d) *C*6 symmetry in $(C_6)_3Li_2$ (all rings with *C*6 symmetry) and (e) *C*3 symmetry in $(C_6)_3Ca_2$ (all rings with *C*3 symmetry). Carbon atoms have grey color, metal atoms are blue, pink, violet and yellow.

Structure	Calculation method	Molecular symmetry	Average bond length between two cyclic C_6, Å	Average bond length in cyclic C_6 in the central ring, Å	Average metal-C_6 bond energy (eV)	Average charge on metal atom	Presence of structural distortion
$(C_6)_5Fe_4$	b3lyp/6-311g*	D6h	3.18	1.41	12.5	0.832	
$(C_6)_5Li_4$	b3lyp/6-311g*	C3	4.06	1.36	2.77	0.581	√
$(C_6)_5Ca_4$	b3lyp/6-31g*	C3	4.84	1.4	10.79	0.982	√
$(C_6)_5Ba_4$	b3pw91/lanl2dz	C3	5.76	1.41	9.56	1.889	
$(C_6)_5Cs_4$	b3pw91/lanl2dz	C3	6.91	1.37	2.51	0.932	√
$(C_6)_5Rb_4$	b3pw91/lanl2dz	near D3h	6.45	1.37	3.83	0.927	
$(C_6)_5Ru_4$	b3pw91/lanl2dz	D6h	3.56	1.46	12.46	0.949	
$(C_6)_5Tc_4$	b3pw91/lanl2dz	D6h	3.54	1.46	12.89	0.927	
$(C_6)_6Fe_5$	b3lyp/6-311g*	D6h	3.17	1.41	16.05	0.835	
$(C_6)_6Os_5$	b3pw91/lanl2dz	D6h	3.54	1.47	29.14	0.982	√
$(C_6)_6Re_5$	b3pw91/lanl2dz	D6h	3.57	1.48	4.38	1	√
$(C_6)_7Fe_6$	b3lyp/6-311g*	D6h	3.16	1.39	14.72	0.836	
$(C_6)_7Mn_6$	b3lyp/6-31g*	C3	3.31	1.41	4.67	0.567	√
$(C_6)_7Ru_6$	b3pw91/lanl2dz	D6h	3.55	1.44	6.18	1.008	
$(C_6)_8Fe_7$	b3lyp/6-311g*	D3h	3.16	1.41	9	0.834	

Table 3-2. Geometry and bond parameters for metal-organic molecules $(C_6)_nM_{n-1}$ with $n >$ 4

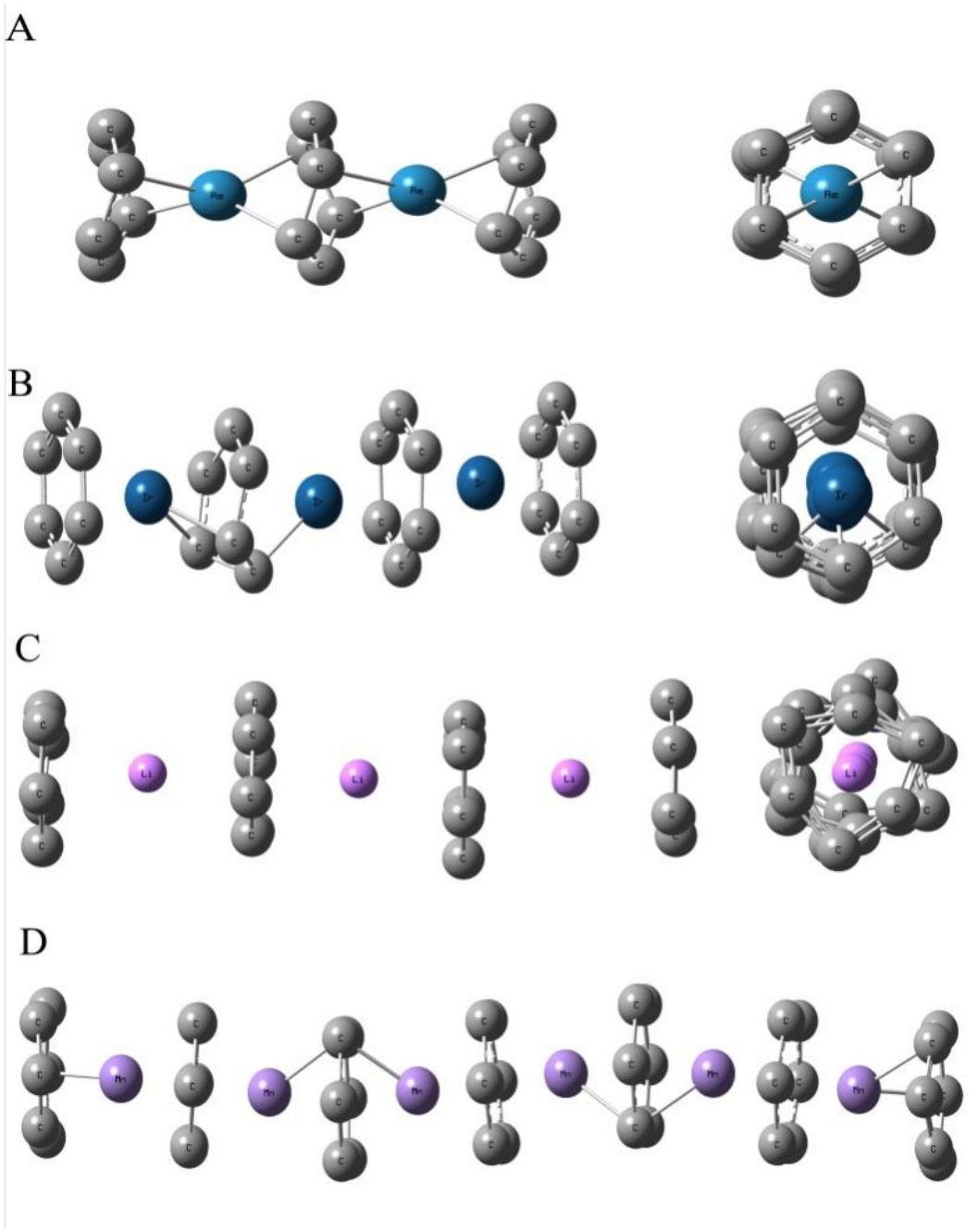

Fig. 3-2. Structural distortion in sandwich molecules *M*-(cyclic C_6): (a) $(C_6)_3Re_2$, (b) $(C_6)_4Ir_3$, (c)$(C_6)_4Li_3$, and (d) $(C_6)_7Mn_6$. Carbon atom have gray color, metal atoms are blue, pink and violet.

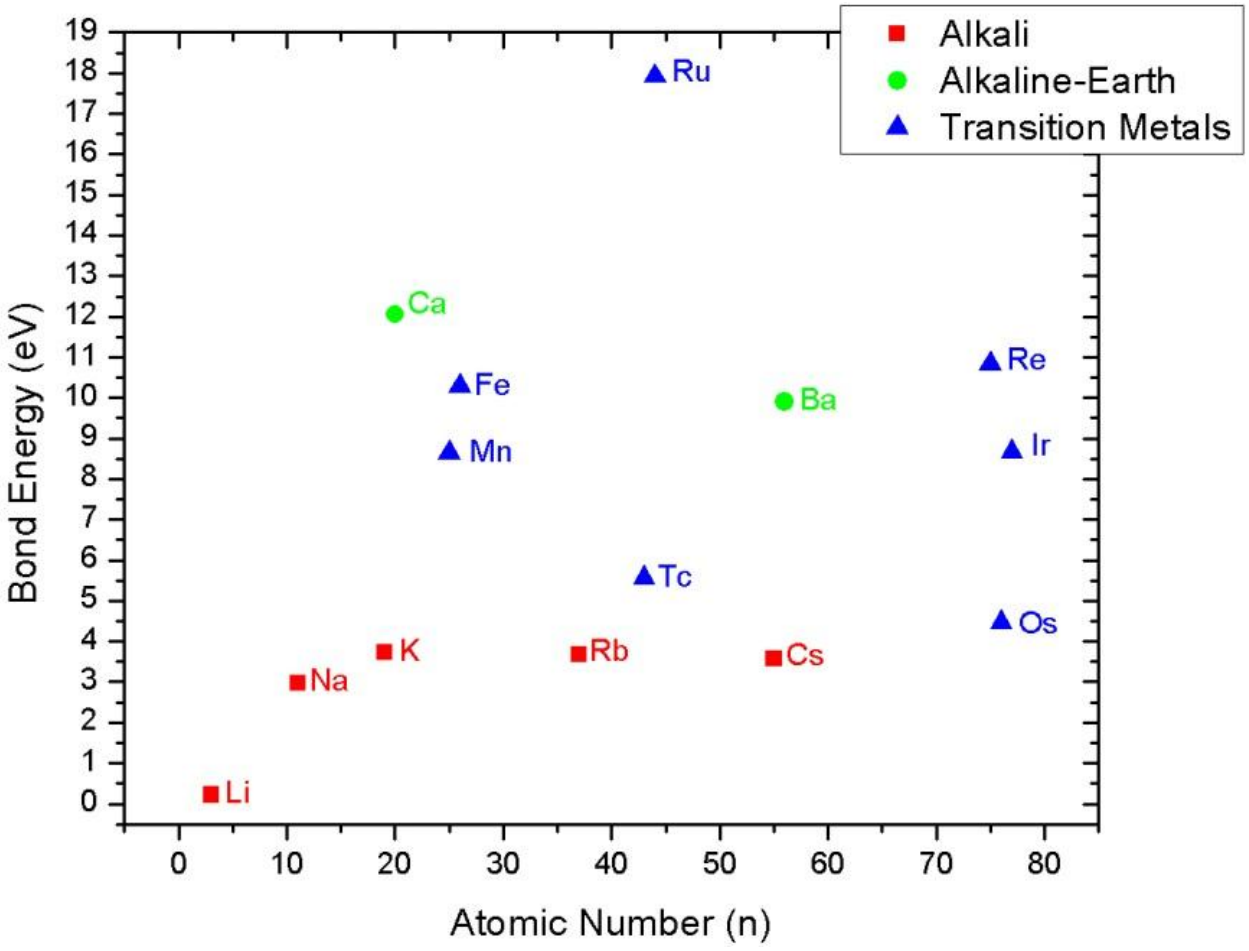

Fig. 3-3. Average bond energy between the metal atom and cyclic C_6 in $(C_6)_3M_2$

Tables 3-1 and 3-2 summarize the symmetries and bond energies for different MC_6 sandwich molecules. It could be seen that molecules incorporating alkali metals are less strongly bonded than those involving transition metals. The average Mulliken charge on the metal atom in this case, with the exception of Li, is ≈0.8–0.9 of an electron. As the rings in these molecules have C3 symmetry, it is apparent that aromatic bonding is less important in these molecules and that the MC6 bond is primarily ionic. A summary of MC_6 bond energies in $(C_6)_3M_2$ is shown in Fig.3-3. It should be noted that the alkaline-earth metals form strong bonds but show some structural instability. This can be attributed to the tendency for a strong interaction to develop between the metal atom and a single carbon atom in the ring which causes a direct bond to form between them. In general, it was found that average bond energy is well correlated with the overall length of the molecule (Fig.3-4) which shows calculated solutions for Rb and Fe compounds. It can be seen that the average bond energy does not change much in larger molecules, particularly for Rb compounds.

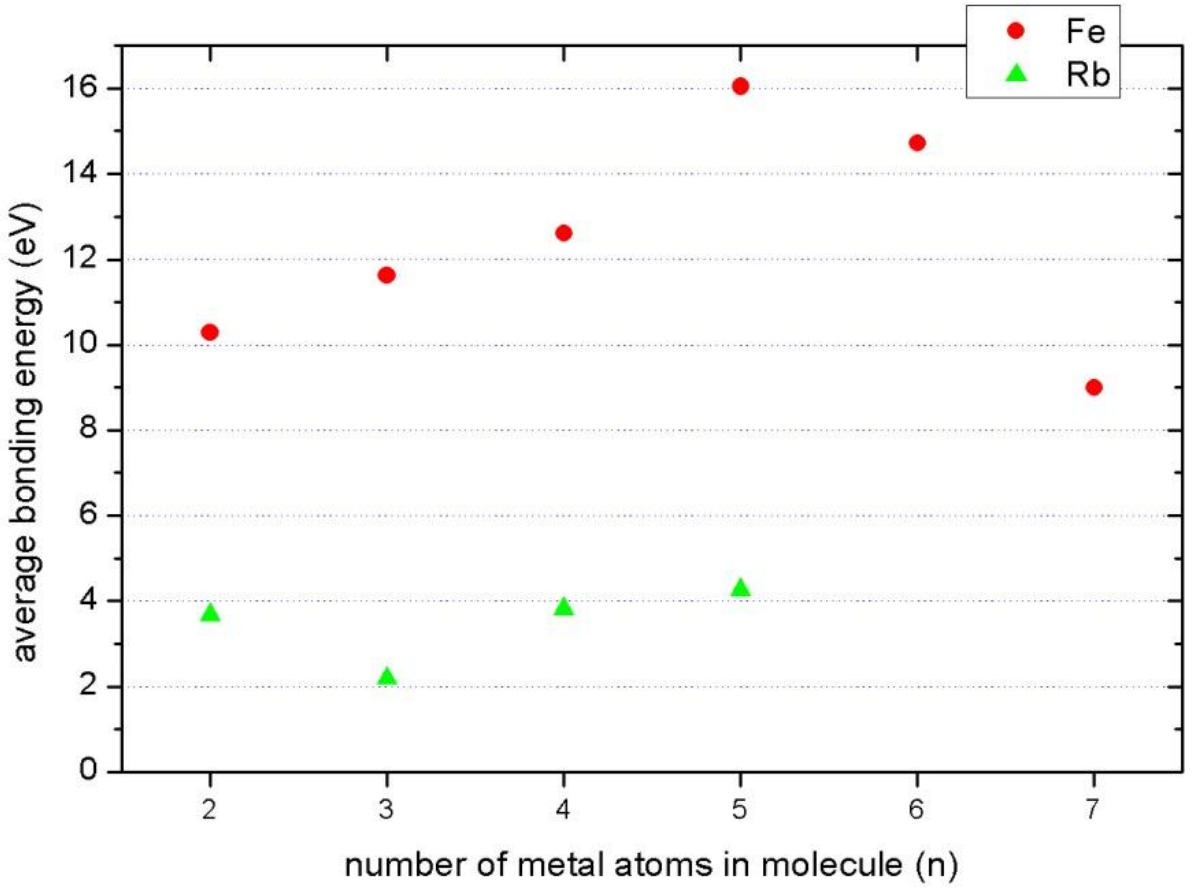

Fig. 3-4. Dependence of the bond energy between the metal atom and cyclic C_6 in $(C_6)_nFe_{n-1}$ and $(C_6)_nRb_{n-1}$ vs. molecule length.

3.2. Electronic properties of metalorganic structures $(C_6)_nM_{n-1}$.

The HOMO-LUMO (lowest unoccupied molecular orbital) energy gap for most molecules is typically <1 eV, indicating that most of these molecules could be intrinsic conductors. The LUMO-HOMO gap vs. molecule length for $(C_6)_nFe_{n-1}$ and $(C_6)_nRu_{n-1}$ with $n \leq 8$ are plotted in Fig. 3-5 and both showed the tendency for this energy

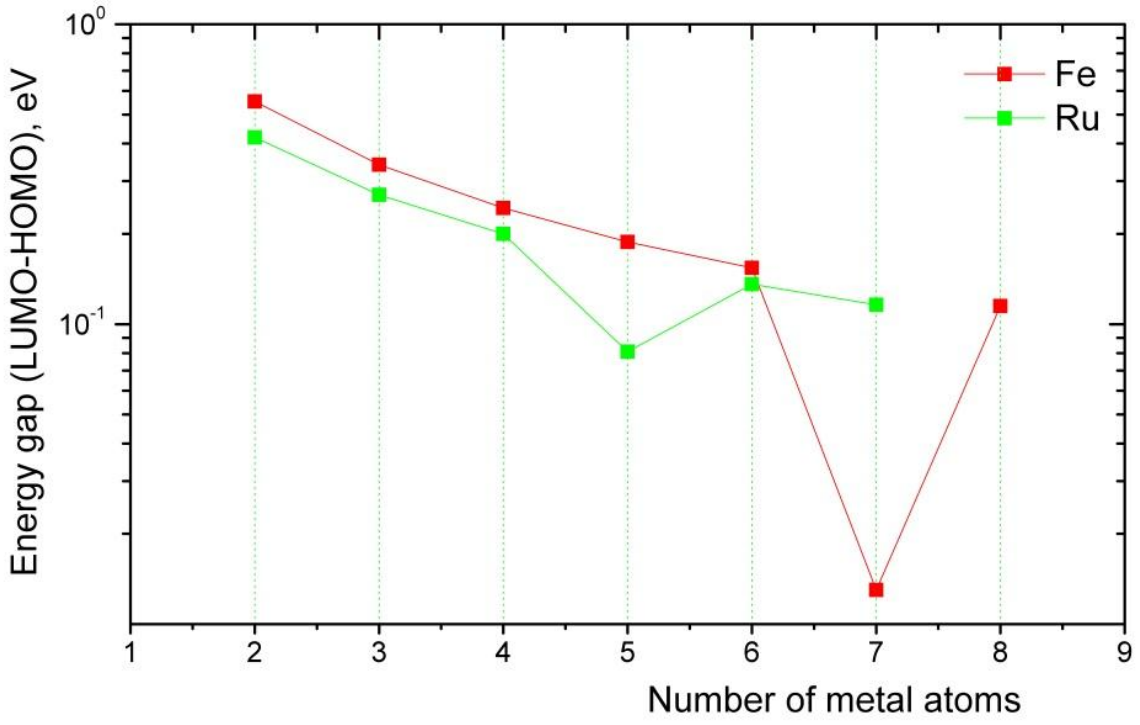

Fig. 3-5.Dependence of the LUMO-HOMO energy gap vs. the number of metal atoms in $(C_6)_nFe_{n-1}$ and $(C_6)_nRu_{n-1}$. The energy gap approaches 0.1 eV in molecules with n >8

to approach 0.25 eV when n exceeds 5. It was also found that most of the orbitals near the Fermi level are delocalized, indicating that long molecules with (C6)nMn-1 composition may exhibit metallic conductivity.

It was shown the bonding and orbital structure in $(C_6)_5Fe_4$ and $(C_6)_5Rb_4$ in Figs. 3-6 and 3-7, respectively. In $(C_6)_5Fe_4$, intercalated by the typical representative of the transition metal, it is an evident that the HOMO and LUMO orbitals correspond to two components of the same doubly degenerate energy level. This is very common feature of electronic structure of metal atoms and clusters. As electrons in these orbitals are highly delocalized, this provides further evidence that the bonding between metal ion and cyclic C_6 ring in molecule $(C_6)_5Fe_4$ has mainly covalent nature, which leads to conductive molecular properties. Additionally, in $(C_6)_5Rb_4$, intercalated by typical representative of the alkali metal, (Fig.3-7) the HOMO and LUMO orbitals and their neighboring orbitals are localized near certain carbon rings. This is a direct consequence of the presence of ionic bonding between individual metal atoms and carbon rings. As a result, although the energy gap in this molecule is very small (≈0.24 eV) and the difference in energy with neighbor energy level is approximately the same, conductivity is possible only by “hopping” of the electrons from one orbital to another. Additional calculations are required to evaluate the role of conduction in this molecule.

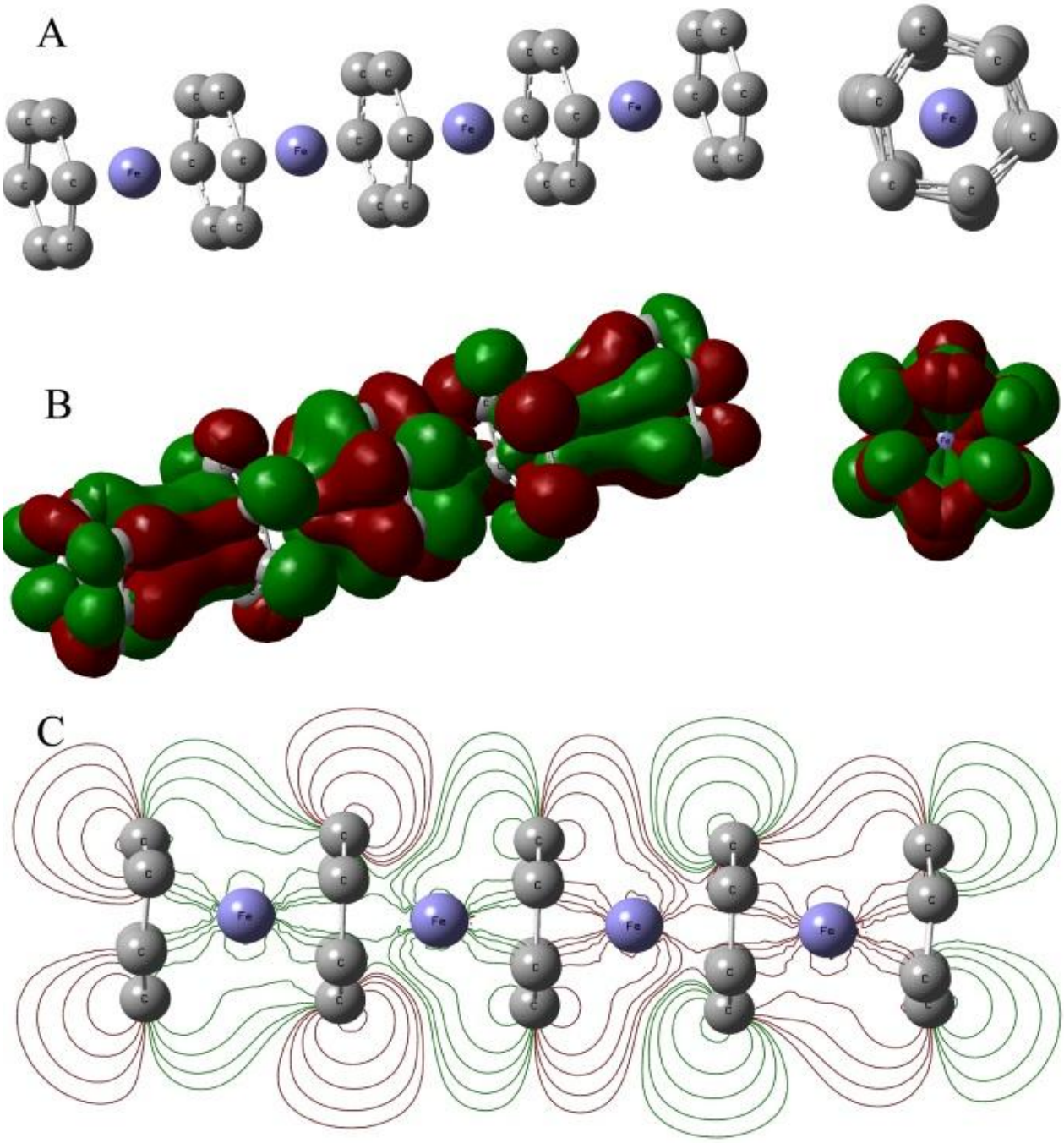

Fig. 3-6.Structure of $(C_6)_5Fe_4$ and its degenerate combined HOMO-LUMO orbital (AO 142-143). (a) Structure, (b) combined HOMO-LUMO orbital (AO 142-143), red and green color corresponds to positive and negative sign of the real part of wavefunction
(c) electron density distribution in the combined HOMO-LUMO orbital.

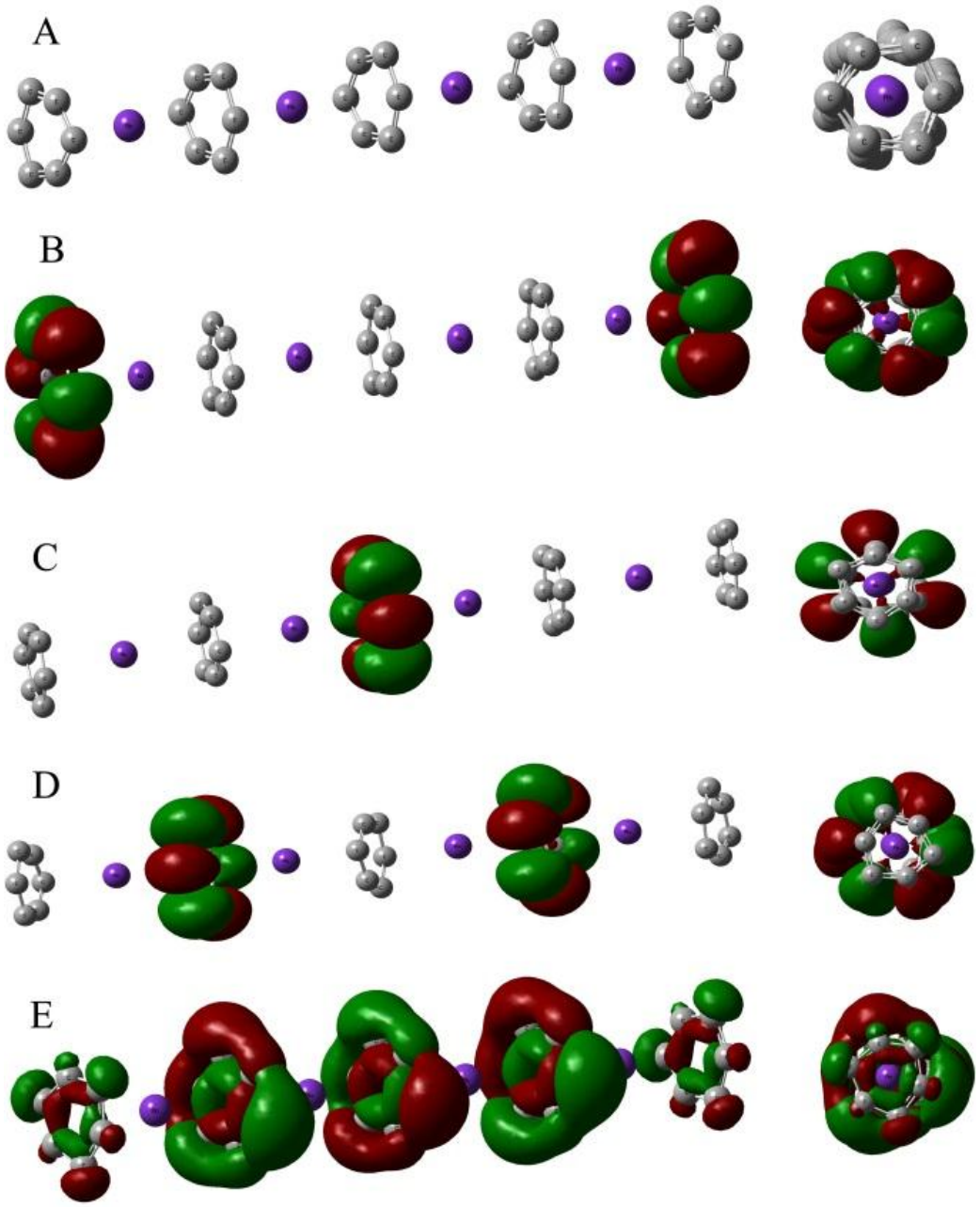

Fig. 3-7. Structure and some of the atomic orbitals in $(C_6)_5Rb_4$:
(a) structure, (b) combined degenerate orbital (AO166-167), (c) LUMO (AO165), (d) combined degenerate HOMO (AO163-164), and (e) combined degenerate orbital (AO160-162).

3.3. Magnetic properties of metalorganic structures $(C_6)_nM_{n-1}$.

The magnetic properties of one-dimensional metal-organic sandwich wires analogous to $(C_6)_nM_{n-1}$ stacks have been subject of many studies. Particular attention has been paid to magnetism in highly stable V-benzene sandwiches [84-87,90,91,95] and in poly-ferrocene sandwich clusters [92,95]. Theoretical calculations have been supported by experimental studies [150,151] and demonstrate that metal-organic molecules containing the transition metals V, Fe, Ti, and Sc are all ferromagnetic. In all cases, the total molecular magnetic moment is determined by the sum of the atomic magnetic moments, orbital magnetic moments, and the spin-orbit interaction.

In 3*d* transition metal-organic sandwich molecules the atomic magnetic moment is determined by the number of uncoupled electrons in the 3*d* orbital shell [95]. For example, in M_nBz_{n+1}, where M denotes transition metal and Bz benzene, the number of uncoupled 3d electrons for V, Ti, and Sc is n = 1, 2, and 1, respectively, and the maximum magnetization in these atoms μ_Z= 1, 2, and 1 respectively (in Bohr magneton units). The calculated total magnetic moment of the unit cell of the polymer molecule with V, Ti, and Sc atoms is, however, 0.88, 1.0, 0.5 μ_B, respectively [90,95]. The reduction of the total magnetic moment is attributable to the spin-orbit interaction [85]. As a result of this term, each benzene ring acquires a small negative magnetic moment along the molecular axis. This is typically ≈0.15 μ_B [86]. Another mechanism for reduction of the molecular magnetic moment involves intra-spin-relaxation (ISR) effects [151]. For molecules like V_2Bz_3, V_3Bz_4, and V_5Bz_6 experiments [150,151] show that the magnetic moments per unit cell are 0.75, 0.77, and 0.72, respectively. A comparative analysis of the magnetic properties of magnetization in 3*d* and some 4*d* transition-metal M_nBz_{n+1}compounds and in polyferrocene molecules has been published by Shen *et al.* [95]. In $Fe_n(C_5H_5)_n$ the ground state corresponds to

magnetic moment μ_B per Fe atom and the total magnetic moment of these molecules is found to be proportional to the number of metal atoms.

These results can be used to predict some magnetic properties of $(C_6)_nM_{n-1}$ sandwich molecules based on multiple layers of cyclic C_6 and are closest in composition to polyferrocene structures. Of most interest is magnetization in compounds such as $(C_6)_nFe_{n-1}$ which represent the most stable stacked C_6 clusters. From Tables 3-1 and 3-2 it is apparent that the Mulliken electric charge of the transition metals atoms in these molecules is nearly unity. This implies that one valence electron of the metal atom participates the chemical bond between metal and cyclic C_6. This is similar to the situation in long polyferrocene molecules where C_5H_5 accepts an electron from the Fe atom. The magnetic moment of the ion Fe+ is nearly μ_B so $(C_6)_nFe_{n-1}$ has a total magnetic moment of $\approx 1\ \mu_B$ per molecular unit cell. In general, the magnetic moment of $(C_6)_nM_{n-1}$ is determined both by the moment of the metal and that resulting from the electron transferred to the cyclic C_6 ring. By inference from the properties of M_nBz_{n+1}, the magnetic moment arising from each cyclic C_6 ring is then expected to be $(0.1–0.3)\mu_B$. It is then expected that the Fe spins in $(C_6)_nFe_{n-1}$ will be aligned ferromagnetically while those in cyclic C_6 will have an antiferromagnetic configuration.

The calculations have been made of the overall molecular energy in $(C_6)_nFe_{n-1}$ for different spin states. It was shown that structures containing iron have ground states corresponding to the ferromagnetic configuration. For example, the ground state in $(C_6)_8Fe_7$ is 13-et corresponding to parallel spins of all iron atoms and a magnetic moment of one Bohr per atom, reduced due to spin-orbit interaction by ~ 16 % [104]. The energy difference between the ideal ferromagnetic and paramagnetic states is ~ 90 meV per electron-electron spin interaction pair. This value is much smaller than the bonding energy between cyclic C_6 and an iron atom.

3.4. Conclusions

The first-principles have been used to investigate the structure and electronic properties of metal-carbon sandwich molecules formed by cyclic C6 rings with intercalated metal atoms. It was found that these structures are quite stable with metal ring bond energies exceeding 11.6 eV in larger molecules. The types of metal atoms that can be incorporated in these molecules form two groups. One of these involves the alkali metals and some of the alkaline earth metals, while the other consists of several transition metals. A unique property of a number of these MC_6 sandwich molecules is that the units repeat on a periodic basis. The most stable compounds are indicated to be $(C_6)_5Fe_4$ and $(C_6)_5Ru_4$. It was found that the MC_6 ring bond energy in $(C_6)_nFe_{n-1}$ and $(C_6)_nRu_{n-1}$ increases with the length of these molecules up to a limiting value suggesting that it may be possible to form long polymer molecules from these compounds. In general, this type of structure constitutes a molecular analog of intercalated graphite, and may possess interesting properties as molecular conductors and superconductors.

CHAPTER 4

ELECTRONIC AND VIBRATIONAL PROPERTIES OF FINIT MOLECULES BASED ON MULTI-LAYER STACKS OF CYCLIC C_6 AND INTERCALATED STACKS OF CYCLIC C_6

The geometry and stability of molecular structures based on first principles calculations for stacks of cyclic C_6 and intercalated stacks of cyclic C_6 have been discussed in Chapters 2 and 3. This Chapter outlines some vibrational and electronic properties of these compounds. As noted previously, structures formed from stacks of cyclic C_6 molecules [4,6] represent carbon nanotubes with the smallest possible diameter. Their topology is, however, differ from that of regular nanotubes. The mechanism of chemical bonding is also different in these two types of nanotube. Chemical bonding in conventional NTs mainly involves sp^2 hybridization and pi-sigma hybridization is important only in nanotubes having diameters < 1 nm [191]. Interlayer bonding is due to hybridization of electron orbitals in structures based on stacks of cyclic C_6 and leads to the delocalization of valence electrons [103,104].

It is known that molecular vibrations are very sensitive to the strength and stability of chemical bonds. Thus a reduction in the energy of characteristic vibrational modes can indicate weak or unstable chemical bonds. It is interesting, then, to compare calculated vibrational energies in molecules based on stacks of cyclic C_6 with those characteristic of other structures. In particular, it is interesting to see how much lower the energy of vibrational modes in these tubular structures is in comparison with those in single-wall carbon nanotubes (SWNTs). The band gap energy in these compounds has also been calculated and is found to depend on the overall length of the molecule.

All calculations of the vibrational properties of these compounds of the finite size molecules were carried out with GAUSSIAN-03/09 [133] using the most precise DFT methods consistent

with computational efficiency. For molecules incorporating Fe, calculations were carried out on a B3LYP/6-311G* (Becke, three-parameter, Lee-Yang-Parr) [132,152,153] and B3LYP/6-31G* basis. For molecules incorporating heavier metals (in this case Ru) a B3PW91/LANL2DZ (Becke, three-parameter, Perdew, Wang)/(Los Alamos National Laboratory 2 double Zeta) basis was used. All molecules were modeled using a restricted closed shell wave function based on the assumption that the ground state is a singlet.

4.1. Vibrational properties of $(C_6)_n$ molecular stacks

Simulated Raman and IR spectra for tubular $(C_6)_n$ molecules having up to 16 layers are shown in Figs. 4-1 and 4-2, respectively. To facilitate comparison with future laboratory spectra, all vibrational energies as calculated from DFT have been scaled to compensate for anharmonicity. Based on the recent studies of the relevant scale factors for different DFT methods in calculation of vibrational spectra of a variety of different organic molecules [155], a scaling factor of 1.005 has been adopted.

Calculated energies for the spectral features shown in Figs. 4-1 and 4-2 are summarized in Table 4-1. An inspection of these data shows that the energies of certain vibrational modes are virtually independent of the length of the molecule, while those of other vibrational modes are strongly dependent. For example, the Raman peak $\omega_7 \approx 840$ cm^{-1}, corresponding to excitation of the radial breathing mode (RBM), occurs at essentially the same energy in all $(C_6)_n$ stacks. This energy is consistent with that of the RBM in Raman spectra of single wall carbon nanotubes (SWNTs), where is found that $\omega_{radial} = (248/d)$ cm^{-1}, and d is the tube diameter in nm [156-158]. Substitution of the calculated frequency for $(C_6)_n$ stacks in this expression gives d = 0.295 nm,

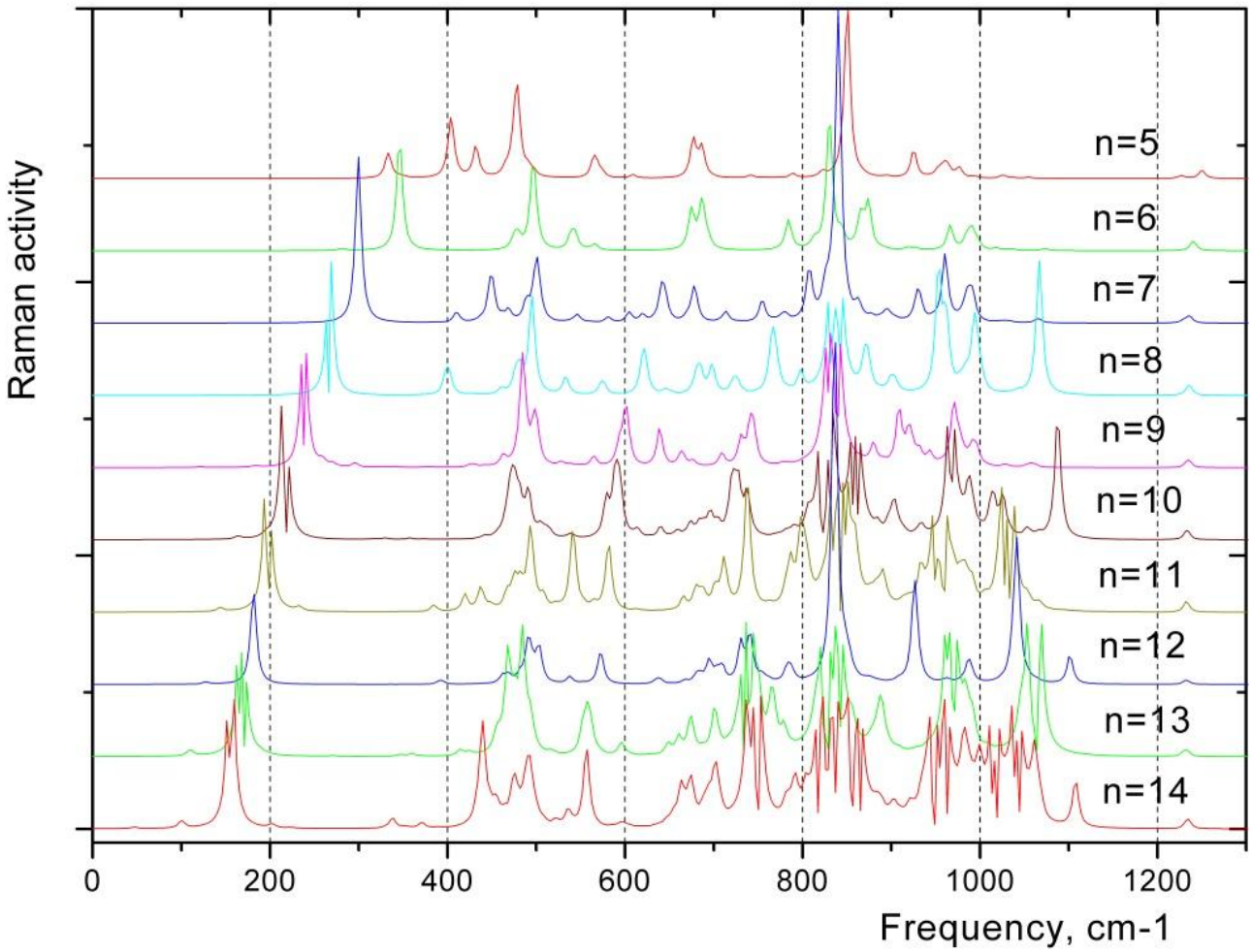

Fig.4-1.Raman spectra of tubular $(C_6)_n$ molecules plotted vs. n. (number of layers in the molecule)

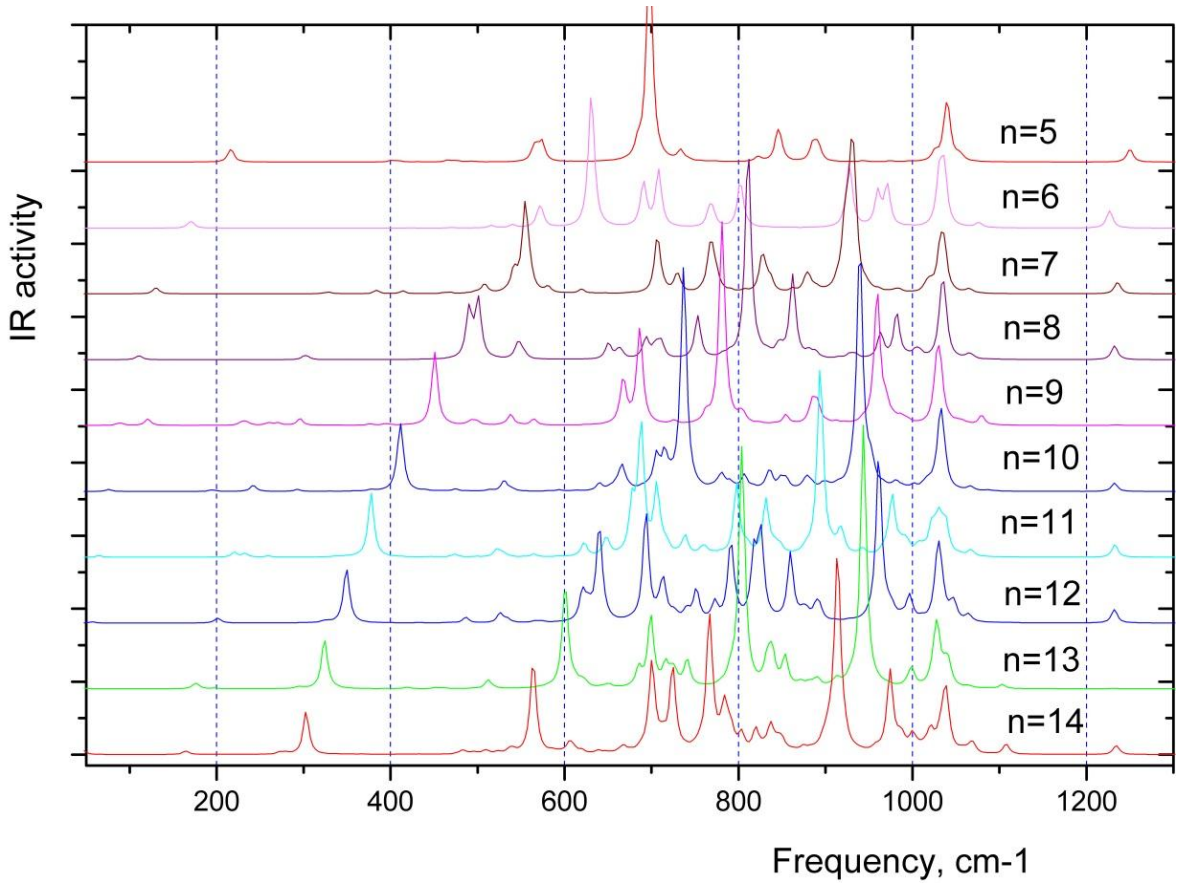

Fig.4-2. Infrared spectra of tubular $(C_6)_n$ plotted vs. n, (number of layers in the molecule)

structure	ω_1 SS1 R	ω_2 SA1 IR	ω_3 MT1 R	ω_4 TL1 R	ω_5 MS1; R	ω_6 LMA1 IR	ω_7 RBM R	ω_8 LS1 R	ω_9 LMA2 IR	ω_{10} MS2; IR	ω_{11} SS2 R	ω_{12} M1 R,IR
$(C_6)_5$	406	--	480	681	688	--	854	--	--	1046	*	1256
$(C_6)_6$	348	--	500	689	697	--	834	--	964	1041	--	1246
$(C_6)_7$	301	557	503	645	717	831	844	965	--	1041	*	1243
$(C_6)_8$	269	503	497	625	730	815	841	*	986	1041	1072	1242
$(C_6)_9$	239	453	487	605	734	785	838	*	964	1035	*	1242
$(C_6)_{10}$	217	413	478	592	731	740	829	972	944	1038	1093	1240
$(C_6)_{11}$	198	379	497	585	741	681	845	959	981	1036	*	1239
$(C_6)_{12}$	182	351	493	575	744	643	840	966	966	1036	1107	1239
$(C_6)_{13}$	168	325	487	560	742	603	836	948	948	1033	*	1235
$(C_6)_{14}$	156	304	497	560	745	567	831	959	979	1043	1113	1242
$(C_6)_{15}$	146	285	490	597	746	534	846	965	965	1036	*	1240
$(C_6)_{16}$	137	269	493	549	748	507	841	971	951	1039	1116	1239

Table 4-1. Energies (cm^{-1}) of major Raman and infrared modes in tubular molecules $(C_6)_n$. SS − stretching symmetrical mode, SA – stretching asymmetrical mode, MT – mixed-torsion mode, TL transverse-longitudinal mode, RBM – radial breathing mode, LS – longitudinal symmetrical mode, LMA – longitudinal mixed asymmetrical mode, MS – mixed symmetrical mode, MA – mixed asymmetrical mode; M- mixed mode; R, IR - Raman and infrared active mode, respectively. An asterisk indicates that this mode does not exist in this molecule.

which is essentially the diameter of a C_6 ring. There is then a clear correspondence between the energy of the RBM in the present molecules and that seen SWNTs. This is a surprizing result as the topology of a rolled single layer sheet of graphene [159] and that present in stacked $(C6)_n$ structures are quite different. This similarity exists because excitation of the radial breathing vibration involves stretching of the CC bonds within C_6 rings in both structures.

The G band, commonly observed near 1590 cm^{-1} in Raman spectra of graphite and carbon nanotubes [156] does not appear in spectra of $(C_6)_n$ since it corresponds to an optical phonon mode between the two dissimilar C atoms in the unit cell of graphitic materials. The 12 IR and Raman modes listed in Table 4-1 appear in the spectra of each molecule and are given in terms of increasing energy. Modes ω_1 and ω_2 are symmetric and antisymmetric stretch modes of the molecule, respectively, along its symmetry axis. The energies of these vibrations are strong functions of the number of C_6 groups and scale as:

$$\omega_1 = 1822.4 / (0.927n)$$
$$\omega_2 = 3126.1 / (0.882n)$$

The vibration with frequency ω_3, appearing at $\approx$ 490 cm^{-1} in all molecules, is identified with a Raman mode in which some rings undergo a rocking motion while pairs of terminal C_6 groups slide back and forth across each other transverse to the symmetry axis. The Raman mode listed as ω_4 in Table 4-1 involves a mixture of transverse and longitudinal vibrations. As a result, the energy of this vibration decreases with the number of C_6 groups in the molecule. The IR mode at ω_6 has a similar dependence on n and corresponds to a hybrid vibration combining a rocking motion of the molecule as a whole together with breathing modes of individual rings. All other IR and Raman modes listed in Table 4-1 have energies that are essentially independent of the number of C_6 groups and therefore the length of the molecule. These are all hybrid modes with the exception of ω_8 and ω_{11}. The symmetric longitudinal mode ω_8 corresponds to a vibration in

which each ring moves back and forth out of phase with its neighbours. For $(C_6)_8$ and $(C_6)_9$, an anti-symmetric vibration occurs with frequency near ω_8. The symmetric vibration ω_{11} involves the vibration of pairs of C_6 rings along the symmetry axis. This mode is Raman active in molecules with n even, but does not exist in molecules with an odd number of C_6 rings. The ω_{12} mode, which is weak in both Raman and IR spectra, is a vibration in which opposing pairs of C atoms within each ring stretch in such a way that the amplitude of this motion increases toward each end of the stack. It is the analog of the G band appearing near 1590cm^{-1} in Raman spectra of graphite and carbon nanotubes [156]. However, the G band characteristic of graphite as well as other Raman bands associated with isolated SWNTs does not appear in the spectra of $(C_6)_n$ stacks. Frequencies of the 12 primary Raman and infrared modes in $(C_6)_n$ molecules are plotted vs. n in Fig.4-3.

4.2. Vibrational properties of the multi-layered intercalated cyclic C_6structures

The overall symmetry of $(C_6)_nMe_{n-1}$ molecules is typically found to be D_{6h}, which is also the symmetry in $(C_6)_7Ru_6$, although, there is a tendency for this to be reduced to D_{3h} as a result of distortion in the C_6 rings at each end of the molecule. Figs. 4-4, 4-5, 4-6, and 4-7 show Raman and IR spectra calculated from first principles of $(C_6)_nFe_{n-1}$ and $(C_6)_nRu_{n-1}$ containing up to eight cyclic C_6 layers. A comparison of vibrational spectra of $(C_6)_nFe_{n-1}$ and $(C_6)_nRu_{n-1}$ shows many similarities as expected from the high symmetry of these molecules. To simplify a discussion of these spectra, eleven primary vibrational modes found in spectra of both types of molecule have been identified. The designations and energies of these modes are summarized in Table 4-2. Based on this classification, these vibrational modes can be divided into two categories: those

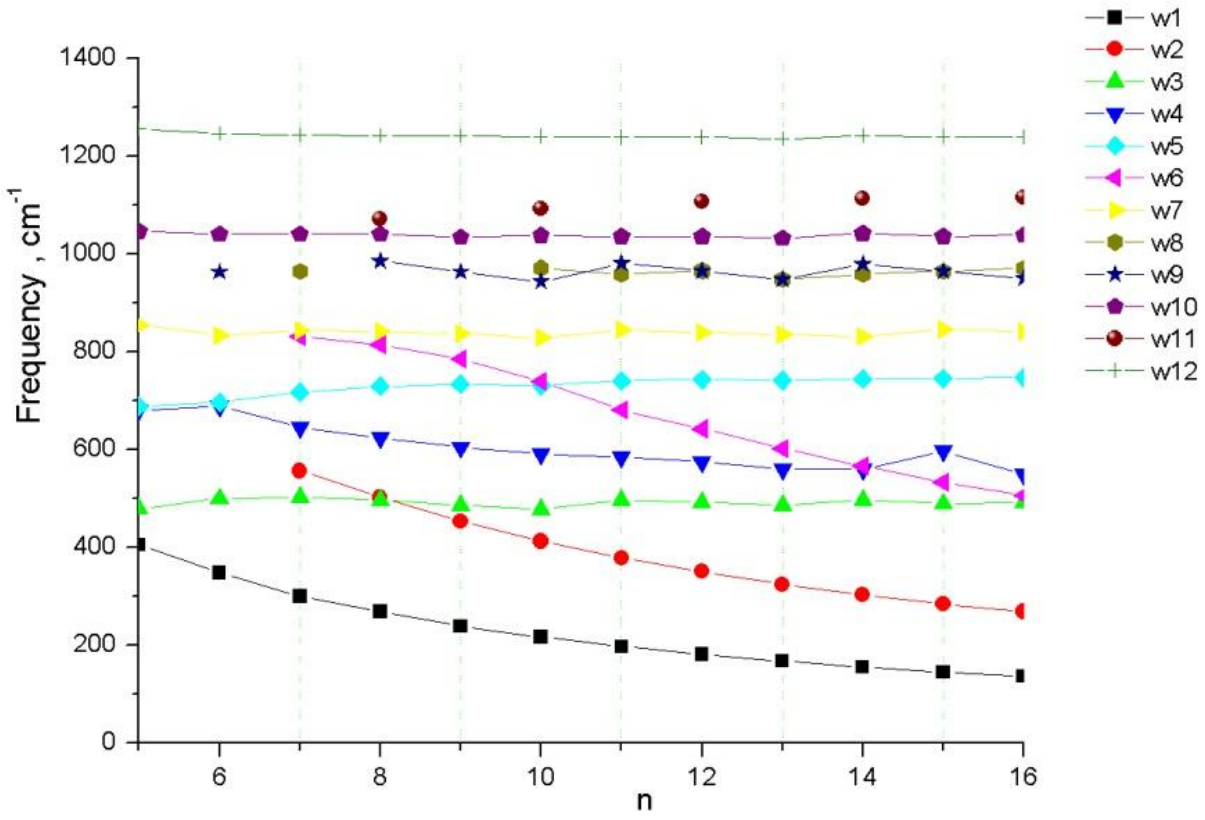

Fig.4-3.Energies of the 12 primary Raman and infrared vibrational modes in $(C_6)_n$ molecules vs. n.

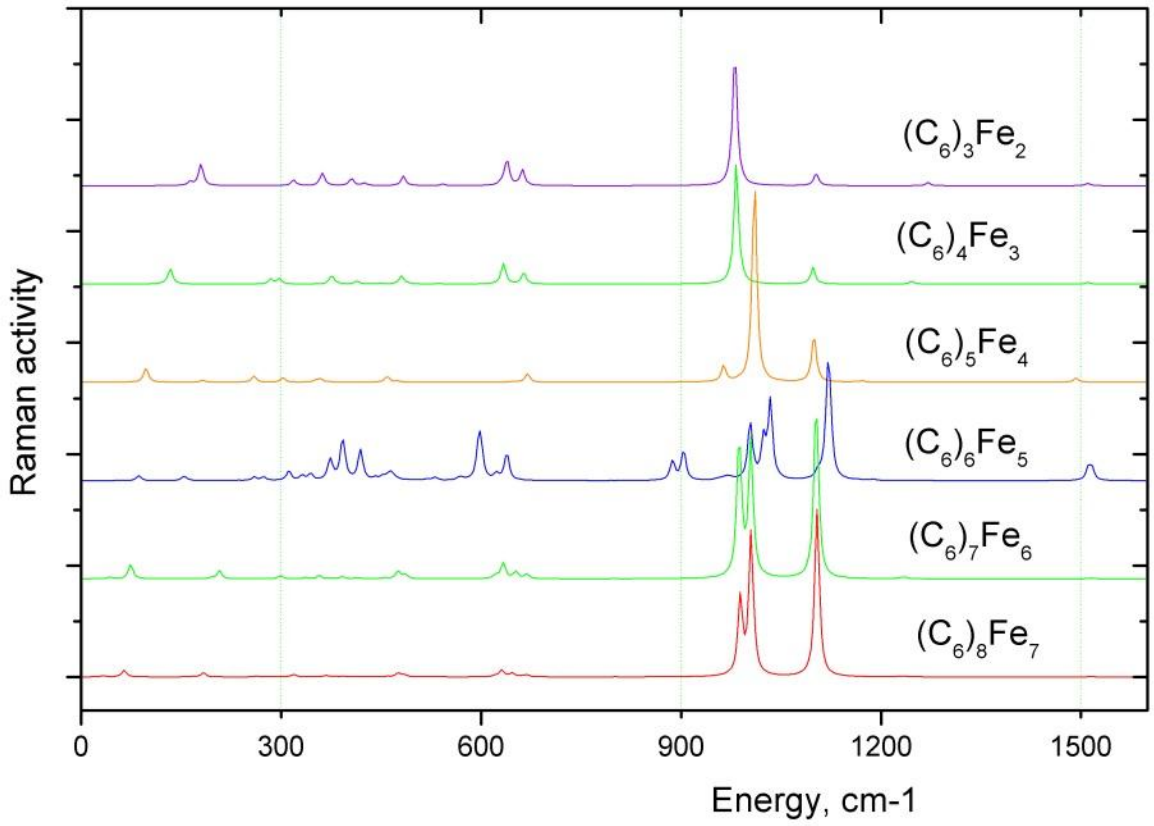

Fig.4-4. Calculated Raman spectra of $(C_6)_nFe_{n-1}$ as a function of, n, the number of layers in the molecule. n changes from 3 to 8.

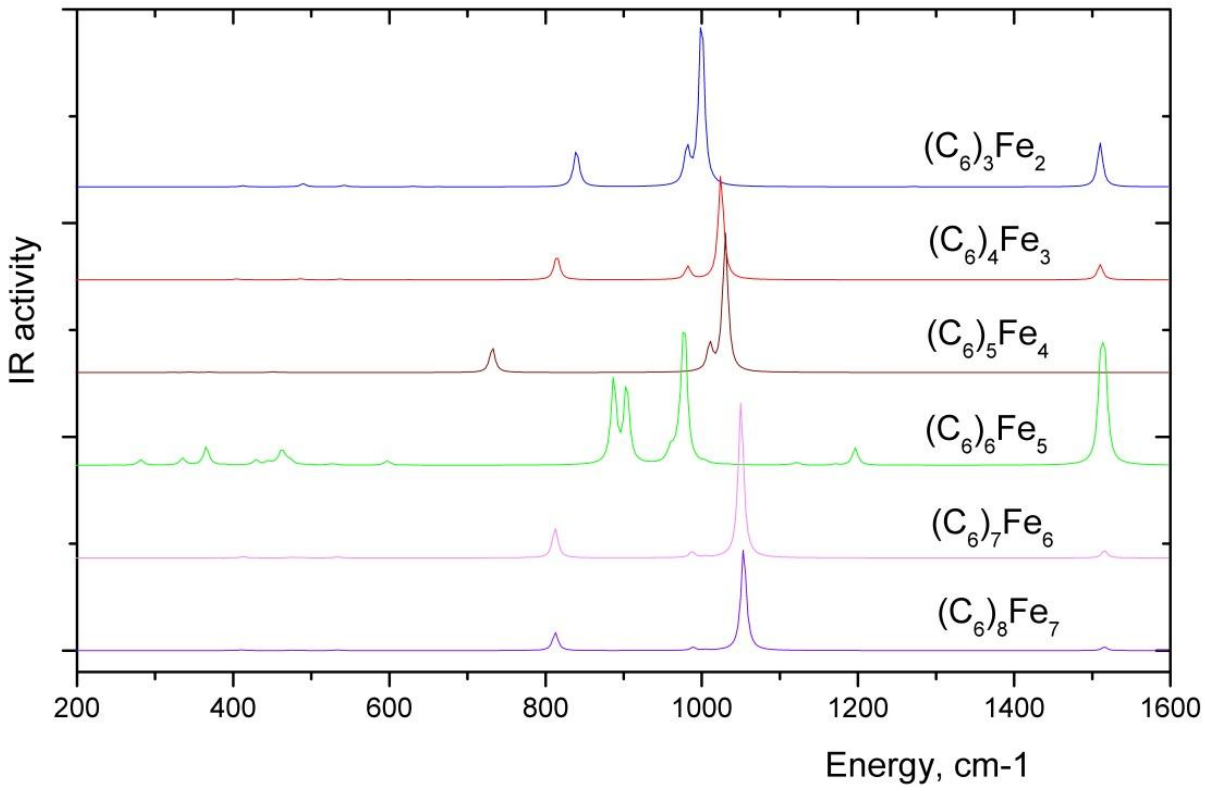

Fig.4-5. Calculated infrared spectra of $(C_6)_nFe_{n-1}$ as a function of, n, the number of layers in the molecule. n changes from 3 to 8.

Structure	ω_1 SS1 R	ω_2 LAMC1 IR	ω_3 LRT1 R	ω_4 DR1 R	ω_5 DR2; IR	ω_6 RBM R	ω_7 ARBEM IR	ω_8 ADRE R	ω_9 SRBEMR	ω_{10} SDRE1 IR,R	ω_{11} SDRE2 IR
$(C_6)_3Fe_2$	196	--	387	675	857	950	980	1000	1080	1540	1000
$(C_6)_4Fe_3$	146	--	403	677	830	967	1004	1002	1076	1540	1002
$(C_6)_5Fe_4$	106	374	384	682	747	945	1009	1030	1077	1524	1030
$(C_6)_6Fe_5$	94	398	399	651	998	1013	1100	905	1100	1546	922
$(C_6)_7Fe_6$	81	390	419	681	828	1003	1029	1006	1080	1545	1008
$(C_6)_3Ru_2$	160	272	374	641	713	845	911	1056	1028	1527	1056
$(C_6)_4Ru_3$	118	282	382	639	697	875	942	1061	1038	1528	1062
$(C_6)_5Ru_4$	94	278	392	636	696	883	956	1060	1040	1527	1060
$(C_6)_6Ru_5$	77	282	397	608	698	885	965	1062	1042	1528	1063
$(C_6)_7Ru_6$	65	297	400	599	862	891	1048	*	1048	1516	*

Table 4-2.Calculated energies (cm^{-1}) of major Raman and infrared modes in $(C_6)_nFe_{n-1}$ and $(C_6)_nRu_{n-1}$. SS: symmetric stretch mode; LAMC: longitudinal asymmetric metal-ring stretching mode; LRT: longitudinal ring tilting mode; DR: ring distortion; RBM: radial breathing mode; ARBEM: asymmetric radial breathing mode of terminal C_6rings; SRBEM: symmetric radial breathing mode of terminal C_6rings; ADRE: asymmetric distortion of terminal C_6 rings; SDRE: distortion of terminal C_6 rings; R, IR: Raman and infrared active modes, respectively. An asterisk indicates that this mode does not appear.

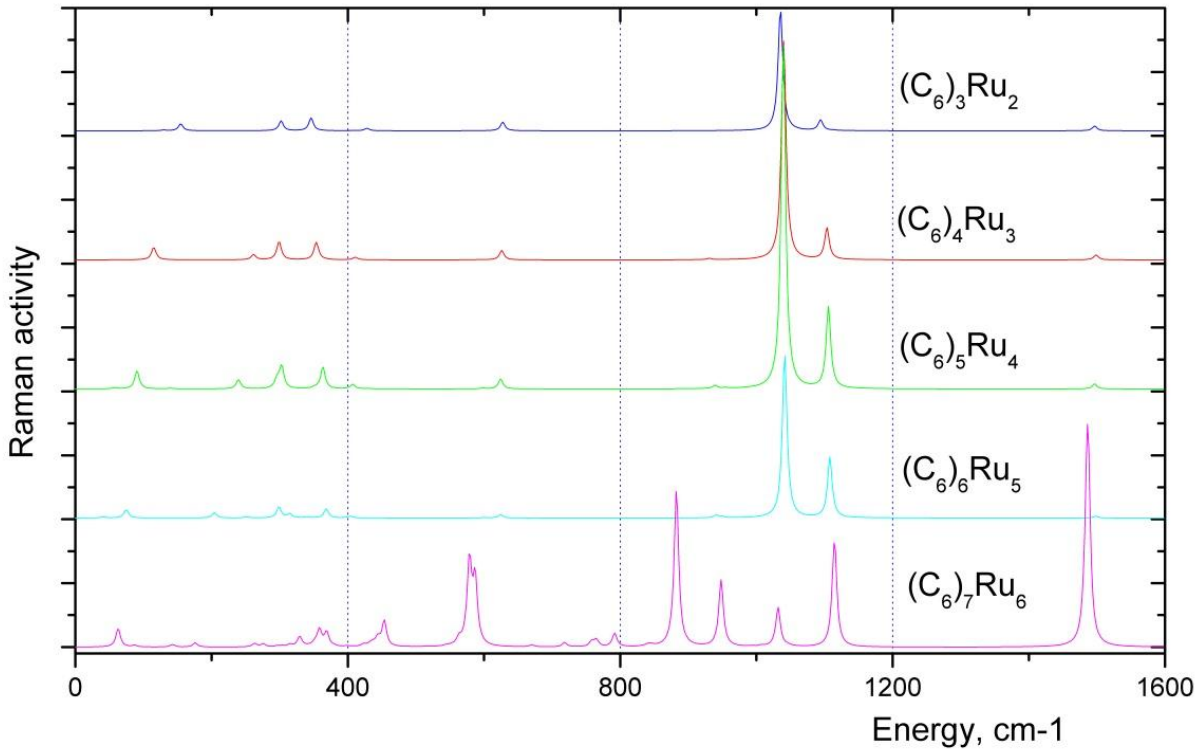

Fig.4-6. Calculated Raman spectra of $(C_6)_nRu_{n-1}$ as a function of, n, the number of layers in the molecule. n changes from 3 to 7.

with energies that are essentially independent of the length of the molecule, and those whose energies are strongly dependent on length. Examples of the latter type include the two modes ω_1 and ω_7. The Raman mode with ω_1 corresponds to a symmetric longitudinal metal-ring stretching vibration of the entire molecule and appears at $\omega_1(cm^{-1}) = 347/(n-1)^{0.817}$ in $(C_6)_nFe_{n-1}$ and at $\omega_1(cm^{-1}) = 279/(n-1)^{0.80}$ in $(C6)_nRu_{n-1}$. The strong infrared-active mode ω_7 is associated with an asymmetric radial breathing vibration of the C6 rings at the ends of the molecule. The frequencies of this mode occur at ω7(cm-1) = 912n0.066 in (C6)nFen-1 and ω7(cm-1) = 835n0.083 in (C6)nRun-1. All other modes showed none, or only very weak correlation with the length of molecule length.

The vibrational mode ω_6, which can be associated with a radial breathing mode (RBM) of C_6 rings within $(C_6)_nFe_n$ and $(C_6)_nRu_{n-1}$, is a characteristic vibration in carbon nanotubes [156-158]. For single wall carbon nanotubes (SWNTs), the symmetric RBM appears at $\omega_{radial} = (248/d)\ cm^{-1}$ with d the tube diameter in nm [156]. Here, the corresponding RBM is found at ω_6 = 845-1015 cm^{-1}

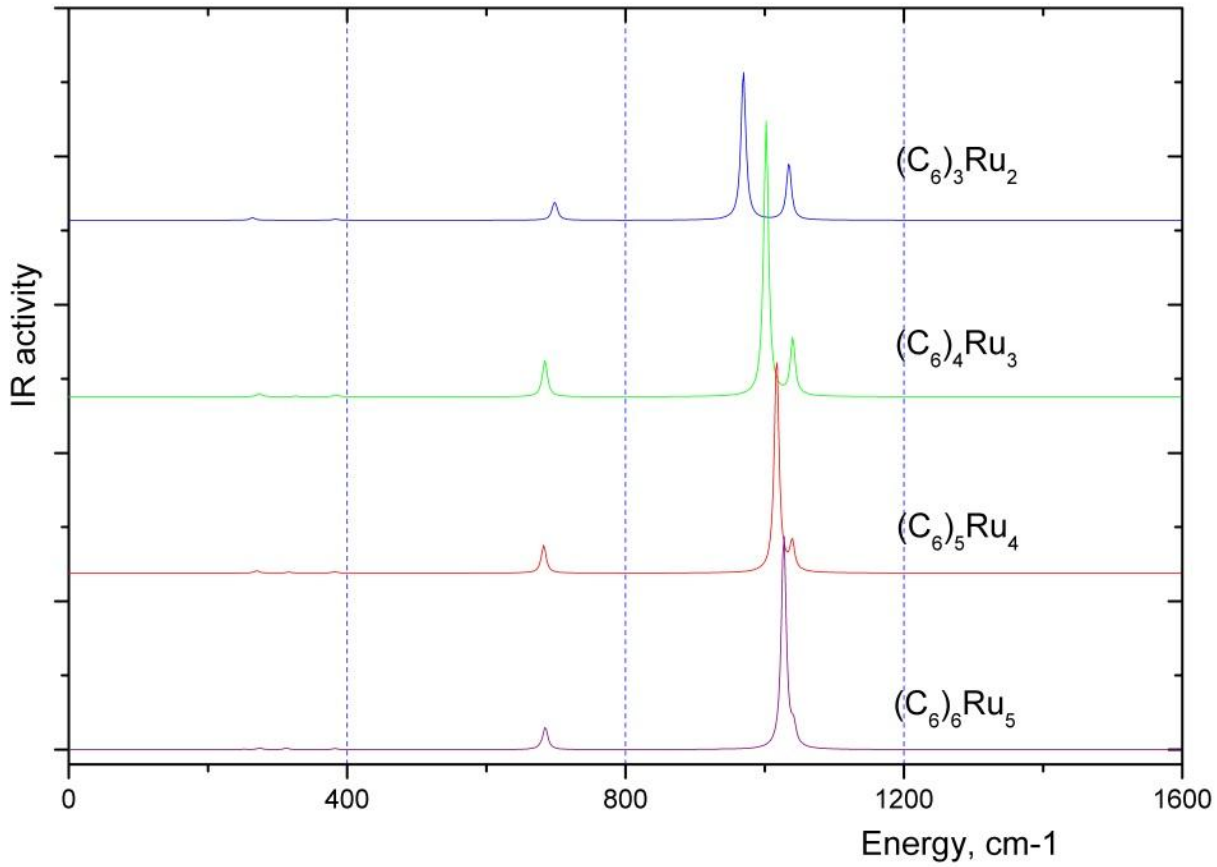

Fig.4-7. Calculated infrared spectra of $(C_6)_nRu_{n-1}$ as a function of, n, the number of layersin the molecule. n changes from 3 to 7.

implying $0.245 \leq d \leq 0.29$ nm, or approximately the diameter of a C6 ring (0.276 nm). Thus, the energy of the RBM mode in these metal-organic molecules closely corresponds with the fundamental breathing mode in the smallest possible SWNT. The finite length of the molecules listed in Table 4-2 resulted in the appearance of two additional vibrational modes involving C_6 rings: ω_7, an asymmetric breathing mode of the terminal C_6 rings, and ω_9, the associated symmetric mode. The relative strength of the mode at ω_9 increased with the overall length of these molecules. Out of seven other vibrational modes in Table 4-2, four (ω_2, ω_3, ω_4, ω_5) were

found to correspond with excitations involving the molecule as a whole, while the other three (ω_8, ω_{10}, ω_{11}) were primarily localized on the terminal C_6 rings. It is notable that Raman spectra of these molecules do not show the G band near 1590 cm^{-1}characteristic of graphite and carbon nanotubes [158].

To aid in a search for these compounds in laboratory spectra, calculated energies have been adjusted using scaling factors determined by a comparison between theoretical (using the present formalism) and experimental energies [162] for the vibrations of ferrocene, $(C_5H_5)_2Fe$. Scaling factors were found to depend on the type of vibrational mode, as well as on the basis used in the first principles calculation. Calculated spectral energies are summarized in the Table 4-2. The scaling factors for the metal-ring stretching vibrations ω_1 and ω_2 were taken to be 1.09 for B3LYP/6-311G* and 1.03 for the B3PW91/LANL2DZ basis, while for ω_3 these were 1.07 and 1.08, respectively. A scaling factor of 1.02 was used for the modes ω_4, ω_5, ω_8, ω_{10}, and ω_{11} in both methods. For ω_6, ω_7, and ω_9 the scaling factors were 0.98 for B3LYP/6-311G* and 0.94 for B3PW91/LANL2DZ.

4.3. Conclusions

First principles techniques have been used to investigate as new class of molecule based on stacks of cyclic C_6 and on cyclic C_6 stacks intercalated with Fe and Ru atoms. It appears that the vibrational properties of elementary carbon nanotubes formed by stacking individual C_6 rings have a good correspondence with those of conventional nanotube having the same diameter. For example, it was found that the RBM mode in a SWNT with d = 0.295 nm is present in the spectrum of each of these tubular molecules but the G band typical of graphitic materials is absent. Other modes have energies that are strongly correlated with the overall length of the

molecule. This may facilitate the characterization of the molecules in laboratory spectra. The correspondence of RBM mode for $(C_6)_n$ with that occurring in conventional NTs suggests that the average bonding energy is similar in both types of nanotube.

Calculation of the vibrational properties of stacks of cyclic C_6 intercalated with Fe and Ru atoms shows the evolution of the energies of Raman and infrared spectral components in these compounds as the length of these molecules increases. These results suggest that these species may exist in the form of infinite polymer chains. While such structures have not yet been produced in the laboratory, the present calculations of vibrational properties of metal-organic molecules will be useful in spectral identification of these compositions.

CHAPTER 5

AB INITIO CALCULATIONS OF THE ELECTRONIC AND VIBRATIONAL PROPERTIES OF INFINITE CHAINS BASED ON CYCLIC C_6 AND CYCLIC C_6 INTERCALATED WITH SOME GROUP VIII TRANSITION METALS.

In Chapter 3 it was shown that small ($n \leq 8$) $(C_6)_nFe_{n-1}$ and $(C_6)_nRu_{n-1}$ compounds have high stabilities due, in part, to strong bonding between the metal atom and cyclic C_6. For example, this bond energy is 11.6 eV in $(C_6)_4Fe_3$. Additionally, high symmetry (D_{6h}, D_{3h}) in these molecules causes an increase in density of electron states near the Fermi level. These two properties combine to make stacks of cyclic C_6 with intercalated metals particularly interesting from a chemical and nano-electronic point of view. This chapter investigates whether these properties are maintained in much longer molecules including infinite structures based on stacked cyclic C_6.

The electronic properties and phonon dispersion of infinite chains based on molecular stacks of cyclic C_6 and on stacks of cyclic C_6 intercalated with Fe and Ru have been calculated using first principles density functional techniques (DFT), [104]. It is shown below that these bands could be associated with rotational states of the structure and cannot be calculated from a simple one-dimensional spatial Fourier transformation of the potential [104], due to additional electronic degrees of freedom in such structures. These degrees of freedom are associated with electron movement around the principle axis. The dimensionality of such structures are often called "one plus zero" [120].

5.1. Some characteristics of band structure in infinite molecular chains having rotational and rotational-translational symmetry

The standard procedure for determining the energy gap structure in one-dimensional periodic molecules involves finding the wave function |x,y,z> of the molecule where the Density Functional Method is used to find the electron density. From the Bloch theorem, the one-dimensional wave function is:

$$\int dxdy \mid x, y, z >= e^{ikz} u(z) \tag{5-1}$$

where u(z) is a function periodic in z and k is wave number.

The most popular software (for example, Siesta [169] and Quantum Espresso [170]) for calculation of energy band structure in periodic substance uses the expansion of the wavefunction and inter-molecular potential in terms of plane waves in k-space. This procedure includes 3-D Fourier transformation of the wave function and inter-molecular potential, followed by substitution into the Hamiltonian, and the solution of self-consistent equations.

This 3D-Fourier expansion of the wave function in one-dimensional structure is then:

$$\mid k >= \frac{1}{2\pi} \iint_{\infty} dydx \int_{\infty} dz \mid x, y, z > e^{-ikz} \tag{5-2}$$

Here we consider one-dimensional molecules with a periodicity along the z-axis corresponding to the lattice constant a. The band energy with eigenvalue n is obtained as the solution

$$\varepsilon_k^{(n)} = \frac{< k \mid \hat{H} \mid k >}{< k \mid k >} \tag{5-3}$$

as in all band structure calculations.

We now take the special case where the molecule has C_n symmetry along its main axis. In cylindrical coordinates the wave function $|\varphi,\rho,z>$ is a periodic function in z and φ. Then, applying the Bloch theorem to both z and φ:

$$\int_0^\infty d\rho\cdot\rho\,|\,\varphi,\rho,z>=e^{ikz}e^{ik_\varphi\varphi}U(\varphi,z) \tag{5-4}$$

where U(φ,z) is a periodic function in z and φ. The corresponding solution in two-dimensional k-space is:

$$|\,k,k_\varphi>=\frac{1}{(2\pi)^2}\int_0^\infty d\rho\cdot\rho\int_0^{2\pi}d\varphi\cdot e^{-ik_\varphi\varphi}\int_{-\infty}^{\infty}dz\cdot e^{-ikz}\,|\,\varphi,\rho,z> \tag{5-5}$$

Here a new parameter k_φ has been introduced that corresponds to the momentum component in the radial direction. At the same time, cyclic boundary conditions lead to the quantization k_φ = m, where m= 0, 1, 2, .. M. Symmetry defines the number of allowed values (M + 1) of the quantum number m and makes this equal to the number of classes in the C_n point group. For example, for the symmetry group C_6 there are 4 allowed values of m corresponding to 0, 1, 2, and 3. These values also determine the number of wave functions with the same k, but different m. All wave functions now satisfy:

$$\int_0^\infty d\rho\cdot\rho\,|\,\rho,\varphi,z>=e^{ikz}\cos(m\varphi+\phi)U(\varphi,z) \tag{5-6}$$

where ϕ – some phase. The corresponding state in k-space is the solution to:

$$|\,k;m>=\frac{1}{2\pi}\int_0^\infty d\rho\cdot\rho\int_\infty^{-\infty}dz\cdot e^{-ikz}\int_0^{2\pi}d\varphi\cos(m\varphi)\,|\,\rho,\varphi,z> \tag{5-7}$$

The term with m = 0 in equation 5-6 corresponds to equation (5-1) in the standard expansion of the wave function in k-space. Terms proportional to cos(φm) correspond to electron states with some rotational component. The energies of these rotational states are

$$\varepsilon_{k,m}^{(n)} = \frac{< k;m \mid \hat{H} \mid k;m >}{< k;m \mid k;m >} \qquad (5\text{-}8)$$

These states are very characteristic of one-dimensional structures combining rotational and rotational-translational symmetries.

It is important that to use circular conditions to find the quantization of the wavefunction pseudo momentum k_φ in the circumferential direction. The same result can be attend by expansion of the wavefunction and intermolecular field by set of spherical or cylinder functions. However, use of the conventional 3D-Fourier transformation that involves projection on a specific direction cannot reveal quantization in circumferential direction.

These states cannot be developed from a standard method that includes a simple plane wave expansion because the spatial components of the cosine function vanish after integration. Thus, in one-dimensional periodic structures with C_n symmetry along the primary axis, there must be additional energy bands corresponding to rotational states whose energies. This implies that each band zone will split to reflect these rotational-translational components. The results given here represent a first step estimation using a tight binding model of band splitting arising from rotational states in these structures.

Some methods of band structure calculation implicitly include rotational states as part of the band structure. For example, the calculation of band structure in nanotubes (NT) whereby the

electronic properties of NTs are evaluated from the electronic properties of graphene rolled from a two-dimensional graphite sheet into a one-dimensional NT [3]. Standard calculations of band structure in one-dimensional geometry use a one-dimensional plane wave Fourier expansion to find the electron states. Therefore, they do not consider any radial component in the motion of the conduction electrons. In the present system, carbon atoms are located off the symmetry axis and this is accompanied by associated rotational or rotational-translational symmetry and the possibility of quantized radial components of the k-vector. For example, the presence of C_6 symmetry along the main axis results in similar symmetry for the wavefunction and quantized rotational components in the k-vector corresponding to rotations by 0, $\pi/3$, $2\pi/3$, π radians around this axis. Hence, band energies for conduction electrons near the Fermi level should split into 4 components.

5.2. Electronic and vibrational properties of the infinite chains based on cyclic C_6 stacks and intercalated C_6 stacks.

The classical band structure of infinite $(C_6)_n$, $(C_6)_nFe_{n-1}$, and $(C_6)_nRu_{n-1}$ chains were calculated from first principles by DFT methods using ADF BAND 2010.02 software [166] as preferred for calculation of the properties of periodic structures. The standard calculations were modified, because the B3LYP/6-311G* method is not supported in ADF BAND software and it was preferable to use a classical method for both types of infinite chains: $(C_6)_nFe_{n-1}$ and $(C_6)_nRu_{n-1}$. The effectiveness of different methods of calculation for finite and infinite structures may vary. Methods that are precise for calculation of the properties of finite molecules are often not precise when used to calculate the properties of infinite structures and vice-versa. For a more precise calculation of the properties of infinite chains TZ2P (triple Zeta with 2 polarization functions) Slater-type orbitals were used in combination with the mPBE (Perdew-Burke-Eruzerhof modified by Adamo and Barone) exchange-correlation functional.

Optimized geometry in an infinite $(C_6)_nFe_{n-1}$ chain was found to correspond to a configuration where the unit cell has length of L=3.1175±0.0003Å and the radius of the C_6 ring is R=1.421±0.001Å. The energy of formation per unit cell was calculated to be E_f=51.426±0.001eV. Corresponding parameters for the unit cell in an infinite $(C_6)_nRu_{n-1}$ chain were found to be L=3.6724±0.0001Å, R=1.424±0.001Å and E_f=50.5014±0.0002eV, respectively.

In both cases the unit cell was found to be centro-symmetric with the metal atom located halfway between the nearest C_6 rings, but the spin-orbit interaction between metal atoms and between metal atoms and C_6 rings is expected to result in slightly lower symmetry. For example, for perfect ferromagnetic orientation between Fe spins in $(C_6)_nFe_{n-1}$, each C_6 ring has an induced spin of ~ 0.07 Bohr magneton and these are oriented in a direction opposite to that of the Fe spins. Consequently, each Fe atom will experience an asymmetric interaction from neighboring

C_6 rings. The energy associated with these terms amounts to ~ 10 meV and is therefore very small compared to the overall bond energy. It was found that Fermi energies in infinite $(C_6)_nFe_{n-1}$ and $(C_6)_nRu_{n-1}$ chains are 5.73 eV and 6.38 eV, respectively. These energies are very similar to those in molecules of finite length.

Calculated band structures for these metal-organic chains are shown in Fig. 5-1. It was found that the Mulliken charge distributions in long $(C_6)_nFe_{n-1}$ and $(C_6)_nRu_{n-1}$ molecules had different locations and that this was related to the chemical bonding in these structures. In $(C_6)_nFe_{n-1}$ chains, Fe atoms had a positive charge of ~ 0.86, while in $(C_6)_nRu_{n-1}$ Ru atoms had a negative charge of ~ 1.04. It appears then that conduction electrons in the Fe compounds are localized near the C_6 ring while those in Ru compounds are found close to the Ru atom. Hence, these differences are reflected in the band structure of the infinite chains. In $(C_6)_nFe_{n-1}$ structures the conduction band crosses the Fermi level at the edge of the Brillouin zone, while in $(C_6)_nRu_{n-1}$ the conduction band crosses the Fermi level at the zone center. The band structures in Fig.5-1 showing an energy gap between the valence and conduction bands is typical of that in semiconductors. However, *ab initio* calculations of the energy gap discussed in the previous chapter predicts that long metal-organic molecules should have metallic properties. In addition, the possibility for conductivity in these molecules is confirmed by the overlap between optical and acoustic phonons branches as seen in Fig. 5-5. It is well-known that conducting CNT have overlapping acoustic and optical phonon branches, while non-metallic CNT have an energy gap between the acoustic and optical phonon branches [167]. It has also been shown that all ultra-small diameter CNTs are conducting [107-109]. All of these factors suggest that intercalated nanotubes of the type investigated here should be conducting.

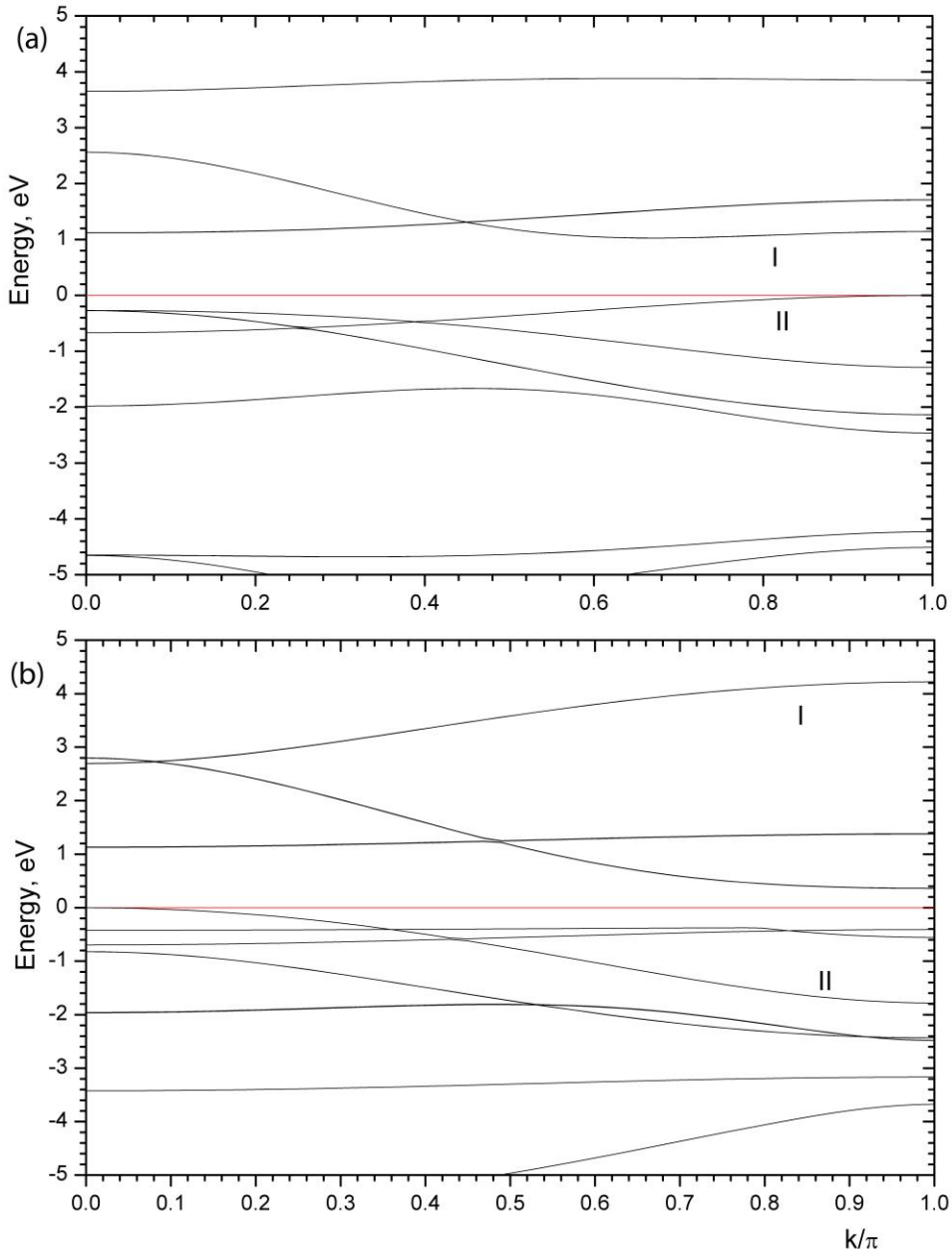

Fig.5-1. Energy band structure for infinite chains: (a) $(C_6)_nFe_{n-1}$;(b) $(C_6)_nRu_{n-1}$. These calculations were carried out using the standard one dimensional plane wave expansion in k-space. The super cell was taken to have 14 atoms (two unit cells).

The absence of conducting states in band structure is a consequence of the imprecision of the conventional method of calculation of band structure in one dimension chains. This suggests that molecules based on cyclic C_6 have metallic properties due to splitting of the some bands that correspond to metal-carbon bonding near the Fermi level.

These states are very characteristic of one-dimensional structures combining rotational and rotational-translational symmetries. They cannot be developed from a standard method that includes simple expansion by plane waves, because the spatial components of the cosine vanish on integration. Thus, in one-dimensional periodic structures with C_n symmetry along the primary axis, there must be additional energy bands corresponding to rotational states. This implies that each band zone will split to reflect these rotational-translational components. The results given here represent the first step estimation using a tight binding model of band splitting arising from rotational states in these structures. A similar result has been found for carbon nanotubes [3]. In Fig.5-2 energy levels are designated I and II corresponding to bonding and anti-bonding bands, respectively, of the metal-carbon interaction near the Fermi level.

To develop a simple tight bonding model for conduction electrons near the Fermi level in these systems we begin with the standard result for tight binding in an infinite one-dimensioned chain of identical atoms [168]:

$$\varepsilon_k = \frac{E_F - 2\Delta\cos(ak)}{1 + 2S\cos(ak)} \qquad (5\text{-}9)$$

where Δ is the bond energy, S is the overlap integral, k is the wave vector, and a is the lattice constant.

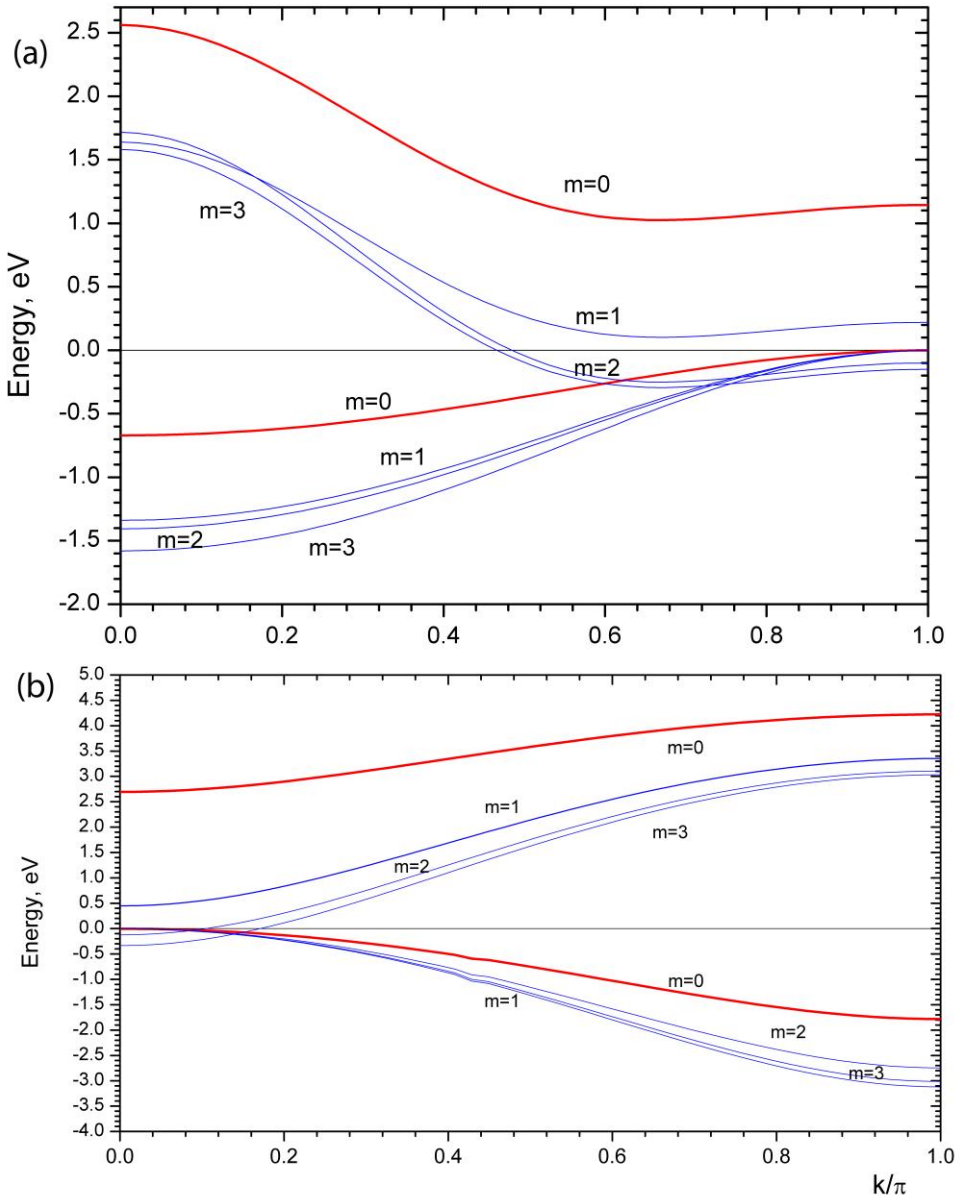

Fig.5-2. Calculated splitting of the bonding and anti-bonding band zones that corresponds to metal-carbon bonding in infinite chains: (a) $(C_6)_nFe_{n-1}$;(b) $(C_6)_nRu_{n-1}$

This can be used now to generate separate tight binding equations for the carbon and metal sublattices in $(C_6)_nRu_{n-1}$. The equations will be the same in the $(C_6)_nFe_{n-1}$ system, but the initial location of the conductivity electron will be shifted from the metal atom to the carbon ring introducing a $\pi/2$ phase shift in the wavefunction. For a chain of non-interacting non-overlapping metal atoms:

$$\varepsilon_k^{\,M} = E_F \tag{5-10}$$

while for a chain of non-interacting identical carbon rings one has:

$$\varepsilon_k^{\,C} = \frac{E_F + 2\Delta_{CC}\cos(\frac{\pi}{3}m)}{1-2S_{CC}\cos(\frac{\pi}{3}m)} \tag{5-11}$$

where Δ_{CC} is the carbon-carbon bond energy inside a ring, m is the rotational quantum number with allowed values m = 0, 1, 2, 3 and S_{CC} is the overlap integral for two adjacent carbon atoms in the ring. If it is assumed that the overlap of wavefunctions between two adjacent carbon atoms on a ring or between two metal atoms is very small, then the Hamiltonian for the two sublattice combination is:

$$\begin{pmatrix} H_C & H_{CM} \\ H_{MC} & H_M \end{pmatrix}\begin{pmatrix} \varphi_C \\ \varphi_M \end{pmatrix} = E\begin{pmatrix} 1 & S_{CM} \\ S_{MC} & 1 \end{pmatrix}\begin{pmatrix} \varphi_C \\ \varphi_M \end{pmatrix} \tag{5-12}$$

where φ_C and φ_M are wavefunctions of the carbon and metal sublattices, respectively.

Calculations give S_{CM}= 0.13 for the overlap integral between carbon and metal atoms. In a zero order approximation where S_{CM} is neglected:

$$\varepsilon_k = \frac{1}{2}(H_C + H_M) \pm \sqrt{(\frac{1}{2}\{H_C - H_M\})^2 + H_{CM}{}^2} \qquad (5\text{-}13)$$

The diagonal element of the Hamiltonian for $(C_6)_nRu_{n-1}$ will be:

$$H_{MC} = -3\Delta_{MC} \sin ka \qquad (5\text{-}14)$$

where Δ_{MC} is the metal-carbon bond energy.

Combining, this becomes for $(C_6)_nRu_{n-1}$:

$$\varepsilon_k = \left(\frac{\Delta_{CC} \cos(\frac{\pi m}{3})}{1 - 2S_{CC} \cos(\frac{\pi m}{3})} \right) \pm \sqrt{\left(\frac{\cos(\frac{\pi m}{3})\Delta_{CC}}{1 - 2S_{CC} \cos(\frac{\pi m}{3})} \right)^2 + \left(3\Delta_{MC} \sin(\frac{a}{2}k) \right)^2} \qquad (5\text{-}15)$$

where the "plus" and "minus" solutions correspond to bonding and anti-bonding bands, respectively. It was found that $S_{CC} = 0.403$.

Equation (5-15) is similar to the standard quantum mechanical equation for bonding and anti-bonding energy levels expanded in terms of plane wave states. The difference from the conventional solution involves the incorporation of rotational states, labeled in terms of m. When m = 0, then this solution reduces to that given by the standard plane wave expansion of the Hamiltonian. The resulting model, while approximate, seems to work well. However, more precise calculations would require reformulating the entire *ab initio* Hamiltonian to include rotational states related to the molecular symmetry.

Fig.5-1 shows band structures for these metal-organic molecules as calculated using standard procedures with m = 0. The bonding and anti- bonding zones corresponding to equation (5-15)

for m = 0 are evident in these solutions. The bonding zone should touch the Fermi level at the center of the Brillouin zone, while the anti –bonding zone should be symmetric with respect to the bonding zone. Both should have a sine character. Thus, lines I and II in the figure can be associated with bonding and anti- bonding zones, respectively. Using zones I and II as solutions defines the other parameters in equation (5-15) and helps in the calculation of band zones corresponding to all allowed values of the quantum number m. The hierarchy of band splitting by rotational states in metalorganic infinite polymers $(C_6Fe)_n$ and $(C_6Ru)_n$ is shown in Fig.5-2. Band structures of $(C_6Fe)_n$ and $(C_6Ru)_n$ (Fig.5-2.a and Fig.5-2.b respectively) shows that the rotational states indicate that these molecules have a relatively high density of electron states at the Fermi level and may be conductors.

Similar calculations have been done for pure carbon chains $(C_6)_n$. All single wall nanotubes (SWNTs) can be represented as a graphene sheet folded into a hollow cylinder [3]. Hence, a good approximation to the band structure in SWNTs can be obtained from the band structure of graphene. Calculation of the band structure includes expanding the electron states by plane waves with wave numbers k_x and k_y. Here the vector k_x is parallel to the main axis of the SWNT and k_y is the axial wave vector. Due to periodicity along the axis, the wave vector k_y is quantized according to equation:

$$l\, k_y = 2\pi m \qquad (5\text{-}16)$$

where l is the circumference of the circle of radius; m=0; ±1; ±2... and only a few values of k_y are allowed inside the first Brillouin zone. This approach can be extended to all infinite polymers having axial symmetry. If the infinite polymer has axial symmetry C_n, then the axial vector k_y can be changed by rotational vector k_φ with quantization rules:

$$k_\varphi = m$$
$$m \leq n/2 \qquad (5\text{-}17)$$

Each of the allowed values of the wave vector k_φ corresponds to an allowed rotational state of the electron determined by the quantum number m. In the following, the wave vector k_x is designated as **k**, because it has only one component for each rotational quantum number. Unfortunately, the standard software does not permit calculation of the band structure of one dimensioned polymers with respect to rotational states. In this case, the contribution of rotational

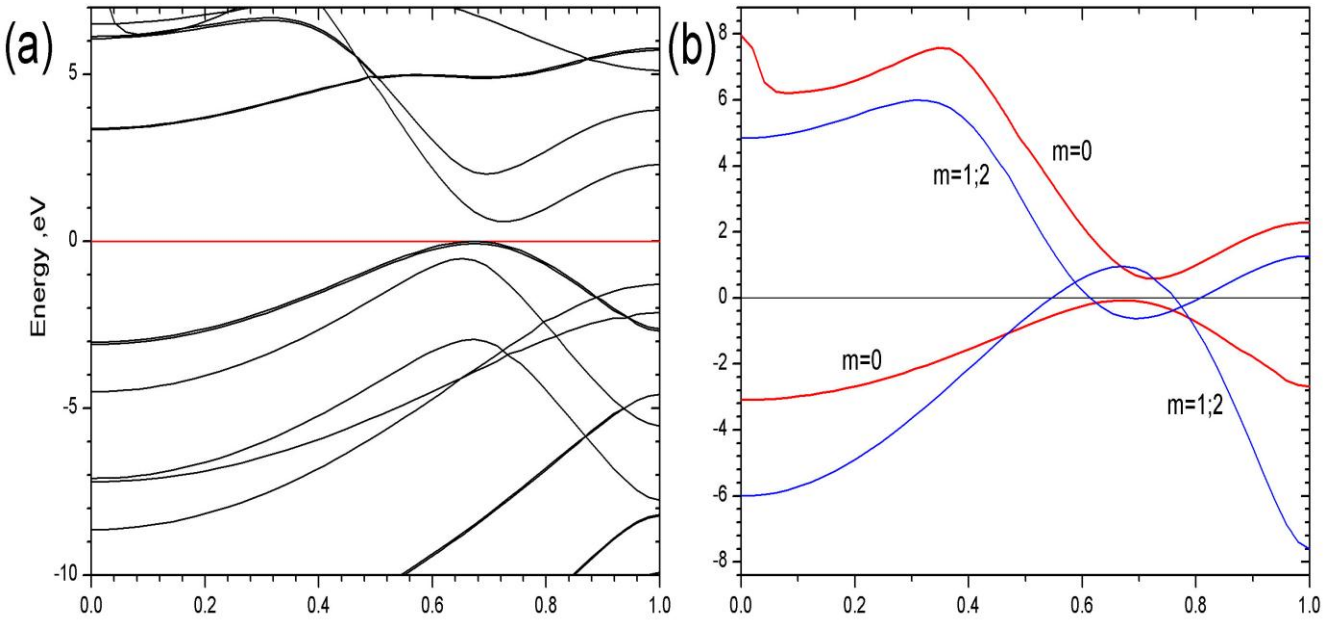

Fig.5-3. Energy band structure for infinite chains $(C_6)_n$;(a) calculations were carried out using the standard one dimensional plane wave expansion in k-space. The super cell was taken to have 14 atoms (two unit cells).
(b) Scheme of possible splitting of the bonding and anti-bonding band zones that corresponds to metal-carbon bonding for infinite chains $(C_6)_n$

states into overall conductivity is not taken into account. Missing of conductivity bands leads to false interpretation of the electron structure of polymers, and underestimation of the number of electron states near Fermi level.

It noted earlier, nearly all SWNTs with diameters less than 1 nm are conducting [107] due to the extensive overlap between electron orbitals. This leads to re-hybridization between π and σ electrons [111] and a decrease in the energy gap between the valence and conduction bands. For carbon nanotubes with diameter less than 1nm the valence and conduction bands overlap.

Molecules based on stacks of cyclic C have D_{6h} symmetry and the principle axis is C_6. Thus, there are 4 allowed rotation numbers corresponding to m = 0, 1, 2, and 3. The energy band structure calculated from the standard software is shown in Fig.5-3.a. In contrast to all other SWNT nanotubes $(C_6)_n$ is obtained not by rolling a honeycomb crystal lattice, but from a rectangular lattice. According to the band structure, this polymer can be characterized as a non-direct gap semiconductor with a band-gap energy of ~ 0.5 eV. Splitting of the conduction bands near the Fermi level due to the inclusion of rotational states is shown in Fig.5-3.b. It is clear from this figure that polymers based on stacked cyclic C_6 are predicted to be good conductors as a result of a relatively high density of electron states at the Fermi level.

5.3. Phonon dispersion in carbon $(C_6)_n$ and metal-organic $(C_6)_nMe_{n-1}$ chains

Phonon dispersion in carbon $(C_6)_n$ and metal-organic $(C_6)_nMe_{n-1}$ chains has been obtained using the Siesta 3.1 [169] and Quantum ESPRESSO 4.3.1[170] software packages. Electronic-structure properties have been calculated in the DFT formalism using a plane-wave basis set and pseudopotentials. The method of calculation involves few steps. First, the force constant matrix is computed using a linear response method. This is then followed by building the dynamical

stiffness matrix from the force constants. The last step is to diagonalize this matrix to obtain phonon frequencies and eigenmodes.

Carbon stacks of cyclic C_6 contain 6 carbon atoms per unit cell. Thus, there are 18 phonon modes in total. At the same time both metal-organic compositions have the same geometry and each contains 7 atoms in the unit cell. Therefore metal-organic structures based on stacks of cyclic C_6 should have 21 phonon modes, including 3 acoustic modes. The D_{6h} symmetry group can be expressed as direct product of the groups D_3, $\{E,\sigma_h\}$, and $\{E,\sigma_i\}$. There are three irreducible representations for group D_3, two one dimensional representations A, and B, and one two-dimensional representation, E. These representations are labelled with subscripts 1, 2. The subscripts u and g are used to denote parity under the operations σ_h or σ_i respectively. The symmetry point group D_{6h} has 12 irreducible representations and can be expanded [98] as follows:

$$\Gamma=4A_{1g}+2A_{2g}+4A_{1u}+2A_{2u}+2B_{1g}+4B_{2g}+2B_{1u}+4B_{2u}+4E_{1g}+8E_{2g}+8E_{1u}+4E_{2u} \quad (5\text{-}18)$$

As a result, there should be 12 phonon branches if this symmetry is maintained in the overall structure. However, one can expect that localized polarization at points within the chain may result in lifting of some of this degeneracy.

The molecular dynamical symmetry of the structure based on cyclic C_6 carbon stacks has only 8 irreducible representations and can be expanded as follows:

$$\Gamma=2A_{1g}+A_{2u}+2B_{2g}+B_{1u}+E_{1g}+2E_{2g}+2E_{1u}+E_{2u} \quad (5\text{-}19)$$

These representations correspond to acoustic modes, twisting modes, tilting modes, circular stretching modes and radial modes. The calculated dispersion of the phonons in the $(C_6)_n$

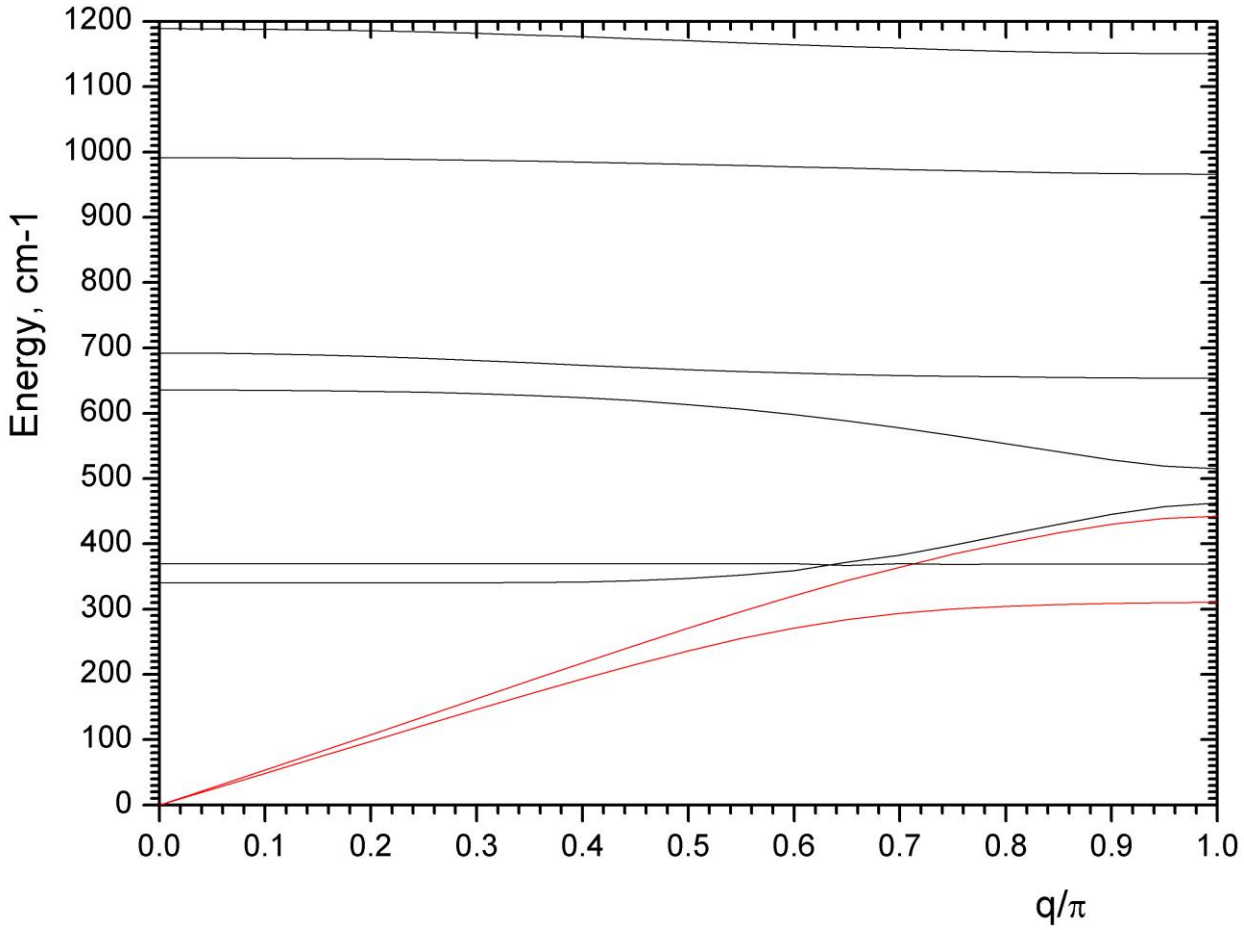

Fig.5-4. Phonon dispersion of pure carbon chain $(C_6)_n$.

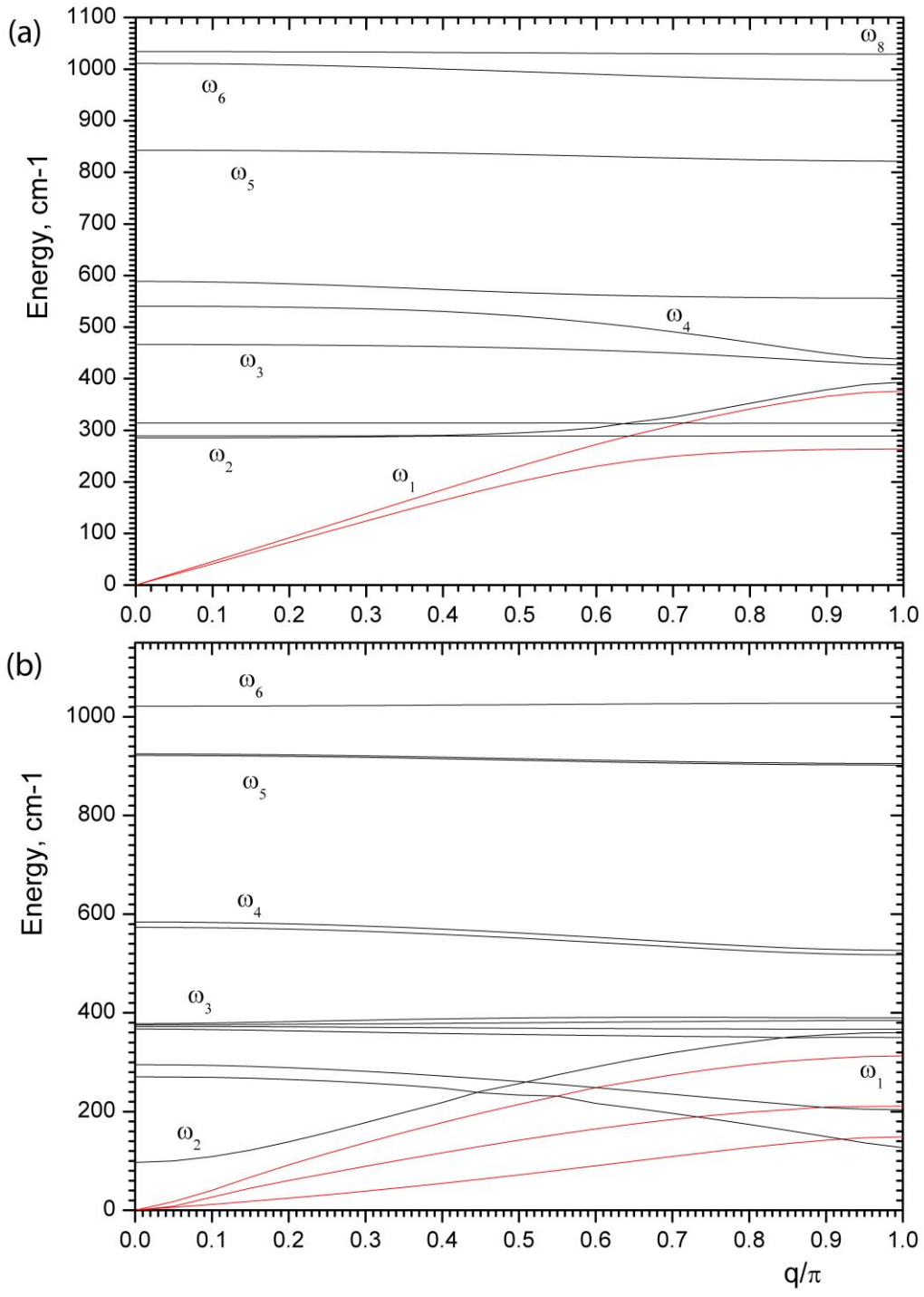

Fig.5-5. Phonon's dispersion for infinite chains: (a) $(C_6)_nFe_{n-1}$;(b) $(C_6)_nRu_{n-1}$ Frequencies ω_1-ω_{11} corresponds to vibrational modes of the finite chains (see previous chapter). Red color corresponds to acoustic modes.

structure is shown in Fig.5-4. Using the same approach, the molecular symmetry of metal-organic molecules based on stacked C_6 can be expanded by irreducible representations as follows:

$$\Gamma=3A_{1g}+ A_{2u}+ 3B_{2g}+B_{1u}+E_{1g}+3E_{2g}+3E_{1u}+E_{2u} \quad (5\text{-}20)$$

Calculated phonon dispersion in metal-organic structures is plotted in Fig.5-5 and is clear that a similar dispersion is found in both compositions. The essential difference in the phonon properties of the Fe and Ru compositions is that the effective charge of the metal atoms strongly influences the phonon spectrum, as a large effective charge localized on the metal atom can cause a high axial polarization within the unit cell. As a result, one sees some removal of degeneracy in the transverse phonon modes in the Ru structure. When compared with $(C_6)_nFe_{n-1}$ the Ru structure has two TA (transverse acoustic) modes and all TO (transverse optic) modes are split away from each other. Another consequence of the large magnitude of the effective charge is the larger separation between TA and TO modes that obey the Lyddane–Sacks–Teller relation [172].

Since the current structures can be considered to be narrow diameter intercalated nanotubes, it is expected that radial, axial and circumferential vibrational modes characteristic of nanotubes will appear in this spectrum [102,173]. By association, a circumferential displacement corresponds to a twisting mode, while the axial mode can be identified with a LA mode. The radial mode arises from optical phonons that have similar dispersion to that of acoustic modes. This peculiarity can be understood if nanotubes are considered to be formed from folded graphite planes. The radial modes can then be associated with out-of plane graphite acoustic phonons [102]. Nanotube spectra are also found to include coupled radial-longitudinal modes [173] and similar coupled modes occur in the present metal-organic structures. The origin of this coupling is presumably due to the interaction between metal atoms and the C_6 rings.

According to the Lyddane–Sacks–Teller relation, pure TO and LO modes are separated from the acoustic modes by an energy gap. This implies that phonon modes appearing in Fig.5-5 at energies < 350 cm^{-1} should be radial, coupled radial-acoustic and radial-optical modes. Fig.5-5 also shows the frequencies of vibrational modes in finite molecules corresponding to phonon modes of the infinite chains. In general, there is a good correspondence between modes in finite and infinite chains.

5.4. Conclusions

It has been found that rotational symmetry of $(C_6)_nFe_{n-1}$ and $(C_6)_nRu_{n-1}$ metal-organic chains about the primary axis results in splitting of band zones near the Fermi level and introduces metallic properties in these systems. The second derivative of the band gap near the Fermi level is very small resulting in a low effective mass for both electrons and holes in these structures. At the same time, the magnitude of the first derivatives of the bands near the Fermi level were all nearly zero, implying that the electron density of states will be very high in this region. These characteristics suggest that cyclic C_6 and cyclic C_6 intercalated structures will exhibit high mobility combined with high conductance. Since the calculated energy bands cross the Fermi level at the edge (or in the center) of the Brillouin zone and a high density of electron states is found at these points called Van Hove singularity [100], these chains may exhibit superconductivity. However, despite these favorable properties, $(C_6)_nFe_{n-1}$ chains are unlikely to be superconducting because of the presence of relatively strong ferromagnetic interactions. This effect does not occur in $(C_6)_n Ru_{n-1}$ chains, and so these materials may be superconducting. The critical temperature in these compounds is expected to be 20-150 K.

CHAPTER 6

SUPERCONDUCTING PROPERTIES OF MOLECULES BASED ON STACKED CYCLIC C_6 AND C_6 INTERCALATED WITH SOME GROUP VIII TRANSITION METALS.

6.1.Introduction.

The classical microscopic theory of superconductivity of Bardeen, Cooper, and Schrieffer [114,119,174] (BCS), modified by Eliashberg [114,119,182,183,184,188,205] in terms of Green's functions still remains the only theory that can give more or less accurate numerical predictions of the properties of conventional superconductors. Also, there have been numerous studies exploring non-phonon mechanisms of electron interaction [114,119]. However, none of these yield quality predictions of superconductive properties for one-dimensional materials that agree with experimental results.

Although the Eliashberg version of BCS methods is an accurate model for most known superconductors, it is not effective in describing low-dimensional superconductors [177,186,187], especially those that are one-dimensional. In particular, all *ab initio* calculations of superconductivity in nanotubes [106-110,175] are in strong conflict with available experimental data. Many alternative mechanisms, including the exciton model [174], have been proposed to explain higher electron binding energy than that predicted by BCS. However, direct optical measurements of the electron-phonon coupling in CN [236] has been confirmed the pure phonon nature of the electron-electron interaction in CN. Interestingly, that in frame of BCS it was theoretically predicted [112] impossibility of the superconductivity in one-dimensional structures.

This prediction is based on the fact that the collective motion of electrons in one dimension does not behave as a Fermi liquid, but as a Tomonaga-Luttinger (TL) liquid [67-70], where charge and spin are carried by separate density waves. Specific properties of TL liquid and strong spatial confinement causes strong fluctuations that should destroy long-ranged order and possible coherent electron states [103,104].

In addition, there are several factors that weakening possible superconductivity in one dimension. Firstly, the density of electron states, as well as phonon states, per unit length is much lower than in bulk 3D materials, although the binding energy of the Cooper pairs depends on these densities of states. Secondary, quantum fluctuations lead to a strong increase in the effective Coulomb repulsion between electrons and a decrease in the electron-phonon interaction [178]. Finally, several recent studies [107,108] have confirmed that a charge density wave (CDW) should appear in one dimensional structures, especially in small radius nanotubes.

It seems, however, that the collective behavior of electrons in carbon nanotubes is not described by a TL liquid. This conclusion was based on the inconsistency between electron properties in NTs with those of a TL liquid. For example, the density of electron states at the Fermi level for a TL liquid should be zero, while in small diameter nanotubes the DOS is high enough to ensure the existence of the superconducting state. A CDW has not been observed in NTs. The electrons in NTs cannot be described in terms of a Landau Fermi liquid because the electron states are highly quantized. The states of conduction electrons near the Fermi level are formed from a superposition of a limited set of one-dimensional solutions. Some authors have proposed [113] that the collective motion of electrons in very small diameter NTs is a Landau Fermi liquid, with extra-strong fluctuations caused by confinement. The critical temperature in

one dimensional superconductors is completely determined by a balance between the strength of the fluctuations and the intensity of the enhanced electron-phonon interaction.

Despite these arguments, superconductivity does exist in one-dimensional structures and has been discovered in a broad class of polymers at high pressure [114]. Superconducting metal nano-wires have been described in numerous studies [115-118]. Superconductivity in small diameter nanotubes exists to a limiting diameter, and has been reported in nanotubes with diameters of nearly 4.2 Å [113], although in these systems, the electron-phonon interaction was depressed by quantum fluctuations. To explain superconductivity in one-dimensional structures it has to be assumed that the effective electron-phonon interaction is much higher than in the bulk material and is enhanced by some mechanism.

This chapter focuses on the superconducting properties of a new class of sandwich molecules, $(C_6)_nMe_{n-1}$, based on stacks of cyclic C_6 intercalated with Fe and Ru, as well as pure carbon molecules $(C_6)_n$. The estimation of superconductivity parameters is made from semi-empirical model by comparison of known superconductive state in 4Å carbon nanotube [113] with possible superconductivity in structures based on cyclic C_6.

6.2.Superconductivity in small diameter nanotubes.

There are several *ab initio* calculations of the superconducting properties of nanotubes using microscopic BCS theory [106-110,175]. Some of these have reported properties estimated from *ab initio* calculations that differ significantly from experimental data [109,175]. Indeed, most predict values of the critical temperature that are much lower than those seen in experiments [115]. The most accurate estimation of critical temperature T_c was derived by McMillan [174]:

$$kT_c = \frac{\omega_{\ln}}{1.2}\exp\{-\frac{(1+\lambda)1.04}{\lambda-\mu^*(1-0.62\lambda)}\} \quad (6\text{-}1)$$

$$\omega_{\ln} = \exp\{-\frac{2}{\lambda}\int_0^{\infty} d\omega\cdot\ln(\omega)\frac{\alpha^2F(\omega)}{\omega}\} \quad (6\text{-}2)$$

$$\lambda = 2\int_0^{\infty} d\omega\cdot\frac{\alpha^2F(\omega)}{\omega} \quad (6\text{-}3)$$

where ω_{ln} is a characteristic frequency, also called the logarithmic frequency, μ^* is the Coulomb pseudopotential, and λ is the mass-renormalization parameter, $F(\omega)$ - sum of phonon densities of states for all modes. It evident that ω_{ln} is averaged over the electron-phonon interaction. In studying the critical temperature for ultra-small diameter nanotubes [109] the Debye frequency is adopted as a characteristic frequency in the McMillan relation. However, this assumption is very imprecise because in most materials the electron-phonon interaction for optical phonons is negligibly small [179], while the frequency of acoustic phonons is much lower than the Debye frequency. This is especially true in carbon materials where the Debye temperature is often high, while dominant electron-phonon interaction is associated with relatively low-frequency breathing mode.

Another source of inaccuracy in these calculations is the uncertainty in the magnitude of the Coulomb pseudopotential. In conventional materials, the Coulomb pseudo-potential is typically $\mu^* = 0.1$. This value is frequently used in calculations [174] of superconductivity in nanotubes. Although, it was shown [107,108] that strong fluctuations in one-dimensional structures make contribution into effective magnitude of the Coulomb pseudo-potential should and it is grew. More precise calculations of the effective Coulomb pseudo-potential in small-diameter nanotubes [107,108] gives $\mu^*=0.16$. This dramatically decreases the calculated critical temperature.

The observation of superconductivity in carbon-based compounds was initially reported in graphite intercalated with alkali atoms (Cs, K), where the superconducting transition was observed between 0.2 and 0.5 K [189]. Much higher temperatures were found in alkali-doped fullerenes [190]. In all these experiments the system had to be chemically doped to observe superconductivity. However, chemical dopants were not present in the ropes of carbon nanotubes reported in [191-194]. For example, ropes containing 40 SWNT with a 1.2 nm diameter showed critical temperatures between 50 and 100 mK [191,192]. On the other hand, it has been found [191,192,194,195] that intentionally doped carbon nanotubes exhibit superconducting fluctuations at much higher temperature (up to 0.4 K).

Resistance measurements on arrays of multiwall boron-doped carbon nanotubes (MWNT) have been shown to exhibit a sharp drop in resistance near 12 K. These results have, however, been found to strongly depend on the way in which the nanotubes were connected, indicating that only small diameter internal shells were exhibiting superconductivity [197]. Superconducting fluctuations have been observed below 20 K in experiments on field-effect transistors made of individual gated undoped SWNT [198] contacted by superconducting electrodes. These fluctuations were found only for high gate voltages indicating that carrier doping was important in these systems.

The most amazing experiment on superconductivity in carbon nanotubes was reported by Tang [113] for a very small diameter (4.2 Å) SWNT grown in a zeolite matrix. The measured critical temperature was ~ 15 K and some superconducting behavior was found up to 20 K. The results of *ab initio* calculations of critical temperature in nanotubes are summarized in Table 6-1.

		Reference [106]				[107,108]				[110]				[109]				[175]			
(n;m)	diameter Å	λ	ω_0 cm^{-1}	μ	T_c K	λ	ω_0 cm^{-1}	μ	T_c K	λ	ω_0 cm^{-1}	μ	T_c K	λ	ω_0 cm^{-1}	μ	T_c K	λ	ω_0 cm^{-1}	μ	T_c K
(5;0)	3.9					0.57	840	0.19	1.1					0.58	972	0	57				
(4;1)	3.6																	1240	0	0.729	
(3;3)	4.1	0.156	665	0	3.60E-01					0.25	488	0	3.0								
(6;0)	4.7					0.12	480	0	0.071												
(4;4)	5.4	0.083	765	0	1.10E-03																
(5;5)	6.8	0.04	858	0	2.00E-09	0.03	1469	0	1.00E-12					0.04	972	0	3.00E-09	1240	0	9.23E-04	
(10;10)	13.6													0.014	972	0	2.60E-30	1240	0	6.46E-10	

Table 6-1. Results of *ab initio* calculations of superconducting properties for SWNTs with ultra-small diameter from different references. Here λ – mass-renormalization parameter, ω_0 – characteristic frequency, μ - Coulomb pseudopotential, T_c – critical temperature

Table 6-1 shows the general tendency for an increase in calculated critical temperature with a decrease in NT diameter. In this respect, it is significant that critical temperatures higher than 0.1K are seen only in nanotubes with diameters less than 4.2 Å. Only the (5;0) NT has a calculated mass-normalization factor λ strong enough to explain the experimentally observed critical temperature of 15 K although, the self-consistent value of the Coulomb pseudo potential μ =0.19 is relatively high, which reduces the calculated critical temperature to 1.1 K. Interestingly, the (5;0) NT should be semiconducting according to the graphene folding model described in Chapter 5. It has been shown [107,108] that due to the small diameter of this NT strong hybridization of the electron orbitals takes place, causing the conduction and valence bands to approach the Fermi level. Calculations using the zone-folding method give a HOMO and LUMO energy gap of 1.4 V, while direct calculations predict overlapping of the conduction

and valence bands by almost 1.6 V. This suggests that all nanotubes with diameters less than 5 Å may be conducting.

The exact phonon mechanism causing superconductivity in doped and undoped fullerenes and nanotubes is still under discussion [171] and there are two hypotheses regarding this question. One group of researchers [2,101,199-201] considers that electron coupling due to mediation of optical phonons is the only way to explain high critical temperatures in fullerenes and NTs. In contrast, De Martino and Egger [195,196] suggest that attractive interactions are mediated by low energy phonon modes specific to the structure of carbon nanotubes, in particular radial breathing modes (RBM). The important role of soft acoustic modes in superconductivity has been stressed by many researchers [174]. A comparison between the role of optical and acoustic phonons in superconducting models has been reported in [179,202].

Most of *ab initio* calculations of the superconducting properties of nanotubes using BCS theory omit the influence of fluctuations. It is especially important to include fluctuations in calculations of superconductivity in one-dimensional structures, since in BCS theory fluctuations destroy the superconducting state [176]. Fluctuations affect all aspects of the terms related to superconductivity, including the intensity of electron-phonon interaction and phase coherence in the superconducting state. The average fluctuation energy is comparable to that of the electron-phonon interaction. The Landau-Ginsburg formalism [179] included the effects of fluctuation, but this phenomenological theory cannot predict superconducting properties from first principles. To date, strong fluctuations as treated in the BCS theory have yielded even lower estimates of critical temperature. Therefore, some factors of enhancement of the common phonon exchange interaction may be needed to explain the mechanism of superconductivity in one-dimensional structures.

6.3. Estimation of superconductivity parameters for molecules based on cyclic C_6

The density of electron states and the electron-electron interaction potential V for small radius nanotubes is strongly dependent on radius as a result of orbital hybridization. Hence, the superconducting properties of ultra-small radius NTs depend primarily on radius. Thus, a first estimation of the superconducting properties of cyclic C6 structures should be based on free energy calculations [154,175,203]. First of all, the electron interaction potential V should be estimated. Analysis of the electron interaction potential, V, in NTs [203] shows that it can be divided as follows into one term that depends on radius and one that is constant:

$$V = V_{flat} + V_{curve}(\frac{R_0}{R})^2 \approx V_{curve}(\frac{R_0}{R})^2 \qquad (6\text{-}4)$$

where R, R_0 are NT radii, and V_{flat}, V_{curve} – components of electron interaction potential that corresponds to flat fullerene surface and curved. It is shown [203] that V_{flat} is negligibly small in compare with another component of potential. The average density of electron states at the Fermi level N(0) also depends on NT radius as follows [105]:

$$N(0) = C\frac{R_0}{R} \qquad (6\text{-}5)$$

where C is some constant

Thus, for any two small-radius nanotubes having different diameters:

$$\frac{N_1(0)V_1}{N_2(0)V_2} = (\frac{R_2}{R_1})^3 \qquad (6\text{-}6)$$

If the characteristic frequencies ω_1 and ω_2 are known, then:

$$\frac{\ln(kT_1/\omega_1)}{\ln(kT_2/\omega_2)} = (\frac{R_1}{R_2})^3 \qquad (6\text{-}7)$$

For comparison, we use the observed parameters for superconducting nanotubes [113]. These correspond to a critical temperature of 15 K and a diameter 4.2 Å. The characteristic frequency for structure $(C_6)_n$ we use calculated in Chapter 4 RBM frequency ω_0= 840 cm^{-1}, while characteristic frequency for conventional CN with diameter 4.2 Å is nearly 600 cm^{-1}. Substitution to equation (6-7) gives us upper limit of estimation of the critical temperature in $(C_6)_n$ structure. In this model the critical temperature approaches $T_c \approx 85$ K.

Metal-organic structures such as $(C_6Ru)_n$ have unit cells that are nearly twice as long as those in $(C_6)_n$ structures. Thus, $(C_6Ru)_n$ is essentially a $(C_6)_n$ structure with half the C_6 rings replaced with Ru atoms. To estimate the critical temperature in this compound, it should be estimated increasing of DOS due to intercalation by ruthenium. The DOS estimation is taken from data on intercalated fullerenes [203]. While in pure carbon structures DOS is nearly 0.20 [105], the intercalation by ruthenium increase this figure up to 0.33. Under these conditions, the semi-empirical equation (6-4) gives estimation of upper limit of the critical temperature $T_c \approx 210$ K.

6.4. Conclusions.

The estimation of the superconductive critical temperature in structures based on cyclic C_6 is calculated from semi-empirical model. The calculated values are over estimated, because they do not take into account stronger spatial confinement in smaller diameter nanotubes. Confinement causes increasing of fluctuations that leads to increasing of the effective the Coulomb pseudo potential and screening of electron interaction potential.

CHAPTER 7

EXPERIMENTAL ATTEMPTS TO SYNTHESIZE MOLECULES BASED ON STACKED CYCLIC C_6 DURING LASER IRRADIATION OF ORGANIC LIQUIDS WITH FEMTOSECOND LASER PULSES

Experimental part of my work devoted to practical attempts to create structures that are studied theoretically in previous sections. It was supposed that creation of structures based on stacks of cyclic C6 by dehydrogenation of benzene in process of irradiation with ultra-short high intensity laser pulses. This method is promising because of the well-known dehydrogenization of organic substances during irradiation with femto-second laser pulses, performed in our lab, and by other research groups [163,14]. For example, under these conditions, dehydrogenization of benzene is expected along with the formation of cyclic C_6 radicals which may self-assemble into $(C_6)_n$ stacks. In the liquid phase, a combination of high temperature, high pressure and plasma should enhance the synthesis of new carbon compounds. In addition, the ultra-short duration and high intensity of the laser pulses will produce nonlinear optical interactions that facilitate a high rate of ionization and the synthesis of new substances.

To study metal-organic species such as $(C_6)_nFe_{n-1}$ ferrocene, $(C_5H_{10})_2Fe$, was dissolved in liquid benzene. The presence of iron is expected to enhance the absorption of laser energy and result in the immediate dissociation and ionization of ferrocene molecules leading to reaction with benzene.

7.1. Generation of carbon nanoparticles and synthesis of organic molecules by irradiation of liquid benzene with high-power femtosecond (fs) laser pulses.

7.1.1. Introduction

The possible formation of carbon compounds based on stacked cyclic C_6 or similar structures was studied in several experiments involving fs laser irradiation of liquid benzene, toluene, benzene-d6, and acetone. Facile generation of carbon nanoparticles was only observed in liquid benzene at laser pulse energies between 0.2 to 2.2 mJ [122]. This observation can be explained [123] by a coincidental correspondence between the third harmonic of the 800 nm laser light and absorption of π-bonds in benzene. Another optical effect that is observed in experiment is strong filamentation at the laser beam. Enhanced filamentation of fs laser pulses (λ=780-810 nm) in liquid benzene can be explained by positive changes in the refractive index due to excitation of the $\pi \rightarrow \pi^*$ resonance absorption via the third harmonic. Filamentation is accompanied by active defragmentation of benzene molecules, the creation of carbon nanoparticles and the synthesis of other organic species. Generation of carbon nanoparticles in this process is critically dependent on the intensity of the third harmonic in the filament and it is suggested that the third harmonic remains coupled to the original laser filament.

In these experiments irradiation of liquids was carried out using high power (10^6-$5 \cdot 10^8$ W/cm^2) femtosecond pulses. As shown below, the laser wavelength corresponds to the resonant absorption of the third harmonics (TH). This leads to an enhancement of the real part of the third order susceptibility and is responsible for both nonlinear optical processes and for the generation of nanoparticles. The presence of the TH filament, coupled to the initial light filament,

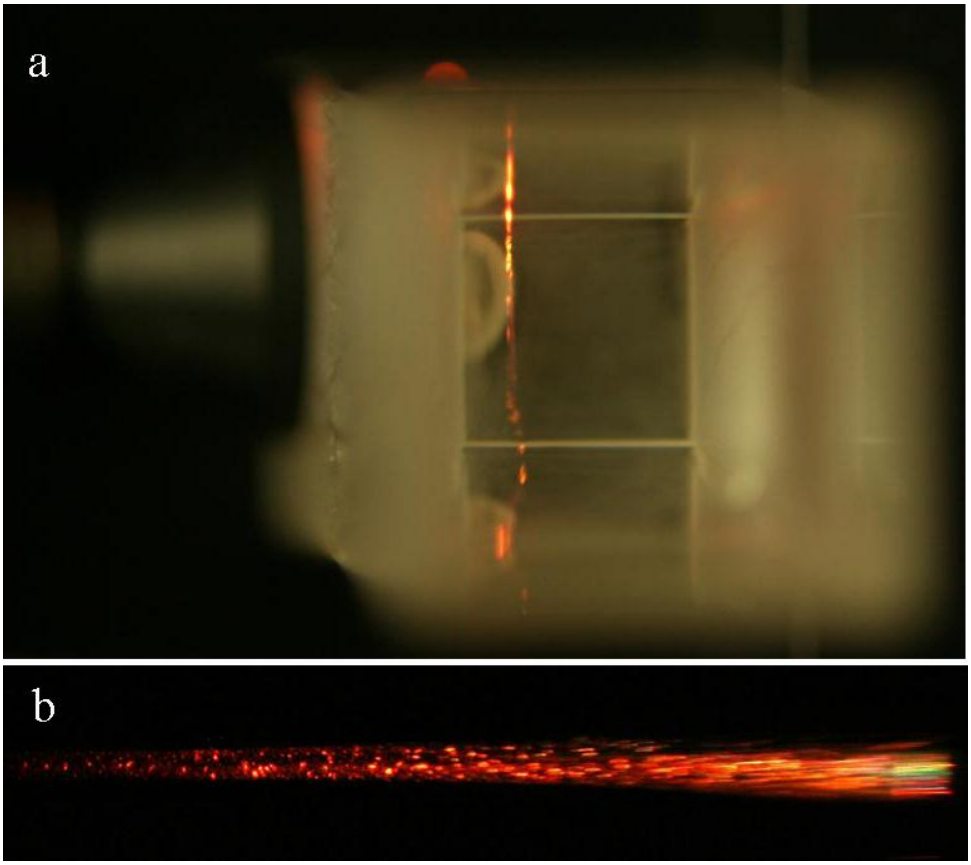

Fig.7-1. Irradiation of liquid benzene by fs laser pulses a. Laser filamentation in liquid benzene (top view). Photo exposure 1/2 s. b. Microphotograph of the light filament for one laser pulse. Bright spots here are multi-focus points. Photo exposure 1/1000 s.

increases the nonlinear interaction resulting in additional focusing. Fig.7-1 shows images of laser filamentation in benzene during irradiation.

Experiments were carried out using radiation from a Ti:Sapphire femtosecond laser. The laser pulses with duration 30 fs and repetition rate 1 kHz had pulse energies between 0.2 and 2.2 mJ. This corresponded to an intensity in the focal spot of up to 10^{18} Wcm^{-2}. The output band extended from 780 to 810 nm. The overall spectrum of the laser output together with the TH and the absorption band in benzene are shown in Fig.7-2.

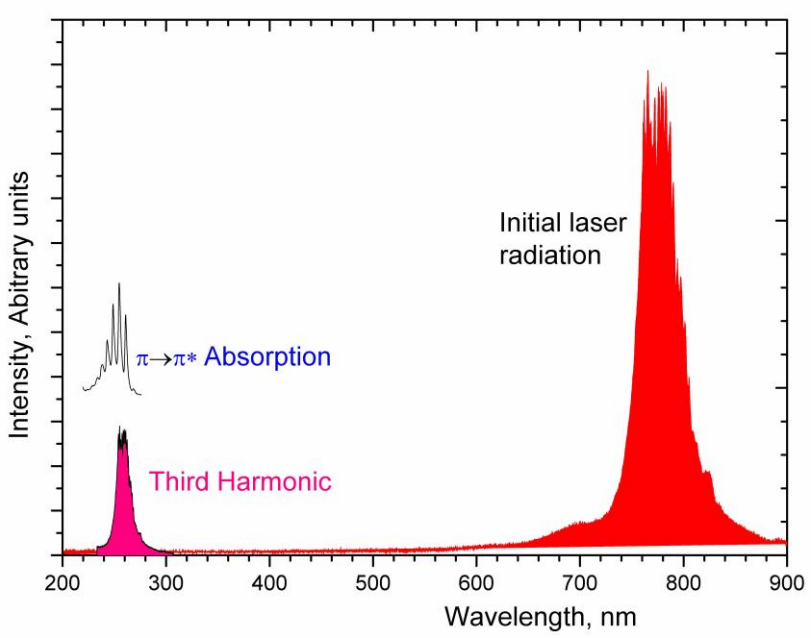

Fig.7-2. Plot of the initial laser spectrum, the spectrum of the third harmonic (TH) and the absorption band π→π* in liquid benzene.

Liquid benzene was irradiated in cuvettes with a square section (1×1 cm) made from quartz and optical glass. Pure benzene 99.8% (Sigma-Aldrich Corporation) was used. Electrodes for measurement of the photocurrent were made from 0.2x4x40 mm stainless steel plane plates placed parallel to each other. The electrodes could be adjusted so that the beam was parallel to the electrodes. The focal distance was 4 cm.

In homogeneous media, second order nonlinear optical processes are weak [206] and there is a very low probability for two photon processes compared to resonant excitation of the π→π* transition. These aspects of the interaction in benzene can be seen from measurements of the photocurrent generated during irradiation. A study of the photocurrent was initiated to clarify some aspects of the dynamics involved in the creation of nanoparticles. It was found that the mass of synthesized molecules can be estimated from the decay of the photocurrent.

Numerous studies of the photocurrent and photoionization in liquid and gas benzene [207-210] have been reported for a variety of laser pulse durations, incident power and laser wavelength. Multiphoton ionization is the dominant term in most of these measurements, but those reported here are the first that study an ionic photocurrent induced by nanoparticles generated by laser irradiation. The efficiency with which nanoparticles are produced is so high that currents can be observed with an electric field of 150-170 V/mm compared with the 1-9 kV/mm field used in other measurements.

7.1.2.The nonlinear optical process during enhanced filamentation in media with resonance absorption of the third harmonic.

Filamentation of femtosecond laser pulses in homogeneous condensed media such as gases and liquids is well known [211-216]. A general feature is an absence of the second harmonic, because the second order nonlinear optical interactions vanish in centro-symmetric media [206]. Another feature is the generation of the strong third harmonic (TH) and existence of strong TH filament that is coupled to the filament of the initial light [217]. It has been shown [211] that the intensity of the TH filament is nearly proportional to the intensity of the filament produced by the original wavelength. The coupling of the initial and TH pulses is caused by cross-phase modulation of the refractive index, imposing a constant phase difference inside the two-coloured filament.

The filamentation and other nonlinear optical phenomena in the present experiment can be described in terms of the third order optical susceptibility $\chi^{(3)}$ [206]. Several specific nonlinear third order processes are related to different components of this susceptibility. For example, self-focusing of the initial light and TH pulses is described by $\chi^{(3)}(\omega+\omega-\omega=\omega)$ and $\chi^{(3)}(3\omega+3\omega-3\omega=3\omega)$ respectively, while generation of the TH is described by $\chi^{(3)}(\omega+\omega+\omega=3\omega)$. Parametric

amplification of the third harmonic by the initial light is given by $\chi^{(3)}(3\omega+\omega-\omega=3\omega)$ and the parametric amplification of the initial light by the TH is related to $\chi^{(3)}(\omega+3\omega-3\omega=3\omega)$. The theory of nonlinear optics [206] tells us that the susceptibility $\chi^{(3)}(\omega+\omega-\omega;\omega)$, responsible for self-focusing of the initial light, increases in the presence of the third harmonic.

The semi-classical equation for susceptibility of the third order for low-intensity light [206] is

$$\chi^{(3)}(\omega_1+\omega_2+\omega_3=\omega_4)=K\prod_{j=1}^{4}\frac{1}{\omega_{res}{}^2-\omega_j{}^2+i\delta\omega_j} \qquad (7\text{-}1)$$

Here K is a constant; ω_{res} is the resonance frequency and δ is the absorption coefficient. When one of the ω_j is close to the resonance frequency ω_{res}, then the susceptibility has a high value for both real and imaginary parts. This causes an enhancement in third order nonlinear effects and with high absorption at the resonance frequency. In the case of high intensity light with saturation, the absorption is given by:

$$\alpha=\frac{\alpha_0}{1-I/I_s} \qquad (7\text{-}2)$$

where α_0 is the absorption coefficient at low-intensity, I is the light intensity, and I_s is the saturation intensity. Thus, when the intensity of light becomes higher the absorption coefficient decreases. A TH filament appears only when the generation of the TH in the laser pulse overcomes absorption. If there is strong absorption at the TH, then a TH filament cannot exist. In addition, the TH filament makes contribution to the nonlinear index of refraction for the initial light, but only the real part of the susceptibility $\chi^{(3)}(\omega+3\omega-3\omega=\omega)$ is responsible. Hence, there is feedback between the intensity of the initial light and that of the TH.

The overall picture of filamentation in benzene is then as follows: initially laser light is self-focused to form a filament, as a result of the third order susceptibility. The third order susceptibility is also responsible for TH generation. Due to saturation of the $\pi\rightarrow\pi^*$ band

absorption near the resonance frequency, absorption at the TH wavelength decreases while the real part of the third order susceptibility is still very high. This effect causes filamentation of the TH coupled to the initial light wave. TH filament also influences the optical conditions for the light filamentation at 800 nm through the parametric process. In regular media this process is negligibly small, but in benzene this process is determined by the real part of the resonance magnitude of the third order susceptibility $\chi^{(3)}(\omega+3\omega-3\omega = \omega)$ which becomes large near resonance.

The linear part of the refractive index can be calculated through the Kramers-Kronig relation that connects the real and imaginary parts of optical parameters. The equation that connects changes in absorption with changes of linear refractive index is [206]:

$$\Delta n(\omega) = \frac{\omega}{\pi c} \int_{-\infty}^{\infty} \frac{\Delta\alpha(\omega')}{\omega' - \omega} d\omega' \qquad (7\text{-}3)$$

where α is the absorption coefficient.

The measured value of the wavelength dependent absorption coefficient for the $\pi \rightarrow \pi^*$ band in benzene was used in these calculations [218-220]. The resulting modification of the refractive index due to excitation of the $\pi \rightarrow \pi^*$ band is shown in Fig.7-3, along with the absorption band corresponding to the $\pi \rightarrow \pi^*$ band. Comparing the spectral distribution of the TH spectrum with that of refractive index, (Fig.7-3) shows that changes in the refractive index has a sharp positive peak with a width of ~ 50nm at the edge of the "blue" side of the TH spectrum. The maximum of this peak corresponds to λ = 253 nm. Absorption at this wavelength is important in the filamentation produced by generation of the TH and this resonance explains why filamentation in liquid benzene is much more intense than that observed in other organic liquids, and why.

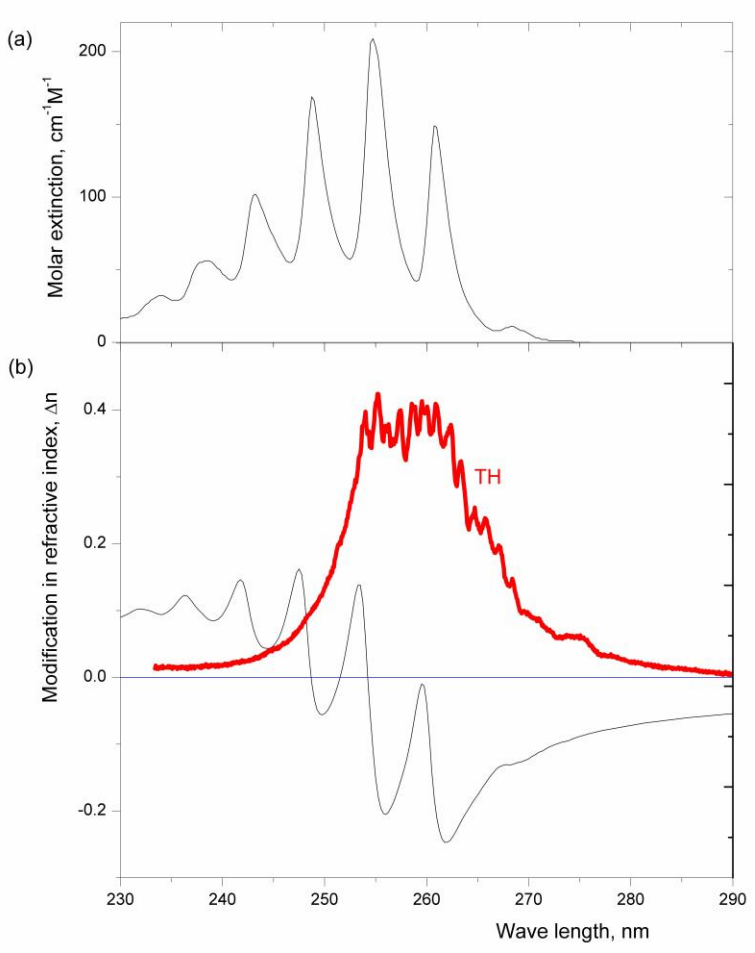

Fig.7-3. Spectral profile of (a) absorption in π→π* band in liquid benzene; (b) modification of the refractive index due to excitation of the π→π* and in liquid benzene

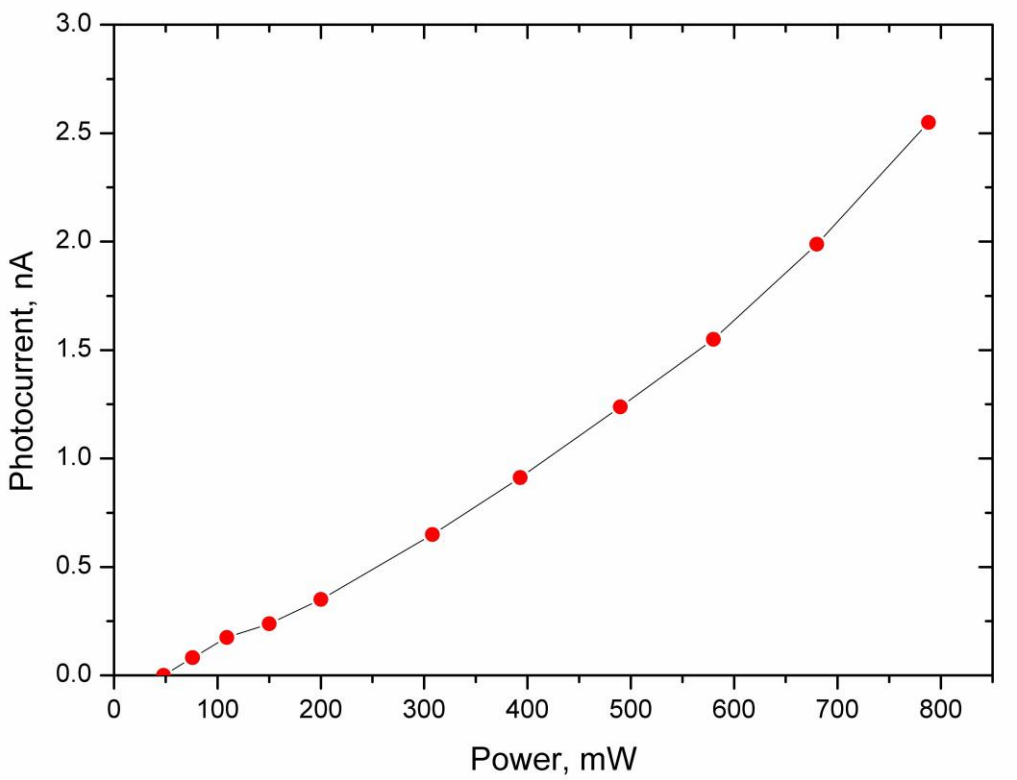

Fig.7-4. Dependence of the ionic photocurrent vs. power of the laser

nanoparticles are detected only in liquid benzene. The small spectral shift in deuterated benzene (C6D6) eliminates this resonance preventing the generation of nanoparticles

The presence of a TH filament can be detected through the presence of the photocurrent carried by nanoparticles generated in this interaction. The dependence of this photocurrent on laser power is shown in Fig.7-4. A threshold photocurrent is clearly seen near 50 mW corresponding to 50 μJ/pulse. This can be identified with the threshold intensity of the initial light requires to initiate TH generation and the production of carbon nanoparticles.

7.1.3. Generation of carbon nanoparticles and synthesis of molecules during enhanced filamentation in benzene.

Experiments on irradiation of liquid benzene by femto-second laser pulses shows that carbon nanoparticles were observed in solution after 10-20 minutes. A similar result has been reported by Nakamura et al. [121]. They report the creation of carbon nanoparticles with an average size of ~ 10 nm after irradiation of benzene with 100 fs laser pulses at a pulse energy of 5 mJ. Fig. 7-5 shows the appearance of benzene after 30 minutes irradiation. An Atomic Force Microscope (AFM) image of the carbon precipitate is also shown in this figure. It is clear that irradiation generates carbon nanoparticles with sizes between 4 and 15 nm.

Many studies have been reported on the analysis of the decomposition products of benzene exposed to high intensity laser pulses [210,231]. The most detailed analysis of this process, with all possible ways of benzene defragmentation in vacuum can be found in [231]. Very few papers describe the decomposition of benzene in the liquid state [210,221-230,233], although the physical conditions of laser irradiation in the gas and liquid states are dramatically different. For example, it has been shown [232] that ultra-short laser pulses (100fs) with an energy of 100 nJ can cause significant heating in the focal region and formation of a plasma. This leads to the creation of a shock wave front that expands out of the focus region. The pressure in the shock wave can reach 1 TPa. Combined with a temperature exceeding 104 K, this results in molecular decomposition and the synthesis of new compounds. In such experiments, the intensity of light is > 1018W cm-2. Irradiation in a gaseous state leads to total decomposition and the formation of

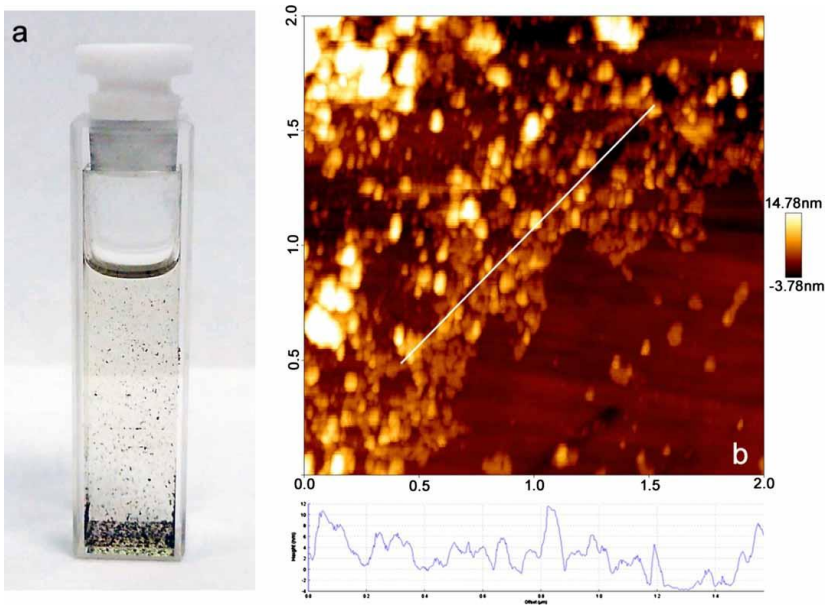

Fig.7-5. Precipitates form in benzene (a) when it is irradiated by fs-laser pulses and are composed of agglomerated polydispersed nanoparticles (b) as seen by AFM. The inset shows the cross-sectional height profile of the white line in the 2 µm by 2 µm micrograph. This Figure is taken from paper [122]

positive ions, while the irradiation of the liquid leads to the synthesis of new chemical compounds. In this case, ionization gives nearly equal quantity of positive and negative ions that also stimulates synthesis. The generation of carbon nanoparticles and growth of polyyne chains have also been reported [122]. Our experiments may also show some evidence for the formation of fullerenes [122]. Fig.7-6 shows an AFM image of a tubular structure that could be interpret as fragment of a carbon nanotube with a diameter of ~ 20 nm. A wide range of different organic molecules are also synthesized during these experiments.

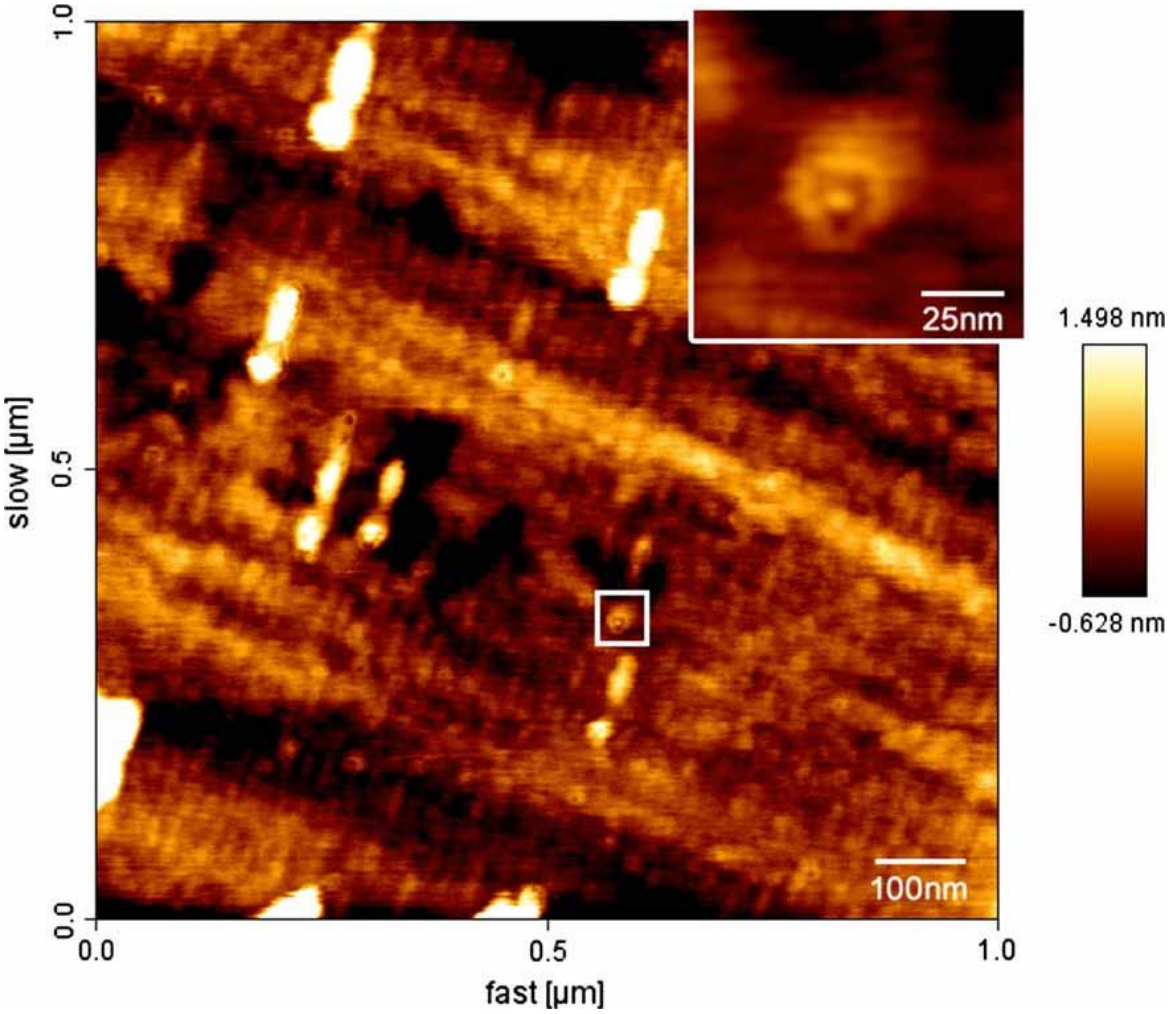

Fig.7-6. Atomic force micrograph of the smallest nanoparticles created by the irradiation of benzene with fs-laser pulses. The inset is a magnified image of the toroid particle contained by the white square. This Figure was copied from [122].

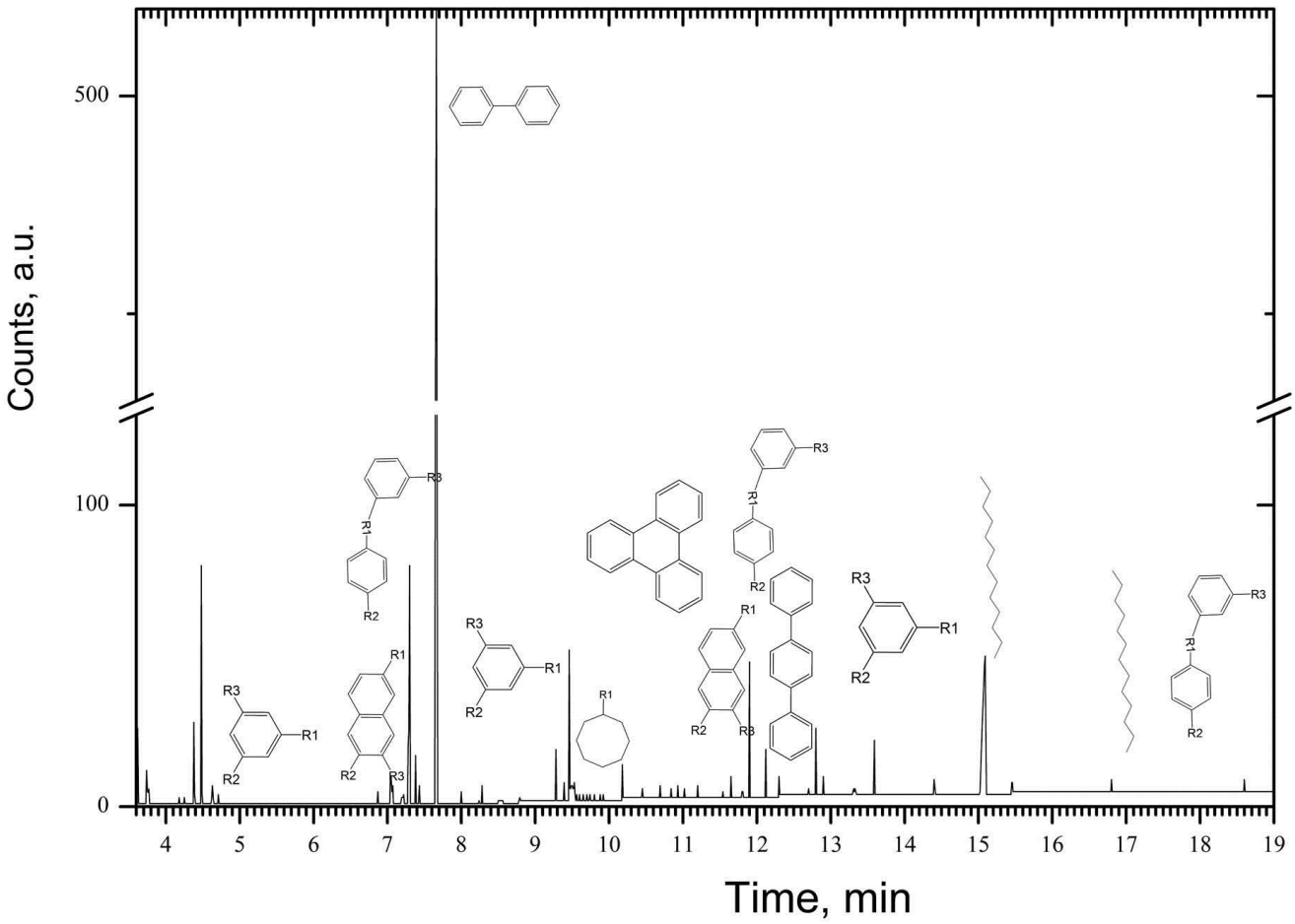

Fig.7-7. A GC/MC chromatogram of substances synthesized in benzene irradiated with femtosecond laser pulses in pure benzene. The chemical structure of some molecules is shown.

From an electrochemical point of view the process of fragmentation in liquid benzene is fundamentally different from that in the gas phase. In the gas phase ionization results primarily in the formation of positive ions while, in the liquid, similar quantities of positive and negative ions are produced. This equality is confirmed by equal quantity of deposited substance on both the cathode and anode electrodes.

Organic compounds formed as a result of irradiation have been studied using gas chromatography. Samples were collected after 30 min irradiation of benzene by laser pulses at pulse energy of ~ 1 mJ. To purify the sample extracted material was centrifuged and filtered through ~ 1 micron pores. Gas chromatography was combined with mass spectroscopy (GC/MS) in a Agilent 5975B inert Series GC/MS System. The GC/MS study shows that ~ 57 different organic compounds can be identified after laser irradiation of liquid benzene.

A comparison of the mass-spectrum of these compounds with standard data base shows that most of them can be identified with standard chemicals. Nearly all of these compounds contain one, two, or three benzene rings connected with chains. The resulting chromatogram is shown in Fig.7-7, together with some identified compounds. As expected, the largest fraction corresponds to biphenyl. The number of counts for biphenyl was nearly equal to the counts of all other species. This can be understood since the laser ionization of benzene liquid gives nearly the same amount of positive and negative ions, so they are naturally combined in biphenyl.

Table 7-1 summarizes some of these compounds. In addition to molecules formed from carbon and hydrogen there were also some involving oxygen and nitrogen. These apparently involves reaction with air. A small amount of silicon and chlorine in some compounds appears from chemical reactions at the walls of the cuvette. It has also been shown [49] that, during

irradiation of benzene with fs laser pulses, polyyne chains can also be formed. These may contribute to bridging groups in the present products.

Another series of experiments was designed to study the ion photocurrent during laser irradiation of liquid benzene. This information provides an estimation of the dynamics of nanoparticle generation, and the mass of ions formed during irradiation. For example, by measuring the relaxation time of different photocurrent components, one can estimate the ion mass spectrum. The connection between the self-diffusion coefficient of an ion and the average velocity of the ion is determined by the Einstein equation [235]:

$$\nu = \frac{eDE}{kT} \tag{7-4}$$

where D is the diffusion coefficient, and E is the electric field. Thus, the expression for an ion created just in the center between the two electrodes is:

$$\frac{d}{2\tau} = \frac{eDU}{kTd} \tag{7-5}$$

where τ is the drift time, e is electron charge, and U is the applied voltage. The simple hard sphere model [234] shows that the diffusion coefficient is proportional to $m^{-1/2}$ where m is the mass of the molecule. The diffusion and mass of an unknown ion can be now compared with these quantities for:

$$D\sqrt{m} = D_{benz}\sqrt{m_{benz}} \tag{7-6}$$

Nomenclature	Quality probability	Arbitrary counts
biphenyl	96	510
benzene, (1,4 –cyclohexadien-1-yl)	96	95
tetradecanamide	87	54
5-phenylcyclohexane-1,3-dione	38	50
2-propenoic acid, pentadecyl ester	91	50
13-docosenamide	91	50
phenol	91	46
p-terphenil	98	30
9- octadecanamide	93	30
benzaldehyde	95	28
phenylethyne	94	26
phthalic acid, 2-ethylhexyl tridecyl ester	50	22
silane [[4-[1,2-bis[(trimethylsilyl)oxy]ethyl]-1,2-phenylene]bis(oxy)]bis trimethyl	53	18
styrene	94	12
naphthalene, 2-methyl	80	12
benzene, 1,4-diethynyl	80	10
2,5 –cyclohexadien-1-yl	93	10
benzene, 1-propynyl	90	8
o-terphenil	93	8
acetophenone, 2-chloro	72	7
furan, 3-methyl	64	7
p-xylene	90	6
4-phenylbut-3-ene-1-yne	50	5
cinnamaldehyde	90	5
2,4,6-triazatricyclo[5,2,2,02,6]undec-8-ene—3,5-dione, 4-methyl-1,7-diphenyl	87	5
all-trans-1,6-diphenyl-1,3,5-hexatriene	64	5
1,4-ethenonaphtalene-1,4-dihydro	76	5
1,3,5,7-cyclooctatetraene	68	5
benzene, 1-ethenyl-3-metyl	58	3
1,2-benzenecarboxylic acid, butyl 2-ethylhexyl aster	64	3
1,1'-biphenyl,2-methyl	96	3
naphthalene	86	3

Table 7-1. A partial list of synthesised organic molecules that were identified with probability > 50%. The data is arranged in descending order of arbitrary count number.

Thus, the ion mass becomes:

$$\frac{m}{m_{benz}} = \left\{ \frac{2eD_{benz}U\tau}{kTd^2} \right\}^2 \qquad (7\text{-}7)$$

In benzene the self-diffusion coefficient $D_{benz}=2.398\cdot10^{-5}$ cm^2/s [104]. This equation is not precise, because the diffusion coefficient for different organic molecules also depends on molecular shape, chemical properties, and the effective radius. However, using this relation the mass spectrum of molecules involved in the ion photocurrent can be estimated.

The relaxation time of photocurrent could be determined only when it was > 1 second. This corresponds to a mass of ~ $1.4\cdot10^3$ carbon atoms. The experiments also showed two different relaxation times. The first, or "fast" component ranged between 1.5 and 10 seconds. The other slow component lasted for 30-60 minutes. The shortest relaxation time was 1.5 s, which corresponds to clusters having ~ $2\cdot10^3$ carbon atoms and sizes ~ 1.3 nm agreeing with the smallest carbon nanoparticles observed (Fig 7-5) [121,122]. The longest relaxation time (50-60 minutes) corresponds to large nanoparticles with masses of up to 10^9 atoms and with sizes of ~ 300 nm. SEM observation clearly show fullerene-like particles with sizes of ~ 25 nm, as well as large clusters aggregated from smaller nanoparticles.

The dependence of relaxation time on laser power is shown in Fig.7-8. It is apparent that small carbon clusters seem to grow in size with increasing laser power they reach some limiting size. A strong spatial dependence of the photocurrent was also found (Fig.7-9) which reveals that the current is highest when the focus is closest to the wall of the cuvette. This shows that the

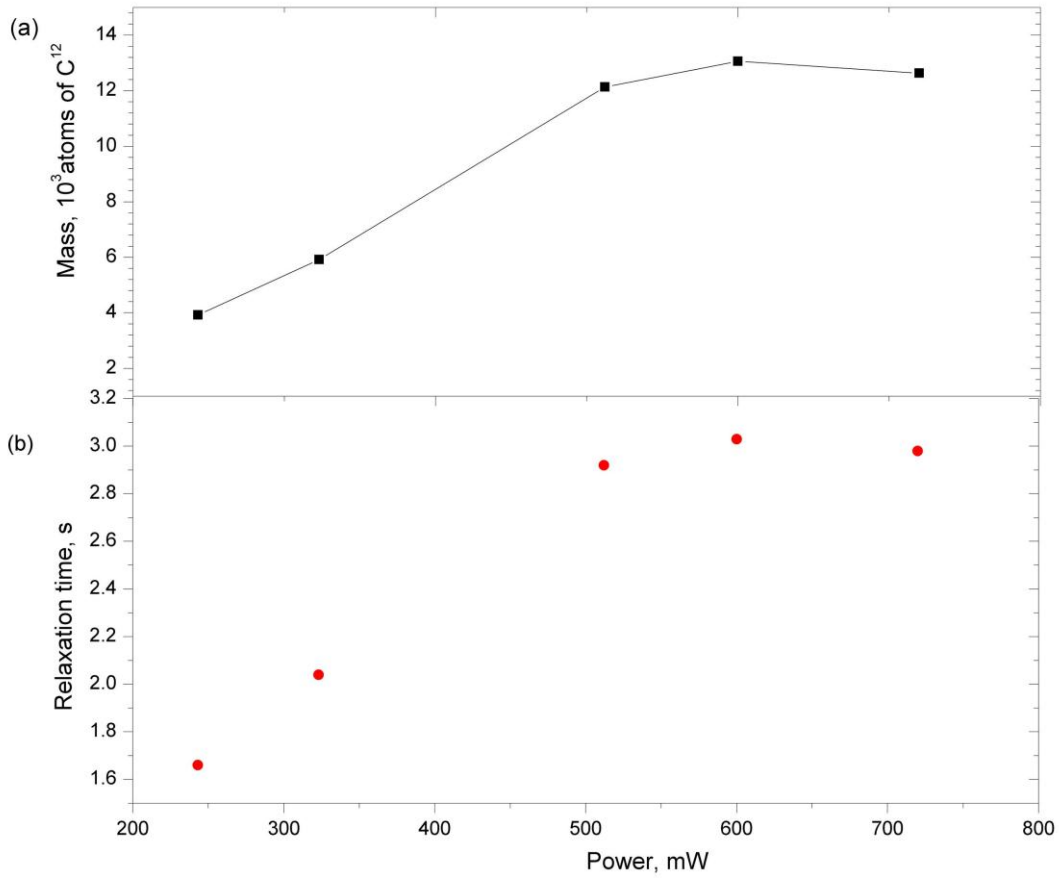

Fig.7-8. Dependence of relaxation time on laser power (a) Estimated number of the carbon atoms in ion nanoparticles (b) Relaxation time

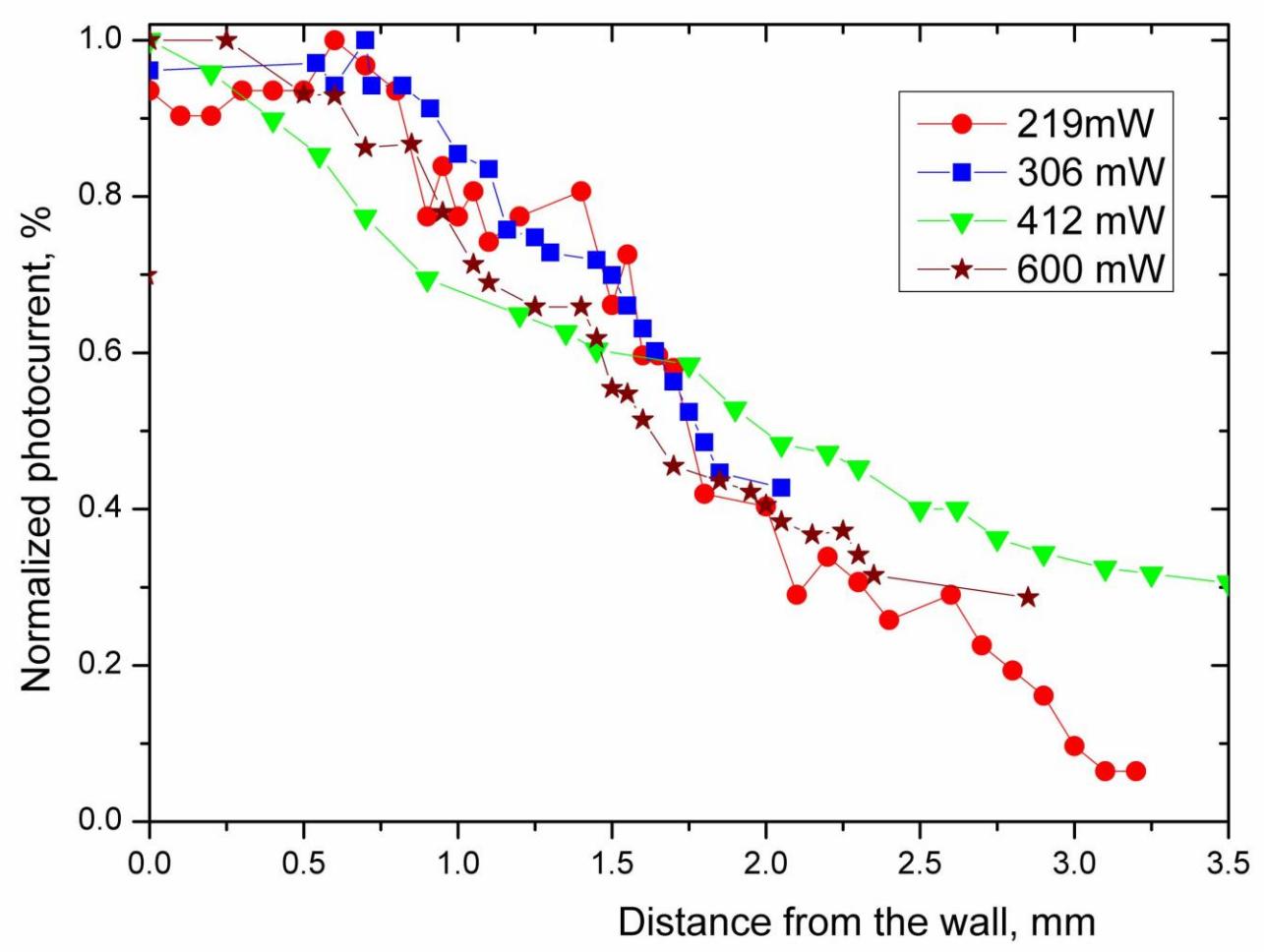

Fig.7-8. Spatial dependence of the ion photocurrent vs. distance of the focus point from the wall of the cuvette

strength of TH filament depends on the value of the TH in the initial (focus) point of filament. This effect can be explained by the fact that the conditions for TH generation are optimized near the wall. This effect might arise from reflection of the shock wave from the wall. Another explanation may be related to the existence of another TH component near the wall, generated as the laser light passes through the wall.

7.2. Formation of metal-organic nanoparticles by laser irradiation of ferrocene in liquid benzene.

In order to try to synthesize sandwich metal-organic molecules such as $(C_6Fe)_n$ the experiment was changed to permit the irradiation of ferrocene/benzene solutions with high-power fs laser pulses. It was hoped that this would yield evidence for structures based on cyclic C_6 rings. Ferrocene, $(C_5H_5)_2Fe$, was chosen as a source of atomic iron as it consists of two cyclopentadienyl (Cp) rings with an iron atom between them combined in a sandwich structure. Ferrocene is a very stable compound that is used as a stabilizing addition for fuel and explosive materials. At room temperature, ferrocene exists in a crystalline state in the form of large bright orange crystals. It also has excellent solubility in benzene. The iron ion in ferrocene absorbs over a range of visible and ultraviolet wavelengths. High intensity laser light should dissociate the ferrocene molecule into atomic iron and some carbon fragments resulting in the subsequent synthesis of some metal-organic compounds possibly including cyclic C_6 and Fe.

In our experiments the optical conditions for laser irradiation of the solution of ferrocene $(C_5H_5)_2Fe$ in benzene are quite those in pure benzene. Pure liquid benzene is highly transparent at the laser wavelength near $\lambda \approx 0.78$ μm, while the absorption of laser radiation in ferrocene

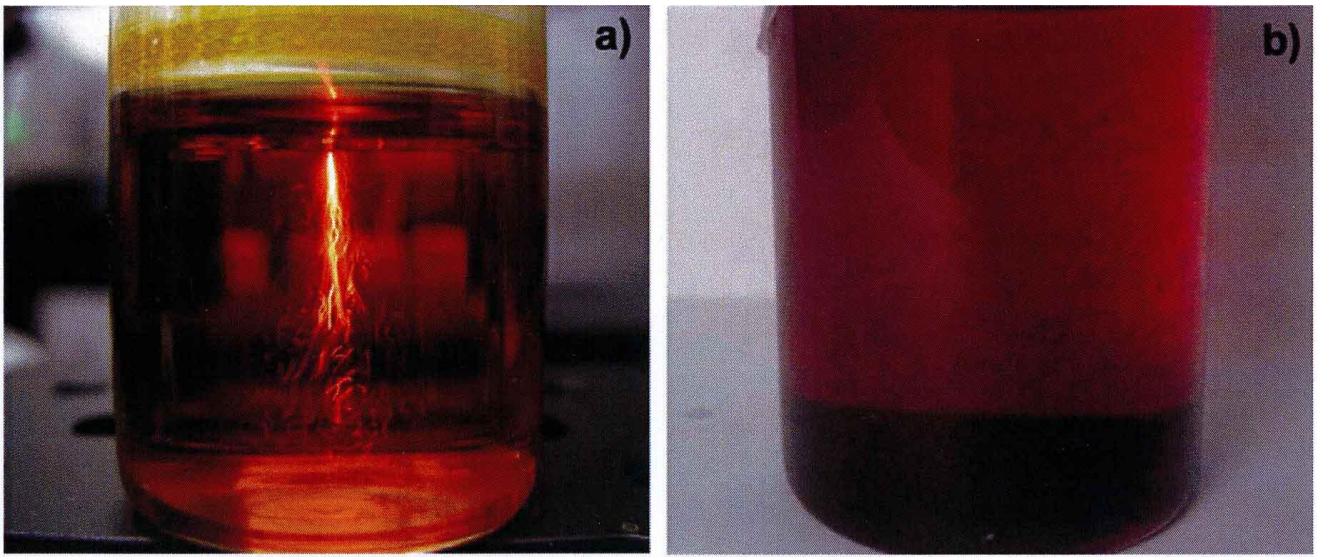

Fig.7-10. Irradiation of a ferrocene/benzene solution with fs laser pulses: a) irradiation from the top; b) resulting product of irradiation after ~ 1hour. The Figure is taken from [47]. The laser pulses had a duration of 30 fs and the repetition rate was 1 kHz. The pulse energy was varied from 200 μJ to 2.2 mJ. Different concentrations of ferrocene solution were used up to the solubility saturation of 0.2 g/ml. The typical concentration of ferrocene was 0.1 g/ml. The solution of the ferrocene in benzene has a deep red to yellow color that depends on concentration.

solution is extremely high. As a result, laser irradiation of ferrocene dissolved in benzene produces a different response. In benzene self-focusing is observed along the laser beam (Fig.7-1), but this is replaced by a series of micro-explosions in the ferrocene solution (Fig.7-10).

The irradiation of the solution was made from the open top of the cuvette downwards. The position of the focus point typically was located near the surface of the liquid inside the solution. In the region near the focus, one could observe small bubbles of boiling benzene. In most of the experiments an orange aerosol was observed. This aerosol consisted of microcrystals of ferrocene. The solution began to change color immediately after beginning irradiation, and

gradually became darker and more opaque (Fig.7-10). After ~ 10 min one could see a suspension of dark particles. When shaken, this suspension formed a uniform emulsion, but after 10 minutes, the suspension would appear again. This suggests that small nanoparticles conglomerated into large clusters that could be observed with the naked eye.

Bright shiny sparks appear from the focus and move down into the liquid. These are seen as bright streaks in Fig 7-10, and appear to be plasma balls where molecular ionization and dissociation have taken place. Single laser pulses having an energy of ~ 1 mJ focused into a ~1 μm spot can produce an energy density of ~ 10^{12} J/m^3 producing strong plasma formation and heating.

7.2.1. The study of nanoparticles created by irradiation of ferrocene solution

As in the previous experiments, insoluble nanoparticles produced by irradiation were centrifuged and then filtered through a glass filter with ~ 1 μm pores. The chemical composition of this sample was compared with that of a ferrocene solution that had not been irradiated. GC/MS did not find that there were any differences in chemical composition between these two samples, and so it can be concluded that all the reaction products were insoluble. As a result, insoluble particles could be easily separated from the irradiated ferrocene solution.

The morphology of nanoparticles was studied with a scanning electron microscope (SEM). Samples were washed in pure benzene to remove any traces of ferrocene and were then deposited on a silicon substrate. A number of different nano and micro-particle morphologies were identified (Fig.7-11). One of these was a dark porous substance that consists mostly of carbon with a 3-5% iron concentration. Fig.7-11.a shows this material in the form of bright

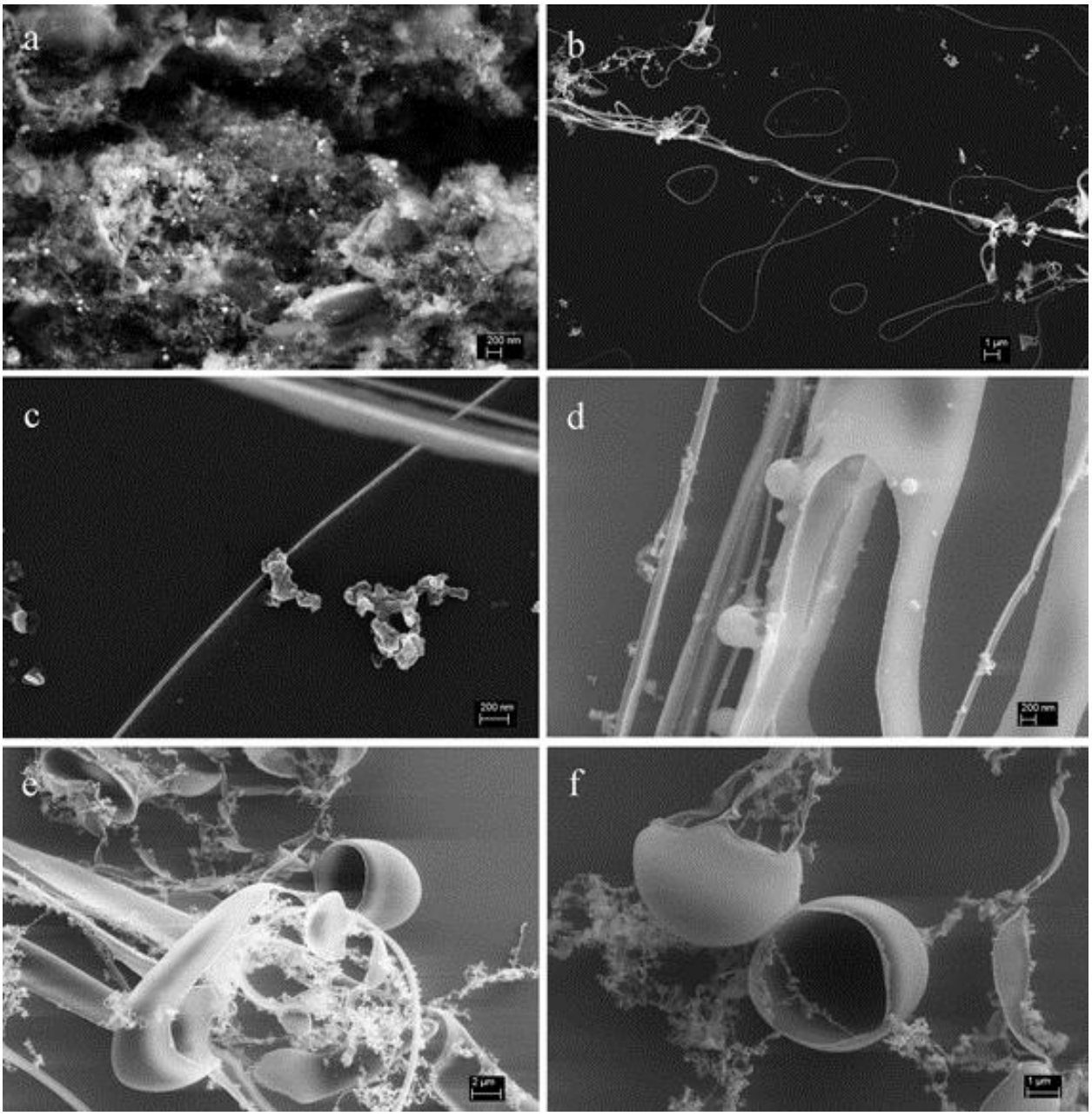

Fig.7-11. Nanoparticles of different morphology produced by laser irradiation of ferrocene solution (The final product was washed off ferrocene). Figures b-f were taken from [47]

inclusions. A range of carbon nanofibers (Fig.7-11.b.), nanotubes (Fig.7-11.c.), ribbons (Fig.7-11.d.) and shells (Fig.7-11.e and f) were also found. The iron content in these substances was found to vary from 3-20%. Previous studies of ferrocene pyrolysis [160] have reported similar structures. During ferrocene pyrolysis iron atoms act as catalysts to facilitate the self-assembly of carbon NTs. We also observe carbon shells, (Fig.7-11.e and f) that have apparently not been previously observed. Nanofibers can form closed loops (Fig.7-11.b) and the conditions under which these unusual structures form needs further clarification.

The laser used in these experiments produces a beam with a gaussian profile. The laser beam is incident from the top of the cuvette perpendicular to the surface of the liquid and was focused a few millimeters below the solution surface. As a result of focusing, strong absorption takes place near the focal point, but absorption also occurs in the surrounding volume. It would appear that the hemispheres seen in Figs.7-11e and f are initially formed in the region where the beam has highest intensity, as the size of these hemispheres (1-2 μm) corresponds to the dimension of the focal region. It is postulated that, in this region, high laser intensity leads to ionization and decomposition of all molecules generating a plasma ball. The asymmetry of the focal region leads to an asymmetrical thermal expansion and ejection of the plasma ball downwards into the liquid. The hemisphere shell is likely formed at the outer boundary of this plasma ball.

The entire region above the focal point is exposed to high intensity laser radiation and thermal expansion of this zone leads to a strong convection current flux perpendicular to the surface of the liquid. Overall, nanotubes, shells, ribbons and other structures appear in this interaction as in the pyrolysis of ferrocene.

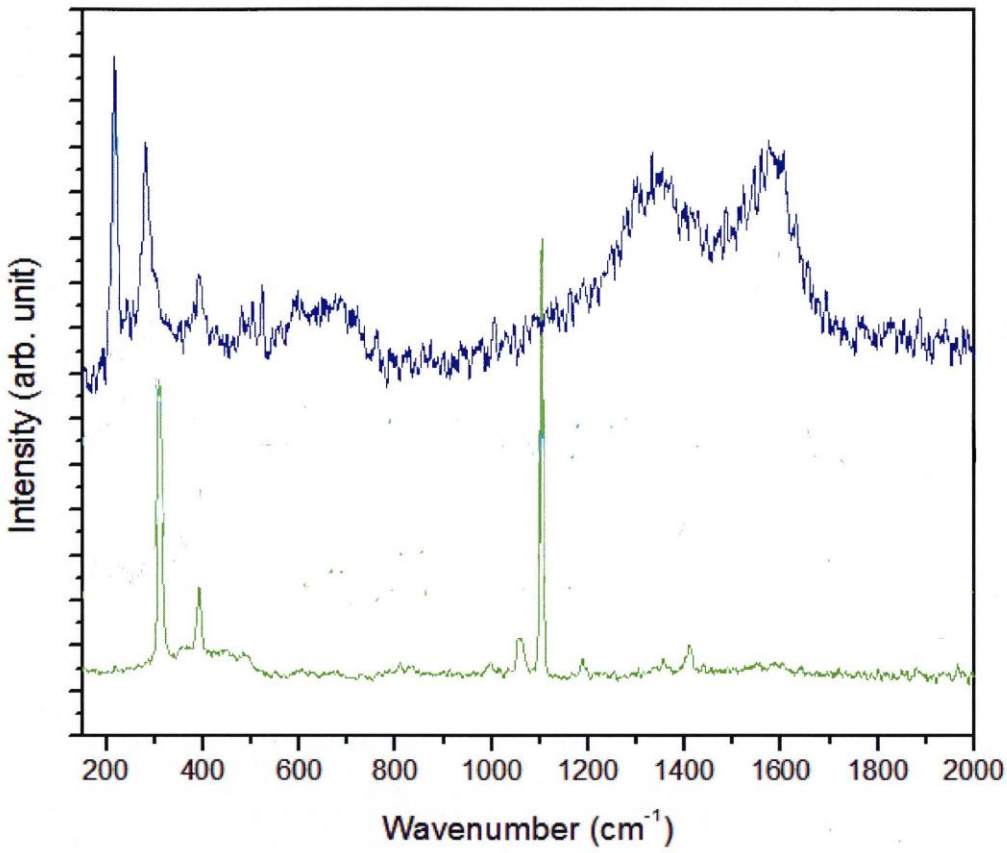

Fig.7-12.SERS spectrum of nanoparticles extracted after laser irradiation of ferrocene solution in benzene. a. Raman spectrum of nanoparticles after removal of ferrocene; b. Raman spectrum of ferrocene crystals. Data is taken from [47]

From the point of view of this thesis, the most important question is the chemical composition and structure of these nanoparticles, and their relation to cyclic C6 structures. Further information on chemical composition, including insight into their chemical structure can be obtained from Surface Enhanced Raman Spectroscopy (SERS) as shown in Fig.7-12.

Comparison Raman spectra of extracted nanoparticles (Fig.7-12.a) with that of ferrocene crystals (Fig.7-12.b) indicates that all ferrocene has been removed from the nanoparticles. Thus, the spectra (Fig.7-12.a) are those of other compounds synthesized during irradiation. Two very broad peaks on the Fig.7-12.a designated D and G, respectively at 1340 cm^{-1} and 1604 cm^{-1} are typical of disordered carbon and correspond to vibrational modes of C=C bonds [156,245]. More interesting is the appearance of two sharp peaks at 216.4 cm^{-1} and 280.9 cm^{-1} that could be assigned to breathing modes of nanotubes, or to stretching vibrations of Fe-C bonds. The latter possibility is supported by x-ray diffraction (XRD) studies of extracted material (table 7-2 and Fig.7-13).

The XRD spectrum of washed nanoparticles is shown in Fig.7-13.a. A list of peaks is shown in Table 7-1. The existence of only two dominant peaks in the spectrum indicates that the molecular structure is highly symmetric. All other XRD peaks were very weak. It is also known that the solid included only carbon and iron and that carbon is the most abundant element. The physical conditions involved in the creation of this substance are so extreme that some exotic molecular structure might be expected. It is then not surprising that the experimental XRD spectrum does not match any spectrum in the Crystallography Open Database (COD) [204]

Peak (2θ)	d-spacing (Å)	Intensity (% of the highest peak)
17.260	5.133	8.0
17.447	5.079	12.3
18.529	4.785	7.2
26.845	3.318	8.8
27.596	3.230	9.6
29.637	3.012	10.3
31.151	2.869	9.6
31.934	2.801	100
45.718	1.983	34.5
56.74	1.621	4.5

Table 7-2. X-Ray diffraction peaks for nanoparticles extracted irradiated ferrocene solution

where XRD spectra of most known chemical substances are listed. It is possible that an allotropic carbon-iron compound might correspond to the experimental XRD spectrum, but this was not found. One possibility is an intercalated graphite as these compounds can incorporate some alkali and alkaline earth metals (K, Na, Rb, Cs, Yb, Li, Ca) [59].

These compounds have D3h or D6h symmetry. In addition, it is known that carbides with Ru and W have hexagonal symmetry and the ratio between metal and carbon is nearly 1:10 [51]. The exact structure of these ruthenium carbides is not quite clear, though it is similar to tungsten carbide WC with lattice symmetry P6m2 (187) known as α-WC. Lattice vectors of RuC with

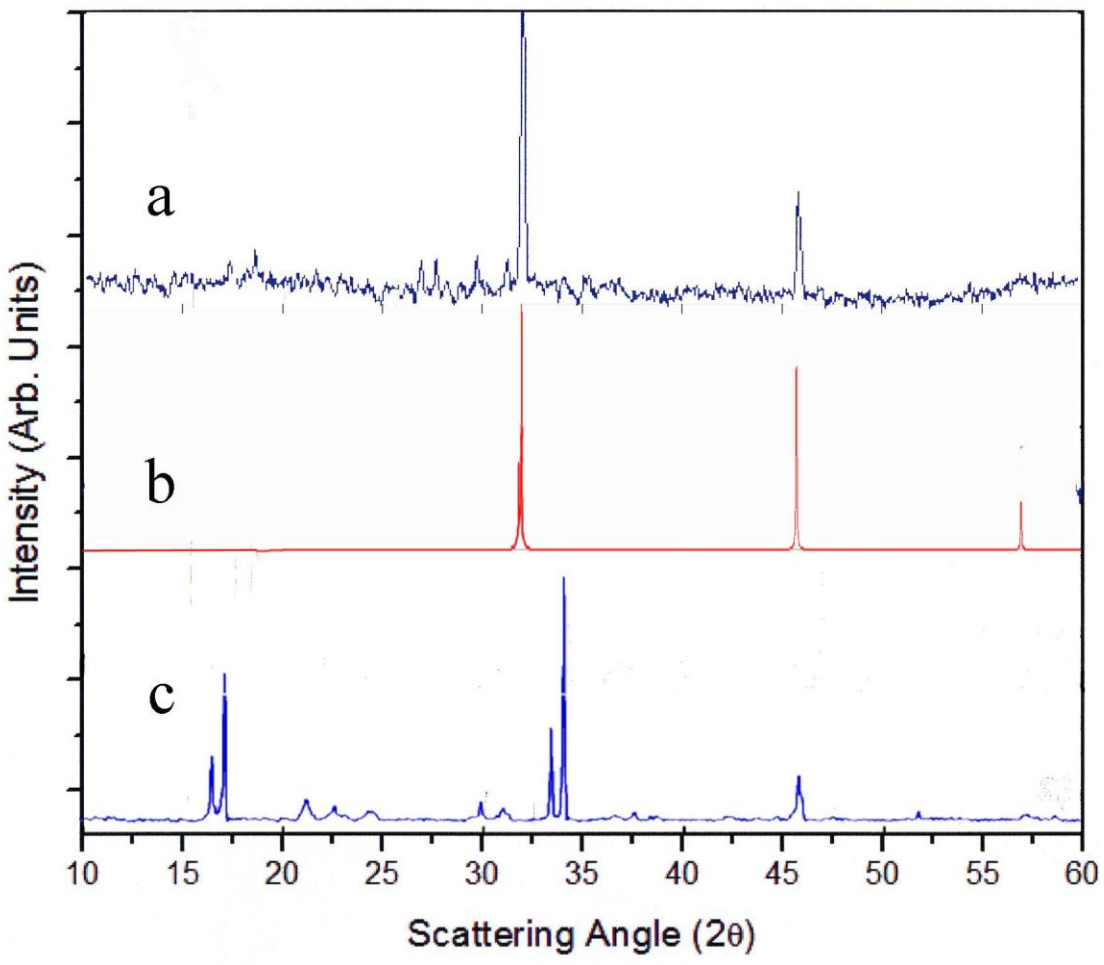

Fig.7-13. X-ray diffraction (XRD) for different types of intercalated graphite;
a. The experimental XRD data on nanoparticles product from ferrocene solution after laser irradiation (from [47]) b. Theoretical simulation of the XRD spectrum for hexagon carbide FeC_2. Experimental XRD data of intercalated graphite C_8K (from [59])

hexagon symmetry are a=2.908 Å, c=2.822 Å and for α-WC lattice the vectors are a=2.906 Å, c=2.839 Å. Hexagonal carbide RuC can be made by heating ruthenium-carbon mixtures up to 2600 C. Since ruthenium and iron are transition metals with very similar properties, this suggests that a new type iron carbide with hexagonal symmetry can be created at high temperature and pressure. It could be expected that the properties of hexagon carbide FeC_n are similar to those of hexagonal RuC and α-WC. The powder XRD pattern was simulated with the help of PowderCell for Windows version 2.4-8.03.2000 [54]. A number of theoretical XRD spectra corresponding to possible carbon-iron compounds with hexagonal symmetry were calculated, and it was found that few of them have a spectrum similar to the experimental one. Hexagonal FeC, FeC_2 FeC_6 and some other compounds have XRD spectra that are very similar to that observed here where the lattice constants are a=3.235 Å, c=2.810 Å. A comparison of the powder XRD spectra for different possible structures is shown in Fig.7-14. Since the exact chemical composition of the carbide is unknown and the difference in XRD is small the new substance obtained in our experiment cannot be precisely identified. All of these spectra have three dominant XRD peaks (at 31.9; 45.7 and 56.7 degrees of 2θ angle). The slight difference in spectra for these carbides is mostly in the relative strength of these three peaks. It is also important to take into account that many published theoretical predictions of the XRD spectra are not precise, especially as they predict peak intensity. Thus, up to date the exact lattice type of hexagonal carbides such as Fe_2C, FeC, FeC_2, FeC_6 (two variants) cannot be determined. XRD spectra of FeC_6 (Fig.7-15) are slightly better fits to the experimental data and are consistent with SEM data.

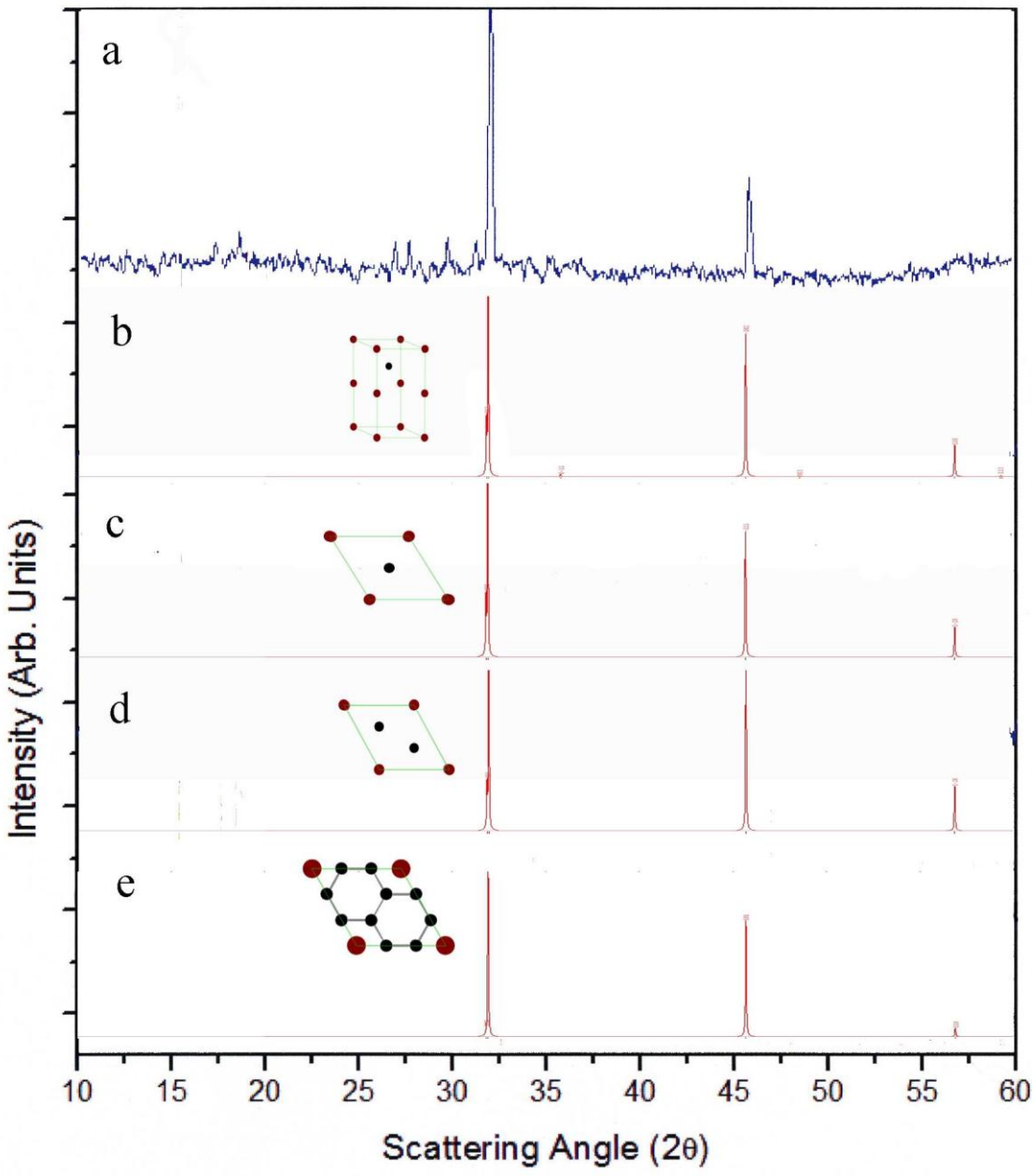

Fig.7-14. Comparison of the experimental XRD spectrum (a) with theoretical XRD spectra for different possible iron carbide structures: b. Fe_2C; c. FeC; d. FeC_2 e. FeC_6. The top view unit cells in c, d, e carbon atoms (black points) and iron atoms (brown points) are located in different parallel planes.

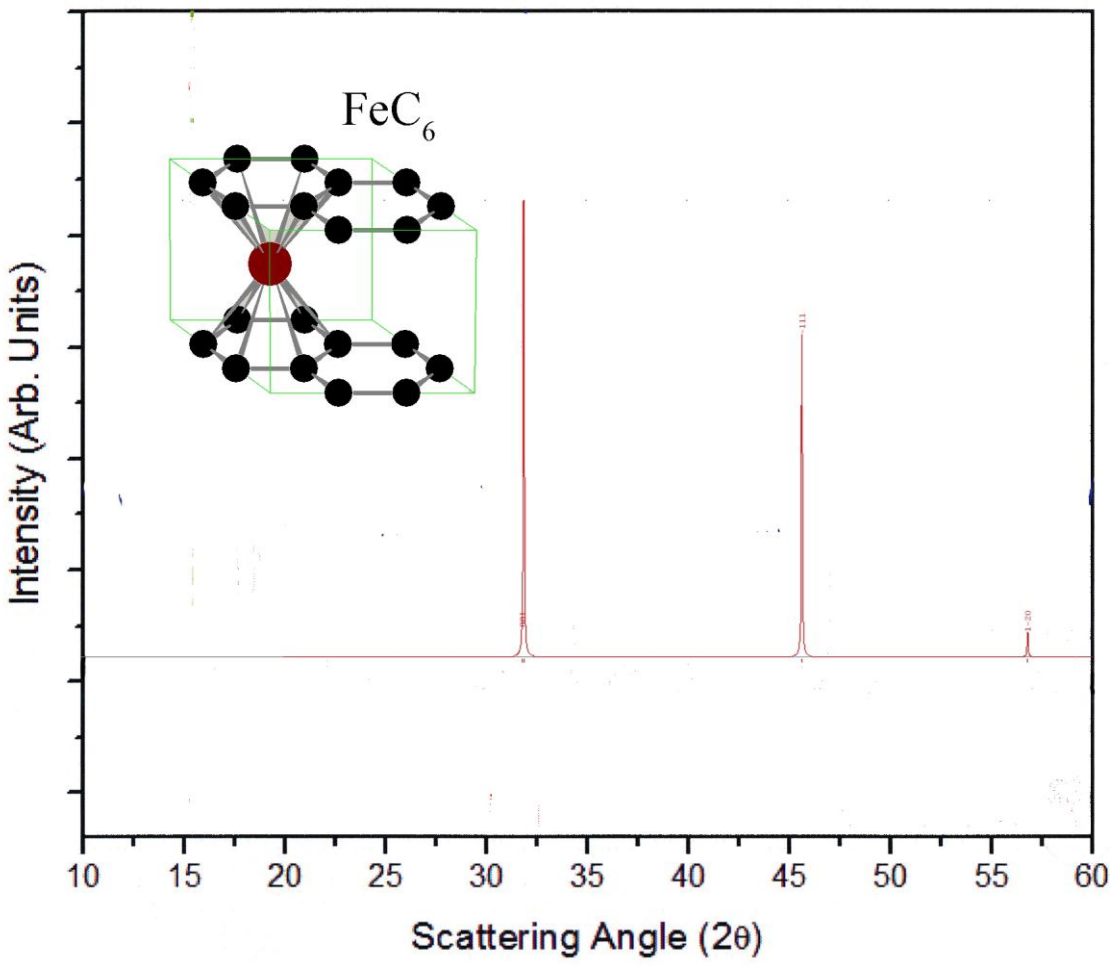

Fig.7-15. XRD spectra and structure of the unit cell of hexagonal carbide or intercalated graphite) FeC_6

It is suggested that carbide FeC_6 (an intercalated graphite from Fig.7-15) is the best candidate composition for the unknown metal-organic substance. This carbide can be synthesized only at temperatures exceeding a few thousand degrees. It is also possible that the high pressure is also needed. If such a compound exists, then its hardness could be comparable (or even higher) than that of tungsten carbide. In both compounds the interlayer distance is nearly the same (2.8 Å).

7.3. Conclusions on experimental studies.

A set of experiments have been carried out in an attempt to find molecules based on cyclic C_6 as predicted theoretically. For this purpose irradiation of the organic liquids fs laser pulses was chosen, since it could be expected that dehydrogenization in combination with total ionization, high temperature and pressure might lead to the creation of the new chemical compounds. Liquid benzene and a solution of the ferrocene in benzene were used for laser irradiation.

Some of these expectations have been confirmed. For example, dehydrogenization and high levels of ionization were observed in both liquids. In benzene filamentation of the laser beam and the emission the "white light" usually associated with a plasma [14] were important. Balls of hot plasma were observed in a ferrocene/ benzene solution under these conditions.

Unfortunately, the predicted substances are not explicitly detected. However, these experiments have yielded further information on the mechanism of nanoparticle formation during laser irradiation of organic liquids. It was also found that fs laser irradiation of liquid benzene was accompanied by a number of unique optical conditions. One of these was the enhanced filamentation of laser pulses caused by positive changes in refractive index due to excitation of the π^* energy level in the $\pi \rightarrow \pi^*$ resonance absorption excited by the third harmonic. This filamentation was accompanied by strong decomposition of the benzene and the creation of carbon nanoparticles. This study shows that this material is an agglomerate of carbon atoms.

Laser irradiation of ferrocene solution in benzene was dominated by the production of a high

temperature plasma. There was then some expectation that $Fe_{n-1}(C_6)_n$ metal-organic molecules based on cyclic C_6 might be produced. These were not detected but a carbide such as FeC_6 may have been formed and can be considered as a three-dimensional analog of the one-dimensional metal-organic structure considered theoretically.

SUMMARY

The electronic and vibrational properties of new type of carbon and metal-carbon molecular structure based on stacks of cyclic C_6 have been investigated in this thesis. These sandwich structures can be considered as a new form of small diameter pure and intercalated nanotubes. Based on first principles calculations, these tubular molecules are shown to have viable structures with high chemical and structural stability. This stability derives from an estimated bond energy of 6.36±0.01 eV in long pure $(C_6)_n$ structures. Theory indicates that the most stable metal-organic chains based on stacks of cyclic C_6 involve iron ($Fe_{n-1}(C_6)_n$) and ruthenium ($Ru_{n-1}(C_6)_n$) compounds with average bond energies of 6.80±0.05 eV and 6.00±0.02 eV, respectively. These bond energies are typical of those found in other highly stable organic compounds.

The vibrational properties of molecules based on stacks of cyclic C_6 showed a strong similarity to those of nanotubes and intercalated nanotubes. Calculations of phonon dispersion indicates that these compounds may be molecular conductors. Using standard methods, the calculated energy bands in these structures are representative of semiconductors. It is shown that molecular rotational and translational-rotational symmetries change the band structure allowing additional bands to appear corresponding to rotational-translational energy levels of the electrons. Applying this correction, the "classical" energy band structure of stacked molecules with C_6 rotational symmetry exhibit additional components that cross the Fermi level. Thus, all molecules based on stacks of C_6 are predicted to have metallic properties. In addition, some of the energy bands in metal-organic molecules such as $Fe_{n-1}(C_6)_n$ and $Ru_{n-1}(C_6)_n$ cross the Fermi level at the edge and at the center of the Brilliouin zone, implying that there is a very high density of electron states at or near the Fermi level.

This combination of high conductivity and a high density of the electron states suggests that these structures may be superconductive, however superconductivity cannot exist in $Fe_{n-1}(C_6)_n$ molecules because of strong ferromagnetic interactions as the presence of a strong molecular magnetic field inhibits creation of Cooper pairs. However, superconductivity in $Ru_{n-1}(C_6)_n$ and in pure carbon $(C_6)_n$ stacks is quite possible.

The possibility of superconductive properties of structures $(C_6)_n$ and in $Ru_{n-1}(C_6)_n$ was analysed. The estimation of transition temperature in such structures is made from semi-empirical model. The superconductive properties of our molecules were compared with properties of the superconductive carbon nanotubes. From published experimental data, this suggests that the upper limit of critical temperatures for superconductivity in $(C_6)_n$ and in $Ru_{n-1}(C_6)_n$ may be as high as 85 K and 210 K, respectively.

Some preliminary measurements designed to produce stacked molecules in the laboratory have been discussed in chapter 7. One approach involved irradiation of liquid benzene with intense fs laser pulses [124]. During laser irradiation of benzene we found that the formation of carbon nanoparticles can be attributed to resonant excitation of benzene by the third harmonic (TH) of incident (780 nm) laser radiation. Excitation of the $\pi \rightarrow \pi^*$ absorption line via the TH produces significant changes in refractive index, as well as nonlinear optical effects, and ionization of the benzene molecule. Decomposition of benzene results in the formation of positive and negative ions, charged carbon nanoparticles and a variety of organic molecules. Traces of fullerenes are also present, but there was no indication of the formation of $(C_6)_n$.

A second set of experiments on the fs laser irradiation of a ferrocene/benzene solution were designed to see if stacked metal-organic structures can be created in the laboratory. Laser radiation is strongly absorbed in this solution reducing the laser intensity at the laser focus.

Despite this attenuation, irradiation produced an intense plasma in the focal region. This was accompanied by the generation of a high transient temperature, high pressure leading to ionization of the surrounding liquid. Under these conditions different carbon and metal-organic structures are synthesized. The most interesting morphologies of these structures were nanofibers, nanotubes and shells. X-ray diffraction of these compounds showed them as having a three-dimensional periodic structure with hexagonal symmetry and lattice vectors a=3.235 Å, c=2.810 Å. Based on diffraction from known carbides, Fe_2C, FeC_2, FeC or FeC_4 are possibly present in this material either as carbides or as intercalated graphite. The micro structure of these compounds is similar to that predicted for one dimensional molecules such as $Fe_{n-1}(C_6)_n$. However, their exact chemical composition needs further clarification. Further experiments to obtain metal-organic molecules $(C_6)_nM_{n-1}$ possibly can be performed by growing them in a zeolite matrix using the method described by Tang at el [113] for the creation of nanotubes with < 4.2Å.

Experimental evidence for pure carbon tubular structures based on cyclic C_6 is reported in the paper written by Zhao et al [78]. They found that the innermost nanotube in a multiwall nanotube has diameter of < 3Å. As no conventional nanotube, formed by rolling graphene, can have such a small diameter, it is possible that this structure corresponds to $(C_6)_n$ as discussed in this thesis.

NOVELTY

Summarizing the major results reported in this thesis:

1. Some chemical, electronic and vibrational properties of a unique type of carbon molecule based on stacks of cyclic C_6 have been calculated from first principles.

2. $Fe_{n-1}(C_6)_n$ and $Ru_{n-1}(C_6)_n$ are found to be the most stable metal-organic structures based on stacks of cyclic C_6 Their chemical, electronic and vibrational properties have also been calculated from first principles.

3. It is shown explicitly that the electron band structure of any polymer chain with rotational or rotational-translational symmetry should include rotational and/or rotational-translational states. Such states cannot be calculated using the standard spatial one-dimensional Fourier transformation and must be directly introduced into the Hamiltonian.

4. According to a simple model incorporating this effect, the critical temperature for superconductivity in $(C_6)_n$ and in $Ru_{n-1}(C_6)_n$ may be in the 50-150 K range.

5. An effect of enhanced generation of carbon nanoparticles during irradiation of liquid benzene by laser femto-second pulses was discovered experimentally, and can be understood from the variation of the refractive index in the spectral region near the resonance corresponding to the third harmonic of the laser light.

6. Laser irradiation of liquid benzene results in the production of at least 75 different chemical compounds, as well as carbon nanoparticles.

7. Laser irradiation of a solution of ferrocene in benzene was used to synthesise metal-organic structures similar to $Fe_{n-1}(C_6)_n$.

8. The new metalorganic compound was synthesized during irradiation of ferrocene in benzene solution. Its X-ray diffraction analysis showed hexagonal lattice structure of new type carbide with lattice vectors a=3.235 Å, c=2.810 Å. The exact chemical content of carbon and iron in this structure yet needs further clarification. However, based on theoretical modeling of the X-ray diffraction spectra, there were few structural possibilities proposed, which potentially can have similar spectrum.

REFERENCES

1. M.S.Dresselhaus,"Future directions in carbon science", Annu. Rev. Mater. Sci., 27 (1997) 1

2. A. Sédéki, L.G. Caron, C. Bourbonnais, "Superconductivity in armchair carbon nanotubes", Phys. Rev. B 65 (2002) 140515

3. J.Y. Park , Chapter 1 from book "Carbon nanotube electronics" Springer 2009

4. O. B. Malcioglu and S. Erkoc,"Thermal stability of benzorods: Molecular-dynamics simulations" Journal of Molecular Graphics and Modelling 24 (2005) 213

5. S. Erkoc," Does tubular structure of carbon form only from graphine sheet?", Physica E 25 (2004) 69

6. S. Kuzmin, and Walter W. Duley," Ab initio calculations of a new type of tubular carbon molecule based on multi-layered cyclic C_6 structures", Physics Letters A, 374 (2010) 1374

7. S. Kuzmin and W. W. Duley, "Multilayer cyclic C_6 structures intercalated with metal atoms", Phys. Rev. A 83, (2011), 022507

8. S.Tennant,"On the nature of the diamond", Philosophycal Transactions of the Royal Society of London 87 (1797) 123

9. E.S.Dana, W.E.Ford, "A Textbook of Mineralogy", fourth edition. John Wiley & Sons. (1932) New York, p.28

10. W.H.Bragg, W.L.Bragg,"Structure of the diamond", Proceedings of the Royal Society of London. Series A. 89 (1913) 277

11. J.D.Bernal,"Structure of graphite", Proceedings of the Royal Society of London. Series A 106 (1924) 749

12. J.C.Lewis, B.Redfern, F.C.Cowlard,"Vitreous carbon as a crucible material for semiconductors", Solid-State Electronics 6 (1963) 251

13. F.C.Cowlard, J.C.Lewis,"Vitreous carbon – a new form of carbon", J of Material Science 2 (1967) 507

14. P. J. F. Harris, "Fullerene-related structure of commercial glassy carbons", Philosophical Magazine, 84 (2004) 3159

15. S.Aisenberg, R.Chabot,"Ion beam deposition of thin films of diamondlike carbon", J. of Applied Physics 42 (1971) 2953

16. F.P.Bundy, J.S.Kasper,"Hexagonal diamond – a new form of carbon", J. of Chemical Physics 46 (1967) 3437

17 C.Frondel, U.B.Marvin,"Lonsdaleite, a hexagonal polymorph of diamond", Nature 214 (1967) 588

18. H.W.Kroto, et al, "Buckminster fullerene", Nature 318 (1985) 162

19. M.Reibold, et al,"Materials: carbon nanotubes in an ancient nanostructured material", Nature 444 (2006) 2215

20. Y.Y.Li, C.C.Hseih, "Synthesis of nanotubes by combustion of a paraffin wax candle", Micro & Nano Letters 2 (2007) 63

21. L.A.J.Garvie, P.R.Buseck, "Nanosized carbon-rich grains in carbonaceous chondrite meteorites", Earth and Planetary Science Letters, 224 (2004) 431

22. S.Iijima,"Helical microtubules of graphitic carbon", Nature 354 (1991) 56

23. M.Monthioux, V.L.Kuznetsov,"Who should be given the credit for the discovery of carbon nanotubes?", Carbon 44 (2006) 1621

24. K.S.Novoselov, et al, "Electric field effect in atomically thin carbon films", Science 306 (2004) 666

25. K.S.Novoselov, et al., "Two-dimensional gas of massless Dirac fermions in graphene", Nature 438 (2005) 197

26. Y.Zhang, Y. W.Tan, H. L.Stormer, and P.Kim, "Experimental observation of the quantum Hall effect and Berry's phase in graphene", Nature 438 (2005) 201

27. R.H.Baughman, "Dangerously seeking linear carbon", Science 267 (2006) 1009

28. R.J.Lagow, et al, "Synthesis of linear acetylenic carbon: The 'sp' carbon allotrope", Science 267 (1995) 362

29. A.V.Rode, et al, "Structural analysis of a carbon foam formed by high pulse-rate lase ablation" Applied Physics A, 69 (1999) S755

30. G.N.Lewis, "The atom and the molecule", J.Amer.Chem.Soc., 38 (1916) 1

31. W.Heitler, F. London, "Wechselwirkung neutraler Atome und homöopolare Bindung nach der Quantenmechanik", Zeitschrift fur Physik, 44 (1927) 455

32. R.S.Mulliken, "Spectroscopy, molecular orbits and chemical bonding", Nobel lecture 1966

33. E.Huchel, “Theory of free radicals of organic chemistry”, Trans.Faradey Soc., 30 (1934) 40

34. L.Pauling, “The nature of the chemical bond. III. The transition from one extreme bond type to another”, J.Americ.Chemic.Soc., 54 (1932) 988

35. A.Szabo, N. S. Ostlund, “Modern Quantum Chemistry”, Dover Publishing. 1996 Mineola

36. P.Hohenberg, W.Kohn. , “Inhomogeneous Electron Gas“, Physical Review B 136 (1964) 864

37. J. E. Field , “The Properties of natural and synthetic diamond”, Academic Press, 1992, London

38. L.Itzhaki, E.Altus, H.Basch, S.Hoz, “Harder than Diamond: Determining the Cross-Sectional Area and Young's Modulus of Molecular Rods”, Angew. Chem. Int. Ed. 44 (2005) 7432

39. C.Lee, et al., “Measurement of the Elastic Properties and Intrinsic Strength of Monolayer Graphene”, Science, 321 (2008) 385

40. W.F.Smith, J.Hashemi, "Foundations of Materials Science and Engineering" (4th ed.) 2006. McGraw-Hill

41. N.N.Greenwood, A.Earnshaw, "Chemistry of the Elements." Pergamon Press. 1984, Oxford, p.318

42. P.R.Wallace, “The Band Theory of Graphite”, Physical Review 71 (1947) 622

43. J.-C.Charlier, P.C.Eklund, J.Zhu, A.C.Ferrari, "Electron and Phonon Properties of Graphene: Their Relationship with Carbon Nanotubes", from Carbon Nanotubes: Advanced Topics in the Synthesis, Structure, Properties and Applications, Springer-Verlag, 2008, Berlin

44. G.W.Semenoff,” Condensed-Matter Simulation of a Three-Dimensional Anomaly”, Physical Review Letters 53 (1984) 2449.

45. P.Avouris, Z.Chen, V.Perebeinos, “Carbon-based electronics”, Nature Nanotechnology 2 (2007) 605

46. A.K.Geim, K. S.Novoselov, “The rise of graphene”, Nature Materials 6 (2007) 183

47. M.J.Wesolowski "Properties of nanomaterials produced by ultrashort pulsed laser irradiation" PhD thesis, Watreloo 2012

48. S.V.Morozov, et al., “Giant Intrinsic Carrier Mobilities in Graphene and Its Bilayer”, Phys. Rev. Lett 100 (2008) 016602

49.J. H.Chen, et al., “Intrinsic and extrinsic performance limits of graphene devices on SiO_2”, Nature Nanotechnology 3 (2008) 206

50. A.Akturk, N.Goldsman, “Electron transport and full-band electron-phonon interactions in graphene”, Journal of Applied Physics 103 (2008) 053702

51. R.P.Elliott; F.A.Shunk; M.Hansen, "Constitution of binary alloys", McGraw-Hill, New York 1965

52. D.K.Efetov, P.Kim, “Controlling Electron-Phonon Interactions in Graphene at Ultrahigh Carrier Densities”, Pys.Rev.Lett. 105 (2010) 256805

53. M.Poetschke, C. G. Rocha, L. E. F. Foa Torres, S. Roche, G. Cuniberti, “Modeling graphene-based nanoelectromechanical devices”, Phys.Rev. B 81, (2010) 193404

54. Nolze, G., and W. Kraus. "PowderCell 2.0 for windows." Powder Diffr. 13 (1998) 256

55. Th.B.Singha, N.S.Sariciftci, et al, “Correlation of crystalline and structural properties of C thin films grown at various temperature with charge carrier mobility”, App.Phys.Lett. 90 (2007) 213512

56. N.Tombros, et al., "Electronic spin transport and spin precession in single graphene layers at room temperature", Nature 448 (2007) 571575.

57. S.Cho, C.Yung-Fu, M.S. Fuhrer. "Gate-tunable Graphene Spin Valve", Applied Physics Letters 91 (2007)123105

58. M.Ohishi, et al., “Spin Injection into a Graphene Thin Film at Room Temperature”, Jpn J Appl Phys 46 (2007) L605

59. M. S. Dresselhaus, G. Dresselhaus, “Intercalation compounds of graphite”, Advances in Physics, 51 (2002) 1

60. G. Csanyi, et al., “The role of the interlayer state in the electronic structure of superconducting graphite intercalated compounds”, Nature Physics 1 (2005) 42

61. G.Savini, A. C. Ferrari, F.Giustino, “First-Principles Prediction of Doped Graphane as a High-Temperature Electron-Phonon Superconductor”, Pys.Rev.Lett. 105 (2010) 037002

62. M.Sluiter, Y.Kawazoe, “Cluster expansion method for adsorption: Application to hydrogen chemisorption on graphene”, Physical Review B 68 (2003) 085410

63. S.Chandrasekhar, B.K.Sadashiva and K. A. Suresh, “Liquid crystals of disc-like molecules”, Pramana, 9 (1977) 471

64. D.Adam, et al., “Fast photoconduction in the highly ordered columnar phase of a discotic liquid crystal”, Nature, 371 (1994) 141

65. K.Ohta, et al., “Discotic liquid crystalline semiconductors”, Mol. Cryst. Liq. Cryst., 397 (2003) 325

66. G.P.Agrawal, “Nonlinear optical properties of one-dimensional semiconductors and conjugated polymers”, Phys.Rev. B 17 (1978) 776

67. N.Kawakami, “Collective Motion of Fermions: Tomonaga-Luttinger Liquid”, AAPPS Bulletin, 16 (2006) 4

68. S.Tomonaga, “Remarks on Bloch's Method of Sound Waves applied to Many-Fermion Problems”, Prog. Theor. Phys., 5 (1950) 544

69. M. Stone, Bosonization, World Scientific, 1994, Singapore

70. J.M.Luttinger, “An Exactly Soluble Model of a Many-Fermion System”, J. Math. Phys. 4 (1963) 1154

71. F. D. M. Haldane, “'Luttinger liquid theory' of one-dimensional quantum fluids. I. Properties of the Luttinger model and their extension to the general 1D interacting spinless Fermi gas”, J. Phys. C 14 (1981) 2585

72. A. A. Belavin, A. M. Polyakov and A. B. Zamolodchikov, “Infinite conformal symmetry in two-dimensional quantum field theory”, Nucl. Phys. B 241, (1984) 333

73. P.M. Krstaji´c, M. Pagano, P. Vasilopoulos, “Transport properties of low-dimensional semiconductor structures in the presence of spin–orbit interaction”, Physica E, 43 (2011) 893

74. J.J.Harris, J.A.Pals, R.Woltjer, “Electronic transport in low-dimensional structures”, Rep. Prog. Phys. 52 (1989) 1217

75. A.A.Shanenko, M.D.Croitoru, A.Vagov, F.M.Peeters, “Giant drop in the Bardeen-Cooper-Schrieffer coherence length induced by quantum size effects in superconducting nanowires”, Phys.Rev. B 82 (2010) 104524

76. L. D.Landau, E. M.Lifshi͡ts, Statistical physics. 2nd rev. and enl. ed., Pergamon Press 1969-1980 London

77. P.Phillips, Advanced Solid State Physics. Perseus Books 2008

78. X. Zhao et al., “Smallest Carbon Nanotube Is 3 Å in Diameter”, Phys.Rev.Lett. 92 (2004) 125502

79. T.Durkop, S.A.Getty, E.Cobas, M.S.Fuhrer, “Properties and applications of high-mobility

semiconducting nanotubes", Nano Letters, 4 (2004) 35

80. X.Wang, Q.Li, J.Xie et al., "Fabrication of Ultralong and Electrically Uniform Single-Walled Carbon Nanotubes on Clean Substrates", Nano Letters 9 (2009) 3137

81. W.Koch, M.C.Holthausen "A Chemist's Guide to Density Functional Theory" Wiley-VCH, 2001, Weinheim

82. C.D.Simpson, J. Wu, M.D.Watson and K.Mullen, "From graphite molecules to columnar superstructures – an exercise in nanoscience", J. Mater. Chem., 14 (2004) 494

83. K. Hoshino *et al.*, "Structures and Ionization Energies of Sandwich Clusters (V_n(benzene)$_m$)", J. Phys. Chem. 99 (1995) 3053

84. T. Yasuike and S. Yabushita, "Ionization Energies and Bonding Scheme of Multiple-Decker Sandwich Clusters: $Mn(C_6H_6)_{n+1}$", J. Phys. Chem. A 103 (1999) 4533

85. Y. Mokrousov *et al.*, "The interplay of structure and spin–orbit strength in the magnetism of metal–benzene sandwiches: from single molecules to infinite wires", Nanotechnology 18 (2007) 495402

86. J. Wang, P. H. Acioli, and J. Jellinek, "Structure and Magnetism of V_nBz_{n+1} Sandwich Clusters", J. Am. Chem. Soc. 127 (2005) 2812

87. R. Pandey *et al.*, "Electronic Structure and Properties of Transition Metal−Benzene Complexes",J. Am. Chem. Soc. 123 (2001) 3799

88. X. L. Wang, M. Y. Ni, and Z. Zeng, "Growth model investigation of Vanadium-Benzene Polymer", e-print arXiv:1002.4323v1[cond-mat.mtrl-sci]

89. H. Xiang, J. Yang, J. G. Hou, and Q. Zhu, "One-Dimensional Transition Metal-Benzene Sandwich Polymers: Possible Ideal Conductors for Spin Transport", J. Am. Chem. Soc.128 (2006) 2310

90. A. Goto and S. Yabushita, "Theoretical study on the spin states and intra-cluster spin relaxation of the one-dimensional metal–benzene sandwich clusters: $M_2(C_6H_6)_3$ (M = Sc, Ti, V)", Chem. Phys. Lett. 454 (2008) 382

91. H. Weng, T. Ozaki, and K. Terakura, "Revisiting magnetic coupling in transition-metal-benzene complexes with maximally localized Wannier functions", Phys. Rev. B 79 (2009) 235118

92. S. Nagao, A. Kato, and A. Nakajima, "Multiple-Decker Sandwich Poly-Ferrocene Clusters", J. Am. Chem. Soc. 122 (2000) 4221

93. T. Yasuike *et al.*, “Why Do Vanadium Atoms Form Multiple-Decker Sandwich Clusters with Benzene Molecules Efficiently?”, J. Phys. Chem. A 101 (1997) 5360

94. J. Kua and K. M. Tomlin, “Computational Study of Multiple-Decker Sandwich and Rice-Ball Structures of Neutral Titanium-Benzene Clusters”, J. Phys. Chem. A 110 (2006) 11988

95. L. Shen *et al.*, “Charge-Transfer-Based Mechanism for Half-Metallicity and Ferromagnetism in One-Dimensional Organometallic Sandwich Molecular Wires”, J. Am. Chem. Soc. 130 (2008) 13956

96. M. Mitsui *et al.*, J. Phys. “Soft-Landing Isolation of Vanadium-Benzene Sandwich Clusters on a Room-Temperature Substrate Using n-Alkanethiolate Self-Assembled Monolayer Matrixes”, Chem. Lett. B 110 (2006) 2968

97. T. Kurikawa *et al.*, “Electronic Properties of Organometallic Metal-Benzene Complexes $[M_n(benzene)_m$ (M)=Sc-Cu)]”, Organometallics 18 (1999) 1430

98. S. Nagaoka *et al.*, “An atomic force microscope study of vanadium-benzene sandwich clusters soft-landed on self-assembled monolayers”, Eur. Phys. J. D 52 (2009) 103

99. J. T. Lyon and L. Andrews, “V, Nb, and Ta Complexes with Benzene in Solid Argon: An Infrared Spectroscopic and Density Functional Study”, J. Phys. Chem. A 109 (2005) 431

100. L. Van Hove, “The Occurrence of Singularities in the Elastic Frequency Distribution of a Crystal”, Phys. Rev., 89 (1953) 1189

101. M. Schluter, M. Lannoo, M. Needels, and G. A. Barafl, “Electron-phonon coupling and superconductivity in alkali-intercalated C60 solid”, Phys.Rev.Lett.68 (1992) 526

102. A. Raichura, M. Dutta, and M.A. Stroscio, Applied Physics of Carbon Nanotubes , Part I, 2005, Springer, Berlin

103. S. Kuzmin and W. W. Duley, "*Ab initio* calculations of some electronic and vibrational properties of molecules based on multi-layered stacks of cyclic C_6", Fullerenes, Nanotubes and Carbon Nanostructures, 20 (2012) 730-736

104. S. Kuzmin and W. W. Duley, " *Ab initio* calculation of the electronic and vibrational properties of metal-organic molecules based on cyclic C_6 intercalated with some group VIII transition metals", (2012) accepted by Ann. Phys. (Berlin)

105. C. T. White, J. W. Mintmire, “Density of states reflects diameter in nanotubes”, Nature 394 (1998) 29

106. D. Connetable, G.-M. Rignanese, J.-C. Charlier, and X. Blase, “Room Temperature Peierls Distortion in Small Diameter Nanotubes”, Pys.Rev.Lett. 94 (2005) 015503

107. R. Barnett et al., “Electron-phonon interaction in ultrasmall-radius carbon nanotubes”, Phys. Rev. B, 71, (2005) 035429

108. R. Barnett et al., “Superconducting and charge-density wave instabilities in ultrasmall-radius carbon nanotubes”, Solid State Commun., 135, (2005) 335

109. K. Iyakutti et al., “Electronic band structure, electron-phonon interaction, and superconductivity of (5,5), (10,10), and (5,0) carbon nanotubes”, Phys. Rev. B, 73, (2006) 035413

110. K.-P. Bohnen, R. Heid, H. J. Liu, and C.T. Chan, “Lattice Dynamics and Electron-Phonon Interaction in (3,3) Carbon Nanotubes”, Pys.Rev.Lett. 93 (2004) 245501

111. S.M.-M. Dubois, Z. Zanolli, X. Declerck, and J.-C. Charlier, “Electronic properties and quantum transport in Graphene-based nanostructures”, Eur. Phys. J. B 72 (2009) 1

112. R.A.Ferrell, “Possibility of One-Dimensional Superconductivity”, Phys. Rev. Lett. 13 (1964) 330

113. Z. K. Tang et al., “Superconductivity in 4 Angstrom Single-Walled Carbon Nanotubes”, Science, 292 (2001) 2462

114. T.Ishiguro, K.Yamaji, G.Saito "Organic superconductors", Springer, 1998, Berlin

115. K.Yu. Arutyunov, D.S. Golubev, and A.D. Zaikin, “Superconductivity in one dimension”, Physics Reports 464 (2008) 1

116. A. Bezryadin et al, J. Phys.: “Quantum suppression of superconductivity in nanowires”, Condens. Matter 20 (2008) 043202

117. P. Xiong, A. V. Herzog, and R. C. Dynes, “Negative Magnetoresistance in Homogeneous Amorphous Superconducting Pb Wires”, Pys.Rev.Lett. 78 (1997) 927

118. M. Zgirski and K.Yu. Arutyunov, “Current-Voltage Dependencies in Ultra-Narrow Superconducting Nanowires in the Regime of Quantum Fluctuations”, Phys. Rev. B 75 (2007) 172509

119. J.Bardeen, L.N.Cooper, J.R.Schrieffer, “Theory of Superconductivity”, Phys Rev. 108 (1957) 1175

120. M. de Llano, “High-Tc Superconductivity via BCS and BEC Unification: A Review”, arXiv:cond-mat/0405071v1 [cond-mat.supr-con]; Book chapter in "Horizons in Superconductivity Research" (Nova Science Publishers, NY, in press)

121. T. Nakamura, Mochidzuki Y, Sato S., “Synthesis of monodispersed DLC nanoparticles in intense optical field by femtosecond laser ablation of liquid benzene”, Conference on Lasers and

Electro-Optics/Quantum Electronics and Laser Science Conference and Photonic Applications Systems Technologies, Optical Society of America; 2007

122. M.J. Wesolowski, S. Kuzmin, B. Moores, B. Wales, R. Karimi, A. A. Zaidi, Z. Leonenko, J. H. Sanderson W.W. Duley,"Polyyne synthesis and amorphous carbon nano-particle formation by femtosecond irradiation of benzene" , Carbon 49 (2011) 625

123. S.L. Kuzmin, M.J. Wesolowski, W. W. Duley, "Enhanced laser filamentation and nanoparticle generation in liquid organic media due to resonance absorption of the third harmonic", (2012), in progress

124. M.J.Wesolowski , S.L.Kuzmin, B.Wales, J.H.Sanderson, W.W.Duley "Carbon superstructures created through catalytic plasma material synthesis", (2012),in progress

125. S. L. Kuzmin and W. W. Duley, "*Ab initio* calculations of novel organic and metal-organic molecules based on multi-layered and intercalated cyclic C_6 structures", Conference "Sharcnet 2010", Toronto

126. F. Chen, J. Hihath, Z. Huang, X. Li, N.J. Tao, "Measurement of Single-Molecule Conductance", Annu. Rev. Phys. Chem. 58 (2007)535.

127. H.W.Ch. Postma, T. Teepen, Z. Yao, M. Grifoni, C. Dekker, "Carbon nanotube junctions and devices", Science 293 (2001) 76

128. A. Akturk, "Terahertz Current Oscillations in Single-Walled Zigzag Carbon Nanotubes", Phys. Rev. Lett. 98 (2007) 166803

129. S. Hong, R. Reifenberger, W. Tian, S. Datta, J.I. Henderson, C.P. Kubiak, "Molecular conductance spectroscopy of conjugated, phenyl-based molecules on Au(111): the effect of end groups on molecular conduction", Superlatt.Microstruct. 28 (2000) 289.

130. M. Yamamoto, K. Wakabayashi, "Control of electric current by graphene edge structure engineering", Appl. Phys. Lett. 95 (2009) 082109.

131. A.H. Castro Neto, F. Guinea, N.M.R. Peres, K.S. Novoselov, A.K. Geim, "The electronic properties of graphene", Rev. Mod.Phys. 81 (2009) 109.

132. A.D. Becke, "Density-functional thermochemistry. III. The role of exact exchange", J. Chem. Phys. 98 (1993) 5648.

133. M.J. Frisch, G.W. Trucks, H.B. Schlegel, G.E. Scuseria, M.A. Robb, J.R. Cheeseman,J.A. Montgomery Jr., T. Vreven, K.N. Kudin, J.C. Burant, J.M. Millam, S.S.Iyengar, J. Tomasi, V. Barone, B. Mennucci, M. Cossi, G. Scalmani, N. Rega, G.A.Petersson, H. Nakatsuji, M. Hada, M. Ehara, K. Toyota, R. Fukuda, J. Hasegawa,M. Ishida, T. Nakajima, Y. Honda, O. Kitao, H. Nakai, M. Klene, X. Li, J.E. Knox,H.P. Hratchian, J.B. Cross, C. Adamo, J. Jaramillo, R. Gomperts, R.E. Stratmann,O. Yazyev, A.J. Austin, R. Cammi, C. Pomelli, J.W. Ochterski, P.Y.

Ayala, K. Morokuma,G.A. Voth, P. Salvador, J.J. Dannenberg, V.G. Zakrzewski, S. Dapprich,A.D. Daniels, M.C. Strain, O. Farkas, D.K. Malick, A.D. Rabuck, K. Raghavachari,J.B. Foresman, J.V. Ortiz, Q. Cui, A.G. Baboul, S. Clifford, J. Cioslowski, B.B. Stefanov,G. Liu, A. Liashenko, P. Piskorz, I. Komaromi, R.L. Martin, D.J. Fox, T. Keith,M.A. Al-Laham, C.Y. Peng, A. Nanayakkara, M. Challacombe, P.M.W. Gill, B. Johnson,W. Chen, M.W. Wong, C. Gonzalez, J.A. Pople, Gaussian, Inc., Wallingford,CT, 2004.

134. J.M.L. Martin, J.P. Francois, R. Gijbelst, "A Critical Comparison of MINDO/3, MNDO, AM1, and PM3 for a Model Problem: Carbon Clusters C_2-C_{10}. An Ad Hoc Reparametrization of MNDO Well Suited for the Accurate Prediction of Their Spectroscopic Constants", J. Comp. Chem. 12 (1991) 52.
135. K. Raghavachari, R.A. Whiteside, J.A. Pople, "Structures of small carbon clusters: cyclic ground state of C_6", J. Chem. Phys. 85 (1986) 6623.

136. T. Torelli, L. Mitas, "Electron Correlation in C4N12 Carbon Rings: Aromatic versus Dimerized Structures", Phys. Rev. Lett. 85 (2000) 1702.

137. J. Hutter, H.-P.Luethi, F. Diederich, "Structures and Vibrational Frequencies of the Carbon Molecules C_2-C_{18} Calculated by Density Functional Theory", J. Am. Chem. Soc. 115 (1994) 750.

138. J.M.L. Martin, J. El-Yazal, J.-P. Francois, "Structure and vibrational spectra of carbon clusters C_n (n = 2-10,12,14,16,18) using density functional theory including exact exchange contributions", Chem. Phys. Lett. 242 (1995) 570.

139. J.M.L. Martin, P.R. Taylor, "Structure and Vibrations of Small Carbon Clusters from Coupled-Cluster Calculations", J. Phys. Chem. 100 (1996) 6047
.
140. J. Haubrich, M. Muehlhaeuser, S.D. Peyerimhoff, "The electronic spectrum of linear and cyclic C_6+. A theoretical study", Phys. Chem. Chem. Phys. 4(2002) 2891.

141. H. Masso, M.L. Senent, "Ab Initio Characterization of C_6+", J. Phys. Chem. A 113 (2009) 12404.

142. Ying Xu, Li-Ling Zhou, Z.X. Dai, "First-principles electronic transport properties study of small carbon clusters: Cyclic C_6", Phys. Lett. A 372 (2008) 4465.

143. W. Weltner, K.R. Thompson, R.L. DeKock, "Spectroscopy of carbon molecules IV", J. Am. Chem. Soc. 93 (1971) 4688.

144. J. Fulara, E. Riaplov, A. Batalov, I. Shnitko, J.P. Maier, "Electronic and infrared absorption spectra of linear and cyclic C_6+ in a neon matrix", J. Chem. Phys. 120 (2004)7520.

145. J.D. Presilla-Marquez, J.A. Sheehy, J.D. Mills, P.G. Carrick, C.W. Larson, "Vibrational spectra of cyclic C_6 in solid argon", Chem.Phys. Lett. 274 (1997) 439.

146. S.L. Wang, C.M.L. Rittby, W.R.M. Graham, “Detection of cyclic carbon clusters. I. Isotopic study of the ν4(e′) mode of cyclicC6 in solid Ar”, J. Chem. Phys. 107 (1997) 6032.

147. W. Scherzer, O. Kratzschmar, H.L. Selzle, E.W.Z. Schlag, “Structural isomers of the benzene dimer from mass selective hole-burning spectroscopy”, Zeitschrift für Naturforschung. A, A Journal of physical sciences 47 (1992): 1248

148. S. H. Khan, M. Husain, “Carbon nanotube and its possible application”, Indian Journal of Engineering and Material Sciences, 12 (2005), 529

149. F. Grein, J. Franz, M. Hanrath, S.D. Peyerimhoff, “Theoretical studies on the electronic spectra of cyclic C_6, in D3h and D6h symmetries”, Chem. Phys. 263 (2001) 55.

150. K. Miyajima, A. Nakajima, S. Yabushita, M. B. Knickelbein,and K. Kaya, “Ferromagnetism in One-Dimensional Vanadium-Benzene Sandwich Clusters”, J. Am. Chem. Soc. 126 (2004) 13202

151. K. Miyajima, S.Yabushita, M.B.Knickelbein, and A. Nakajima, “Stern-Gerlach Experiments of One-Dimensional Metal-Benzene Sandwich Clusters: $M_n(C_6H_6)m$ (M = Al, Sc, Ti, and V)”, J. Am. Chem. Soc. 129 (2007) 8473

152. A. D. Becke, “Density-functional exchange-energy approximation with correct asymptotic behavior”, *Phys. Rev.* A 38 (1988) 3098

153. C.Lee,W.Yang, R.G.Parr, “Development of the Colle-Salvetti correlation-energy formula into a functional of the electron density”, Phys. Rev. B 37.2 (1988) 785

154. R. Moradian and A. Fathalian, “Investigation of superconductivity in the single-walled carbon nanotubes”, J of Physics and Chemistry of Solids, 69 (2008) 2589

155. S. Z. Fairchild, Charles F. Bradshaw, Wansheng Su, and Samar K. Guharay, “Predicting Raman Spectra Using Density Functional Theory”, Applied Spectroscopy, 63 (2009) 733

156. M.S. Dresselhaus, G. Dresselhaus, R. Saito, A. Jorito, Physics Reports, “Raman spectroscopy of carbon nanotubes”, 409 (2005) 47

157. M. Paillet et al, J. Phys. “Raman Spectroscopy of Free-Standing Individual Semiconducting Single-Wall Carbon Nanotubes”, Chem. B, 110, (2006) 164

158. J. C. Meyer, M. Paillet, A. Moreac, A. Neumann, G.S. Duesberg, S. Roth, J.-L. Sauvajol, “Raman modes of index-identified freestanding single-walled carbon nanotubes”, Phys. ReV. Lett. 95 (2005) 217401.

159. R. Saito, G. Dresselhaus, M.S. Dresselhaus, Physical Properties of Carbon Nanotubes, Imperial College Press, Singapore, 1998, p.35

160. C. N. R. Rao and Rahul Sen, “Large aligned-nanotube bundles from ferrocene pyrolysis”, Chemical Communications, 15 (1998) 1525

161. T. Giamarchi, "Quantum Physics in One Dimension", Glarendon press, 2003, Oxford

162. J. Bodenheimer, E.Loewenthal, W.Low, “The Raman spectra of ferrocene”, Chem. Phys. Lett., 3 (1969) 715

163. H. Zhang, Y. Miyamoto, A. Rubio, “Laser-induced preferential dehydrogenation of graphane”, Phys. Rev. B 85 (2012) 201409

164. C.T. Fleaca et al., “Fe-inserted and shell-shaped carbon nanoparticles by cluster-mediated laser pyrolysis”, Applied Surface Science 258 (2012) 9394

165. M.S. Dresselhaus, A. Jorio, R. Saito, “Characterizing Graphene, Graphite, and Carbon Nanotubes by Raman Spectroscopy”, Annu. Rev. Condens. Matter Phys. 1 (2010) 89

166. G. te Velde, F.M. Bickelhaupt, S.J.A. van Gisbergen, C. Fonseca Guerra, E.J. Baerends, J.G. Snijders and T. Ziegler, “Chemistry with ADF”,. Journal of Computational Chemistry 22, 931 (2001)

167. R. Saito, M.S. Dresselhaus, G. Dresselhaus. Physical properties of carbon nanotubes, Imperial College Press, 1998, Singapore, p.163

168. J. C. Slater, G. F. Koster., “Simplified LCAO method for the periodic potential problem.”,Physical Review, 94, (1954) 1498

169. J.M. Soler, E. Artacho, J.D. Gale, A. García, J. Junquera, P. Ordejón, D. Sánchez-Portal. “The SIESTA method for ab initio order-N materials simulation", J. Phys.: Condens. Matt. 14, (2002) 2745

170. P. Giannozzi, S. Baroni, N. Bonini, M. Calandra, R. Car, C. Cavazzoni, D. Ceresoli et al. “QUANTUM ESPRESSO: a modular and open-source software project for quantum simulations of materials." Journal of Physics: Condensed Matter 21 (2009) 395502.

171. M.S. Dresselhaus et al., Science of fullerenes and carbon nanotubes, 1996, Academic Press, N.Y., p.965

172. S. Nakashima and H. Harima, “Spectroscopic analysis of electrical properties in polar semiconductors with over-damped plasmons”, J. Appl. Phys. 95, (2004) 3541

173. M. Mitra and S. Gopalakrishnan, “Vibrational characteristics of single-walled carbon-nanotube: Time and frequency domain analysis”, J. Appl. Phys. 101, (2007) 114320

174. J.P.Carbotte , “Properties of boson-exchange superconductors”, Reviews of Modern Physics 62 (1990) 1027

175. S.-D. Liang, “Bardeen–Cooper–Schrieffer formalism of superconductivity in carbon nanotubes”, Physica B 403 (2008) 2288

176. N. Giordano, “Superconducting fluctuations in one dimension”, Physica B 203 (1994) 460

177. W.A. Little, “Decay of persistent currents in small superconductors." Physical Review”, 156 (1967) 396

178. J. M. Graybeal, P. M. Mankiewich, R. C. Dynes, M. R. Beasley, “Apparent destruction of superconductivity in the disordered one-dimensional limit”, Pys.Rev.Lett. 59 (1987) 2697

179. G.Rickayzen, "Green's functions and condensed matter", Academic press, 1980, London

180. J.A.Reissland, “The physics of phonons”, J. Willey and sons ltd., 1973, London

181. A.Migdal, “Interaction between electrons and lattice vibrations in a normal metal”, Sov.Phys. JETP 7 (1958) 916

182. P.B.Allen, “Neutron Spectroscopy of Superconductors”, Phys.Rev.B, 6 (1972) 2577

183. W.H.Butler, H.G.Smith, N. Wakabayasky, “Electron-Phonon Contribution to the Phonon Linewidth in Nb: Theory and Experiment”, Phys.Rev.Lett. 39 (1977) 1004

184. J.P.Carbotte "Critical temperatures" from book "Superconductivity" Gordon and Breach Science Publishers Inc., N.Y.,1969

185. D.Chandler "Introduction to modern statistical Mechanics" Oxford University press" 2010 NY

186. O. A. E. Cherney, J. Shewchun, “Enhancement of superconductivity in thin aluminium films”, Canadian Journal of Physics 47 (1969) 1101

187. D. G. Walmsley,. K. Campbell, R. C. Dynes, “Superconductivity of very thin aluminium films”, Canadian Journal of Physics 46 (1968) 1129.

188. S.Y.Savrasov, D.Y.Savrasov, “Electron-phonon interactions and related physical properties of metals from linear-response theory”, Phys. Rev. B 54 (1996) 16487

189. N.B. Hannay, T.H. Geballe, B.T. Matthias, K. Andres, P. Schmidt, D. MacNair, “Superconductivity in Graphitic Compounds”, Phys. Rev. Lett. 14 (1965) 225.

190. O. Gunnarsson, “Superconductivity in fullerides”, Rev. Mod. Phys. 69 (1997) 575

191. M. Ferrier, A. Kasumov, R. Deblock, S. Guéron, H. Bouchiat, “Superconducting properties of carbon nanotubes”, C. R. Physique 10 (2009) 252

192. M. Ferrier, et al., “Superconductivity in ropes of carbon nanotubes”, Solid State Commun. 131 (2004) 615

193. L.C. Venema, J.W.G. Wildöer, J.W. Janssen, S.J. Tans, H.L.J. Temminck Tuinstra, L.P. Kouwenhoven, C. Dekker, “Imaging electron wave functions of quantized energy levels in carbon nanotubes”, Science 283 (1999) 52.

194. A.A. Odintsov, “Schottky Barriers in Carbon Nanotube Heterojunctions”, Phys. Rev. Lett. 85 (2000) 150.

195. A. De Martino, R. Egger, “Acoustic phonon exchange, attractive interactions, and the Wentzel-Bardeen singularity in single-wall nanotubes”, Phys. Rev. B 67 (2003) 235418

196. A. De Martino, R. Egger, “Effective low-energy theory of superconductivity in carbon nanotube ropes”, Phys. Rev. B 70 (2004) 014508.

197. I. Takesue, et al., “Superconductivity in Entirely End-Bonded Multiwalled Carbon Nanotubes”, Phys. Rev. Lett. 96 (2006) 057001.

198. J. Zhang, A. Tselev, Y. Yang, K. Hatton, P. Barbara, S. Shafraniuk, “Zero-bias anomaly and possible superconductivity in single-walled carbon nanotubes”, Phys. Rev. B 74 (2006) 155414.

199. J. Gonzalez, “Consistency of Superconducting Correlations with One-Dimensional Electron Interactions in Carbon Nanotubes”, Phys. Rev. Lett. 87 (2001) 136401

200. J. Gonzalez, “Microscopic Model of Superconductivity in Carbon Nanotubes”, Phys. Rev. Lett. 88 (2002) 076403

201. J. Gonzalez, “Superconductivity in carbon nanotube ropes”, Phys. Rev. B 67 (2003) 014528.

202. E.G. Maksimov, D. Y.Savrasov, “Lattice stability and superconductivity of the metallic hydrogen at high pressure”, Solid State Commun. 119 (2001) 569

203. L.X. Benedict et al, “Static conductivity and superconductivity of carbon nanotubes: Relations between tubes and sheets”, Phys Rev B 52 (1995) 14935

204. S.Grazulis at el, "Crystallography Open Database – an open-access collection of crystal structures", Journal of Applied Crystallography 42 (2009) 726

205. E.G.Maksimov, D.Yu.Savrasov, S.Yu.Savrasov, “Electron-phonon interaction and the physical properties of metals”, Phys. Usp. 40 (1995) 337

206. R.W.Boyd, Nonlinear optics, 3-d edition Academic Press, Elsevier, 2008 London

207. J. S. Greever, J. B. M. Turner, J. F. Kauffman, “Multiphoton Excited Conductance Spectroscopy. 1. Application of the Born Model to Femtosecond Laser Excited Multiphoton Ionization of Nonpolar Liquids”, J. Phys. Chem. A 105 (2001) 8635

208. V. O. Saik and S. Lipsky, “The Photoionization Spectrum of Liquid Benzene”, J. Phys. Chem. 98 (1994) 11858

209. T-W.Scott, A.J. Twarowski and A-C. Albrecht, “Multiphoton ionization of liquid benzene: The ionization mechanism”, Chem. Phys. Lett., 66 (1979) 1

210. I. A. Shkrob and M. C. Sauer, “Electron Localization in Liquid Acetonitrile”, J. Phys. Chem. A 106 (2002) 9120

211. W. Liu, S. Petit, A. Becker, N. Akozbek, C.M. Bowden, S.L. Chin, “Intensity clamping of a femtosecond laser pulse in condensed matter “, Optics Communications 202 (2002) 189

212. M. Centini at el, “Inhibition of Linear Absorption in Opaque Materials Using Phase-Locked Harmonic Generation”, Pys.Rev.Lett. 101 (2008) 113905

213. S.L.Chin at el, Some fundamental concepts of femtosecond laser filamentation, Springer, 2008, Berlin

214. A. Couairon, A. Mysyrowicz, “Femtosecond filamentation in transparent media”, Physics Reports 441 (2007) 47

215. C. D’amico, B. Prade, M. Franco, A. Mysyrowicz, “Femtosecond filament amplification in liquids”, Appl. Phys. B 85 (2006) 49

216. H. Schroeder, S.A. Hosseini, Q. Luo, S.L. Chin, “Self-steepening is an abrupt process”, Optics Communications 266 (2006) 302

217. N. Akozbek, A. Iwasaki, A. Becker, M. Scalora, S. L. Chin, and C.M. Bowden, “Third-Harmonic Generation and Self-Channeling in Air Using High-Power Femtosecond Laser Pulses”, Phys Rev Letters 89 (2002) 143901

218. T. V. K. Sarma and C. Santhamm, “The near ultraviolet absorption spectra of 2,3-, 2,4- and 2,5- dimethylbenzonitriles”, Spectrochimica Acta, 43A (1987) 929

219. I. B. Berlman, “Handbook of Fluorescence Spectra of Aromatic Molecules”, 1965, Academic Press,1965, N.Y.

220. T. Inagaki, “Absorption spectra of pure liquid benzene in ultraviolet region”, The Journal of Chemistry Physics, 57 (1972) 2526

221. T. Ogawa, M. Mizutani, and T. Inoue, “Dependence of the Laser Two-Photon Ionization Process in Solution on the Laser Pulse Width”, Anal. Chem., 73 (2001) 2066

222. V. S. Antonov and V. S. Letokhov, “Laser Multiphoton and Multistep Photoionization of Molecules and Mass Spectrometry”, Appl. Phys., 24 (1981) 89

223. V. S. Antonov, V. S. Letokhov, and A.N. Shibanov, “Photoionization Mass-Spectrometry of Benzene and Benzaldehyde Molecules with an Excimer KrF Laser”, Appl. Phys., 22 (1980) 293

224. V. R. Bhardwaj, K. Vijayalakshmi, and D. Mathur, “Dissociative ionization of benzene in intense laser fields of picosecond duration”, Phys Rev A 59 (1999) 1392

225. H. M. Boechat-Roberty et al, “Dissociation of the benzene molecule by UV and soft X-rays in
circumstellar environment”, Mon. Not. R. Astron. Soc. 394 (2009) 810

226. W. Fub, W. E. Schmid, and S. A. Trushin, “Time-resolved dissociative intense-laser field ionization for probing dynamics: Femtosecond photochemical ring opening of 1,3-cyclohexadiene”, J of Chem Phys 112, (2000) 8347

227. R. Itakura, J. Watanabe, A. Hishikawa, and K. Yamanouchi, “Ionization and fragmentation dynamics of benzene in intense laser fields by tandem mass spectroscopy”, J of Chem Phys 114, (2001) 5599

228. P. M. Johnson, “The multiphoton ionization spectrum of benzene”, J of Chem Phys 64, (1976) 4143

229. D. J. Smith et al, “Time-of-flight Mass Spectrometry of Aromatic Molecules Subjected to High Intensity Laser Beams”, Rapid Commun. Mass Spectrom. 12 (1998) 813

230. L.Zandee and R.B.Bernshtein, “Resonance-enhanced multiphoton ionization and fragmentation of molecular beams: NO_2, I_2, benzene, and butadiene”, J.Chem.Phys. 71 (1979) 1359

231. V. V. Kislov, T. L. Nguyen, A. M. Mebel, S. H. Lin, and S. C. Smith, “Photodissociation of benzene under collision-free conditions: An ab initio/Rice–Ramsperger–Kassel–Marcus study”, J. Chem. Phys. 120, (2004) 7008

232. A. Vailionis, E. G. Gamaly, V. Mizeikis, W. Yang, A. V. Rode, S. Juodkazis, “Evidence of superdense aluminium synthesized by ultrafast microexplosion”, Nature Communications (2011) 1

233. J. Momigny, C. Goffard and L. D'or, “Photoionization studies by total ionization measurements. I. Benzene and its monohalogeno derivatives”, International Journal of Mass Spectrometry and Ion Physics, 1 (1968) 53

234. H. J. Parkhurst, Jr. and J. Jonas, “Dense liquids. I. The effect of density and temperature on self-diffusion of tetramethylsilane and benzene-d6”, J. Chem. Phys. 63, (1975) 2698

235. E.W.McDaniel, E.A.Mason, "The mobility and diffusion of ions in gases", John Willey and sons, 1973, N.Y.

236. Y. Yin, et al., “Optical Determination of Electron-Phonon Coupling in Carbon Nanotubes”,Phys.Rev.Lett. 98 (2007) 037404